2015-04-24

Study of Composite Sorbent Pellets for Integration of Calcium Looping and Chemical Looping Combustion

Recio Delgado, Alvaro

UNIVERSITY OF CALGARY

Study of Composite Sorbent Pellets for Integration of Calcium Looping and Chemical Looping Combustion

by

Alvaro Recio Delgado

A THESIS

SUBMITTED TO THE FACULTY OF GRADUATE STUDIES

IN PARTIAL FULFILMENT OF THE REQUIREMENTS FOR THE

DEGREE OF MASTER OF SCIENCE

GRADUATE PROGRAM IN CHEMICAL ENGINEERING

CALGARY, ALBERTA

APRIL, 2015

Abstract

Carbon capture and storage (CCS) technologies were developed to address the problem of increasing CO_2 emissions. Two of the most promising technologies are calcium looping (CaL) and chemical looping combustion (CLC). The integration of CaL and CLC has been studied in this thesis with CuO/CaO composite sorbent pellets. The pellets were tested over multiple cycles and the stability in terms of chemical looping combustion was excellent, although agglomeration was observed. In contrast, a significant decay in the rate of CO_2 uptake was observed in the first 3-4 cycles. Both a thermal pretreatment and the presence of steam enhanced the stability, while the addition of potassium hydroxide hindered the performance. Steam will be present with the flue gases in an industrial application, and so it is important that steam did not detract from the performance of the pellets.

Acknowledgements

First and foremost, I would like to thank Dr. Josephine Hill for giving me the opportunity of joining her group and provide me the tools, advices and support to perform my work at the Laboratory for Environmental Catalytic Applications (LECA). For me, this has been an invaluable opportunity, which has made me grow as a person and as an engineer. The last two years will always be an important part of my life, in which I have had the chance to work alongside outstanding colleagues, make extraordinary friends and push my boundaries to limits that two years ago would have seemed impossible to me.

Also, I would like to thank Dr. Arturo Macchi for his advices and suggestions to make my project move forward, and for spending some time with us while I visited Ottawa. Special thanks to Dr. Dennis Lu for making possible for me to go to CanmetENERGY – Ottawa. The time was an enriching (and freezing) experience in which I had the chance to work with excellent professionals. As part of the team at Canmet and the University of Ottawa, I also want to thank Ryad Rahman for the good moments while at Ottawa, and prior to that, for providing me with the pellets when needed.

Thank you to Dr. Karan, for encouraging me to put more effort into the heat transfer model and guiding me throughout the complicated study.

Special thanks to my LECA fellows, Sip Chen, Dr. Andrei Veksha, Dr. Benjamin Feist and Luis Virla for their invaluable help, teachings, inputs and patience. I really believe that part of my work is also yours.

Thank you to Andres, Beatriz and Tania, who have been my safety net since the very first day.

I cannot forget about my cousin Oscar and his wife Eva, because the two of you were the first ones to encourage me to go abroad. I really do not know what would have happened if we would not have had that coffee, that day. In any case, if all this happened because of that, the only thing I can do is to thank you.

Thank you to all my friends back in Spain, for being so patient with me, and be willing to find a spot to see me every time I could visit, even when I said it with very short notice and it was almost impossible. But here I have to make a special mention to the two best friends I could have ever met, Marta and Salva. For me they are more than friends, they are my family too, and I really want to thank them for being there no matter the distance. You have no idea of what it meant to me knowing that I could always count on you, and that you really believed in me, on no condition.

Last but not least, thank you to my parents, Luis and Pilar, my sister, Diana, my brother-in-law, Oscar, and my wonderful family. Your unconditional support really gave me strength in some moments. The biggest thanks are to you.

Dedication

This thesis is dedicated to my parents, my sister, my brother-in-law and my recently arrived niece Vera and nephew Dario, because one day I will tell you the story of uncle Alvaro travelling to faraway lands.

Table of Contents

List of Tables

List of Figures and Illustrations

List of Abbreviations

AGR	Acid Gas Removal
BET	Brunauer-Emmett-Teller
BJH	Barrett-Joyner-Halenda
CaL	Calcium Looping
CE	Cement
CC	Carbon dioxide Capture Capacity
CCL	Carbon dioxide Capture Capacity Loss
CLC	Chemical Looping Combustion
EDS or EDX	Energy Dispersive X-Ray Spectrometry
EOR	Enhanced Oil Recovery
LECA	Laboratory for Environmental Catalytic Applications
MEA	Monoethanolamine
MFC	Mass Flow Controller
OC	Oxygen Capture Capacity
OCL	Oxygen Capture Capacity Loss
SEM	Scanning Electron Microscopy
SP	Set Point
SV	Solenoid Valve
TGA	Thermogravimetric Analysis or Analyzer
TT	Thermal Treatment
XRD	X-Ray Diffraction

Chapter One - Introduction

1.1 Overview

The constant increase of emissions of carbon dioxide (CO_2) and its concentration in the lower level of the atmosphere (troposphere) are problems that are being addressed currently. Carbon dioxide belongs to the group of gases known as greenhouse gases (GHG), in which are also included water vapour, methane, nitrous oxide, ozone and CFCs (chlorofluorocarbons)[1]. Although CO_2 is not the gas with the strongest greenhouse effect, it is largely the most emitted worldwide[2]. For instance, in 2011, according to the International Energy Agency, approximately 31.6 billion tonnes of CO_2 were emitted worldwide, which accounted for almost 80% of the total emissions of GHG[3]. That makes CO_2 the main GHG to be reduced.

In Canada, the emissions of CO_2 in 2010 accounted for 1.8% of the global emissions[4]. The main sources of CO_2 emissions in Canada are in the province of Alberta, where 48.5% of the reported emissions in Canada in 2011 were located. This province has an intensive oil and gas industry that was responsible for 46.4% of emissions in 2011, and also a number of coal-fired power plants that generated a large portion of the electricity for the province. The generation of the electricity involved 35.4% of the emissions of CO_2 in 2011[5]. Thus, the oil and gas industry and the energy supply, together, accounted for more than 80% of the emissions of CO_2 in the province of Alberta, which in turn was almost 40% of the total emissions in Canada.

From 2005 to 2012, the emissions of CO_2 in Canada were reduced by 5.1%[4], but the commitment for 2020 is to reduce the emissions by at least 17% below the levels of 2005. Therefore, further efforts to make possible such decline of the emissions are necessary. Some of the policies that have been implemented aim to reduce the emissions of CO_2 from coal-fired

power plants. For example, the *Reduction of Carbon Dioxide Emissions from Coal-Fired Generation of Electricity Regulation (SOR/2012-167)* report set 420 tonnes of CO_2/GWh as the limit for coal-fired electricity generation units. The purpose of this regulation is to force a shift to lower- or non-emitting units, such as those of natural gas, renewable energy, or fossil fuel-fired with carbon capture and storage (CCS)[6]. With regards to CCS, in the last years, the Government of Canada has invested approximately $3 billion in research and study of these technologies, resulting in Canada becoming a world leader in this area[7].

Carbon capture and storage technologies offer the possibility of avoiding the emission of CO_2 into the atmosphere by treating the flue gases of the industrial process. The CO_2 is separated from the other gases (mainly N_2), and is obtained in a pure stream (>98%)[8]. Once the CO_2 is prevented from being emitted, it is injected into the ground, for instance, in depleted oil and gas reservoirs. It is important to note that, in order to store the CO_2, first, it is necessary to separate it from the other gases because otherwise the energy and costs required to compress the mixture of gases would make the process infeasible[9].

Some of the CCS technologies, such as amine capture, have been implemented at commercial scale. For instance, in October 2014, SaskPower started to operate the Boundary Dam Integrated CCS plant, which was the first CCS plant in the world, and it is expected to capture approximately one million tonnes of CO_2 a year[10]. Another example is the case of the Shell's Scotford Upgrader, located near the city of Edmonton (Alberta), which has implemented the Quest Carbon Capture and Storage project. This project is expected to capture and store deep underground (~2300 m) more than one million tonnes of CO_2 per year[11]. This second example shows that not only coal-fired power plants, but also other industrial processes can benefit from CCS technologies.

However, there are several issues associated with the use of amine based compounds for CO_2 capture. First, it involves a high energy penalty (~9-12.5%), which decreases the efficiency, and consequently increases the price of the energy. Second, the cost of manufacturing the absorbent is high: monoethanolamine (MEA) costs $1,250 US/tonne [12,13]. Third, there are environmental and health risks related to the handling and disposal of large quantities of degradation products and waste solvent[14].

Thus, intensive research is focused on addressing these problems, and alternative solutions to the commercial processes are currently being developed. One of them is the calcium looping (CaL), which has arisen as one of the most promising technologies because it presents a number of advantages that are explained herein. This process is based on the use of lime (CaO) as sorbent, which is widely available and environmentally benign. Lime reacts with CO_2 to produce calcium carbonate ($CaCO_3$, see Eqn. 1-1), and then returns to its initial state when heated to high temperatures, releasing the CO_2 at the same time. Thus, 1) the CO_2 is obtained in a pure stream, and 2) the CaO can be recycled multiple times.

$$CaO + CO_2 \leftrightarrow CaCO_3 \qquad (1\text{-}1)$$

Additionally, the CaL process is carried out at high temperatures, which enables the possibility of recovering energy to drive a steam cycle. This, in turn, would result in a lower energy penalty of the process, minimizing the impact on the energy efficiency. Also, CaL involves the use of fluidized bed technology, which is a well-established technology, extensively applied in the industry. Furthermore, the materials used in CaL have a certain affinity to SO_2, which results in simultaneous desulphurisation of the flue gases[12]. On the other hand, the main drawback of CaL is the need to provide the energy required to carry out the decomposition of the

carbonate. Also, although the CaO can be recycled multiple times, the reactivity decreases significantly after a few cycles[15].

Another promising alternative is chemical looping combustion (CLC). This technology uses metal oxides, known as oxygen carriers, instead of air for the combustion of fuels. As Figure 1.1 shows, the oxygen carrier is put in contact with the fuel, and it provides the oxygen required for the combustion. As a consequence of the combustion, the metal oxide is reduced, but it can be regenerated by exposure to air. Hence, the oxygen carrier can be recycled multiple times.

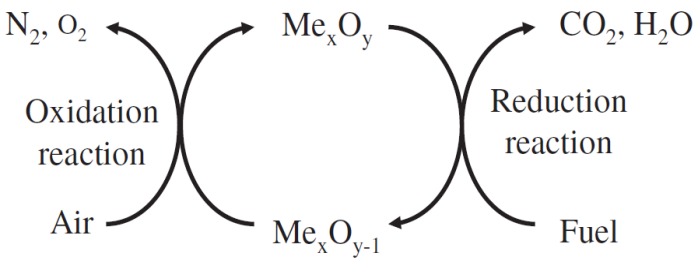

Figure 1.1. Schematic of chemical looping combustion for gaseous fuels[13]. (Reproduced with permission from the publisher, Elsevier. A copy of the permission is provided in Appendix A.1).

These technologies are just two examples of the multiple alternatives to the amine-based processes. A more thorough and detailed review of the current state-of-the-art is provided in Chapter Two. Nonetheless, CCS technologies are expected to play a significant role in the reduction of CO_2 emissions, not only in Canada, but globally. Its implementation can help to extend the lifetime of high-emitting coal-fired power plants that otherwise would need to terminate their activity. Also, other industrial processes, such as bitumen upgraders, can benefit from these technologies, and reduce their emissions.

1.2 Motivation and objectives

The work reported in this thesis was part of a collaborative project carried out between the University of Ottawa, the École Polytechnique de Montréal, CanmetENERGY-Ottawa, and the University of Calgary. The project involved the study of the performance of composite sorbent pellets developed by researchers at CanmetENERGY-Ottawa[14,16] with the purpose of combining the two alternative technologies mentioned in Section 1.1., i.e., calcium looping (CaL) and chemical looping combustion (CLC). The idea of providing the energy required for an endothermic reaction by means of chemical looping combustion was first proposed by Lyon and Cole[17], applied by Abanades et al.[18,19] for steam reforming, and even suggested by the same authors for CCS purposes. However, this idea was based on simulations - no experimental work had been done[20].

The developed pellets contained a mixture of CaO (adsorbent for CaL) and copper oxide (CuO), which was the oxygen carrier selected for the CLC process. In addition to these two compounds, calcium aluminate cement (CE) was included as part of the mixture with the purpose of acting as a binder and providing mechanical strength to the pellets[14,20].

Thus, a simplified diagram of the CaL-CLC process is depicted in Figure 1.2. Three reactors are required, namely 1) the carbonator, where the reaction of the adsorbent with CO_2 takes place, 2) the calciner, where the reduction of the metal oxide and subsequent decomposition of the carbonate occur, and 3) the air reactor, where the oxygen carrier is re-oxidized by exposure to air.

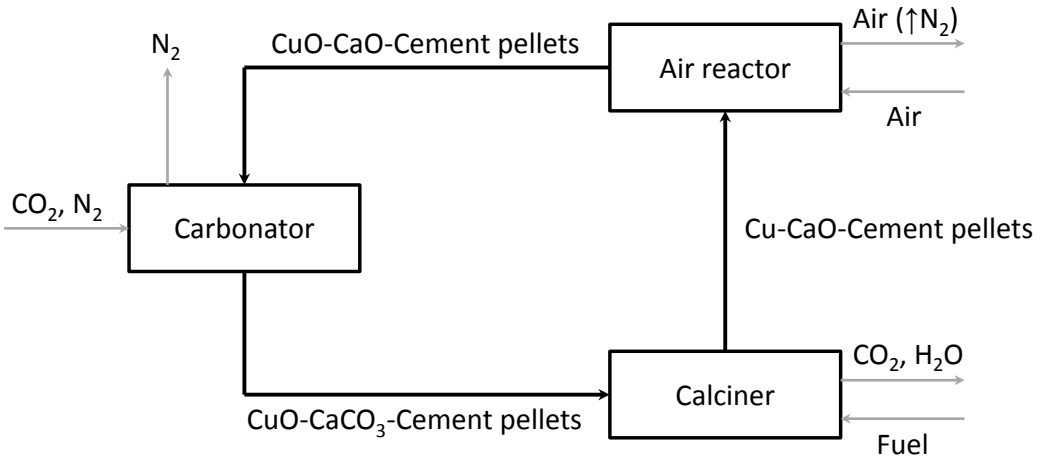

Figure 1.2. Schematic of the combined CaL-CLC process (black solid arrows represent flow of solids, while gray solid arrows represent flow of gases).

In addition to this configuration for the CaL-CLC process, a second configuration was proposed by collaborators at the University of Ottawa[21]. The second option was named dual loop configuration because instead of one global loop, there are two local loops, as illustrated in Figure 1.3.

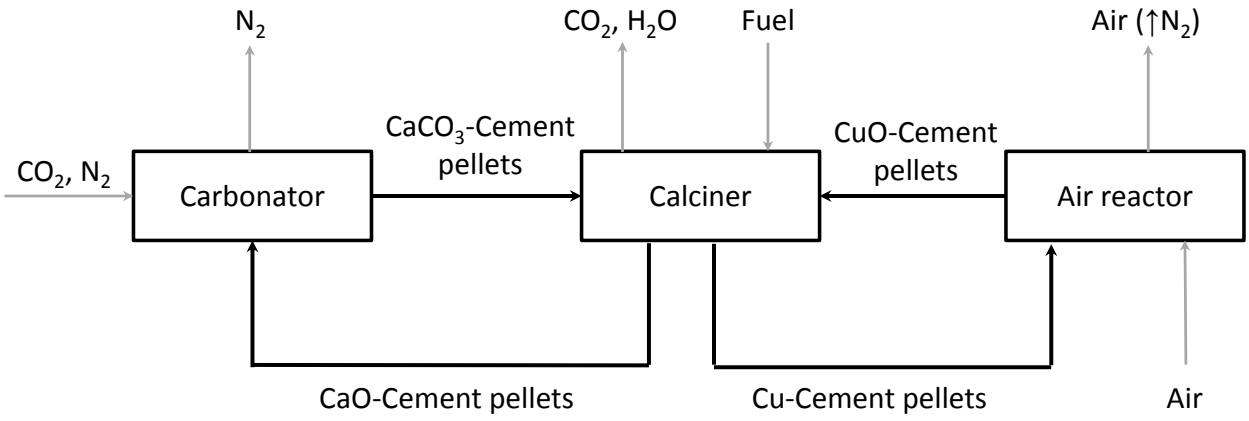

Figure 1.3. Schematic of the dual loop configuration of the CaL-CLC process (black solid arrows represent flow of solids, while gray solid arrows represent flow of gases).

For this configuration, instead of pellets in which CuO, CaO and cement are mixed, pellets with only CaO and cement, and pellets with only CuO and cement are used. In this case, the pellets containing CaO circulate between the carbonator and the calciner, while the pellets containing CuO circulate between the calciner and the air reactor. This configuration simplifies the manufacturing of the pellets, but it may involve separating the two different pellets that reach the calciner. In such case, it could be possible to accomplish the separation by controlling the gas velocity, taking into consideration the different densities and sizes of the pellets[21].

Therefore, based on the novelty of the pellets developed and the two configurations of reactors proposed, this thesis focuses on the study of the performance of the composite sorbent pellets and dual loop pellets. The specific objectives are:

1) Determine the capacity of the composite pellets to capture CO_2 over multiple carbonation/calcination/oxidation cycles, and the capacity of the dual loop pellets that contain CaO over multiple carbonation/calcination cycles.
2) Determine the capacity of the composite pellets to be re-oxidized over multiple carbonation/calcination/oxidation cycles, and the capacity of the dual loop pellets that contain CuO over multiple reduction/oxidation cycles.
3) Address the decay of the capacity of CaO to capture CO_2 over cycles.

1.3 Organization of the thesis

This thesis has been structured in seven chapters. Chapter Two provides a brief literature review on CCS technologies and their fundamentals, as well as information regarding the deactivation of CaO over cycles. Chapter Three explains the characterization techniques used on the pellets, the experimental methods followed for the study of the pellets, and preliminary

results. Chapter Four offers a heat transfer model for which mass transfer is taken into consideration by means of the shrinking core model. The heat transfer model estimated the temperature profiles within the pellets over time. Chapter Five provides the results of the performance of both composite and dual loop pellets. Chapter Six is focused on the enhancement of the capacity of pellets that contain CaO to capture CO_2 over cycles. Three different approaches were taken and the results are presented in this chapter. For one of the approaches, the experiments were performed at CanmetENERGY-Ottawa, and a brief description of the experimental methods used at those facilities is included in this chapter. Last, Chapter Seven presents the conclusions and recommendations for this thesis.

Chapter Two - Literature Review

2.1 Carbon Capture and Storage (CCS)

The Carbon Capture and Storage are a set of technologies developed to avoid CO_2 produced from the use of fossil fuels to generate electricity, and that of industrial processes, from being emitted into the atmosphere[22]. This thesis focuses on the carbon capture, and consequently in this review the technologies related to this process are covered. There are four main technologies, 1) pre-combustion or decarbonisation, 2) oxy-fuel combustion, 3) post-combustion and, 4) chemical looping combustion[15]. All of these technologies aim to obtain a stream of pure CO_2 (98%)[8] that can be later transported and stored in geological formations, or used in other processes such as Enhanced Oil Recovery (EOR), production of urea and methanol, food processing, preservation and packing, coffee decaffeination and production of beverages[23–25]. Among these four main technologies, post-combustion methods are the most appropriate for existing coal-fired plants because they can be retrofitted to the plant by adding the capture unit downstream of the process, without impacting the original structure of the plant[15,26].

2.1.1 Pre-combustion capture or fuel decarbonisation

This technology is based on the partial oxidation of a fuel, for instance, by gasification, to produce a mixture of hydrogen (H_2), carbon monoxide (CO) and CO_2. The mixture is treated to convert the CO into CO_2, which is usually accomplished by means of the water-gas shift reaction. Then, the remaining mixture, which contains mainly CO_2 and H_2, is treated to separate the CO_2 from the H_2[26,27]. Therefore, in this process, the CO_2 is captured prior to the combustion of the fuel. Figure 2.1 shows a simplified diagram of these steps. Ultimately, H_2 can be used in

many processes, but usually its application as a fuel is preferred, for instance in Integrated Gasification Combined Cycles (IGCC), in which H_2 is combusted in a gas turbine[26]. In addition, H_2 has applications in other processes, such as the upgrading of heavy crude oils [28], metallurgy industry, pharmaceutical industry and fuel cells[29].

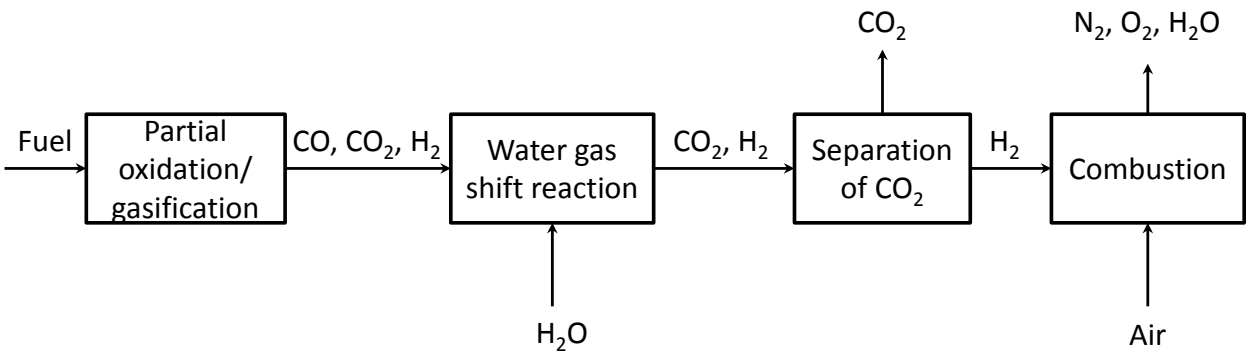

Figure 2.1. Schematic of the pre-combustion technology.

However, the pre-combustion technology presents several disadvantages. The separation of CO_2 and H_2 is usually performed by acid gas removal (AGR) processes, which involve energy penalties[30]. Additionally, the retrofit to existing coal-fired plants is not a viable option because considerable modifications to the structure of the plant would be necessary. Therefore, pre-combustion technologies would be more suitable for future plants, in which the capture of CO_2 can be included as part of the initial design of the plant. In this regard, its application is normally suggested to be done in connection with Integrated Gasification Combined Cycle (IGCC) power plants rather than coal-fired plants[26].

2.1.2 Oxy-fuel combustion capture

The principle of oxy-combustion capture is to avoid the separation of CO_2 and nitrogen by using oxygen of high purity (at least 95%)[31] instead of air, which prevents the CO_2 from being diluted in N_2. As depicted in Figure 2.2, the typically suggested configuration for a plant with oxy-fuel combustion technology involves the recirculation of part of the combustion gases to control the temperature within the burner[26,32]. The limitation in the temperature is based on the capability of the materials currently available to withstand high temperatures[31]. This configuration was first suggested in the early eighties with the purpose of producing large amounts of CO_2 for Enhanced Oil Recovery (EOR), and also reducing the environmental impacts from the use of fossil fuels in energy generation[12,13].

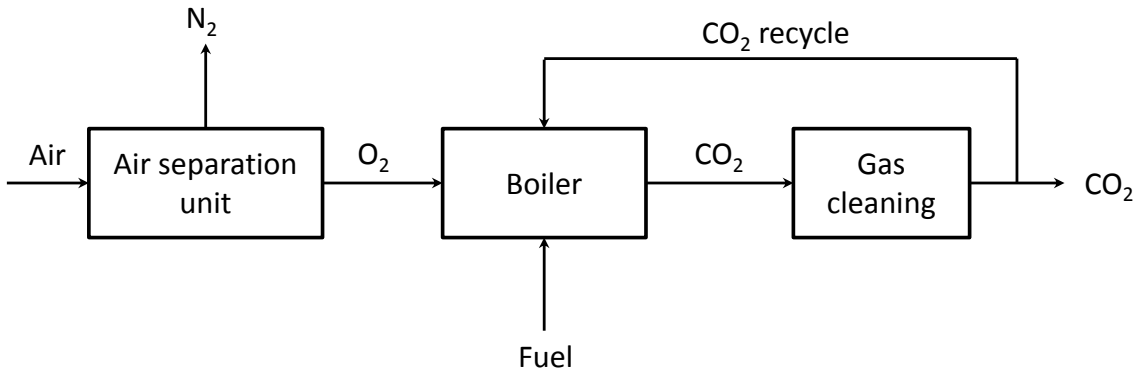

Figure 2.2. Conceptual diagram of the oxy-fuel combustion process.

This technology offers several advantages, and it is considered one of the most promising options for capturing CO_2 from coal-fired power plants. The CO_2 capture efficiency of this process can be very high, ranging from 90% to 95%[31,35]. The use of oxygen of high purity (>95%) reduces the formation of thermal NO_x to almost zero, which results in low overall-NO_x emissions[32,36]. The reduction of these pollutants ranges between 50% and 70%[11,12]. Note that,

even though the formation of thermal NO_x is prevented, these pollutants can still be formed due to the presence of nitrogen in the fuel. Additional reductions in the SO_2 emissions, as high as 90%, could be accomplished economically if limestone would be added to the process[36,37].

The main disadvantage of oxy-fuel combustion is the energy penalty and costs associated with the air separation unit needed to produce oxygen of high purity. Currently, at commercial scale, pure oxygen can be produced only by cryogenic distillation, which is expected to cause a penalty of 15-30% of the generated electricity, depending on the initial efficiency of the plant[26,32]. Additionally, retrofitting this technology to existing plants involves a number of changes in the configuration of the plant. Figure 2.3 shows a schematic of an existing coal-fired power plant in which the major modifications due to the implementation of oxy-fuel combustion have been depicted[26].

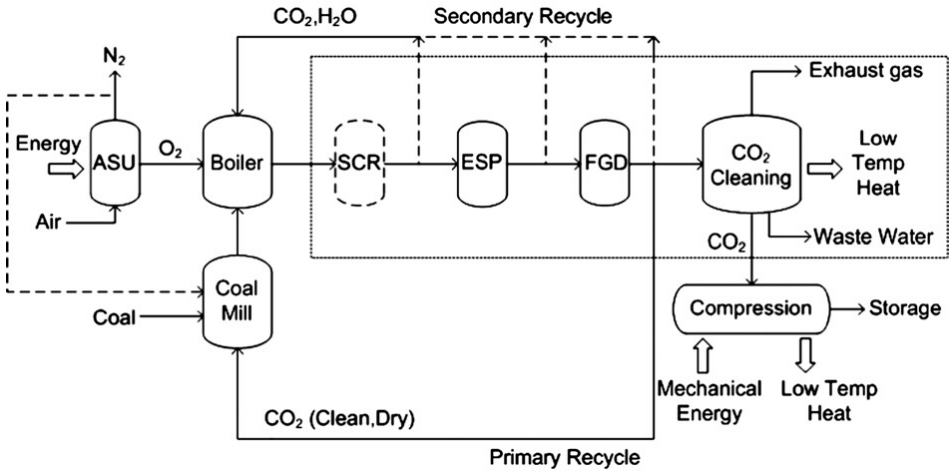

Figure 2.3. Configuration of a coal-fired power plant with implementation of oxy-fuel combustion technology. ASU - Air Separation Unit, SCR - Selective Catalytic Reduction reactor (deNO$_x$), ESP - Electrostatic Precipitators, FGD - Flue Gas Desulphurization[26]. (Reproduced with permission from the publisher, Elsevier. A copy of the copyright permission is provided in Appendix A.2).

Implementing the oxy-fuel combustion technology requires addition of an air separation unit upstream of the process, in order to provide the high purity oxygen, and final processing (cleaning) of the CO_2 downstream. The final processing involves removal of water and other non-condensable gases, such as O_2 and N_2 to meet the requirements regarding purity of the CO_2 stream, and the compression step prior to its transportation and storage.

2.1.3 Post-combustion capture

The post-combustion technology is based on the removal of CO_2 from the flue gases stream produced in a power plant. In these facilities, as air is used for the combustion, the fraction of CO_2 in the flue gases is low, normally between 13-15% for coal-fired power plants[38–40], and 7-8% for gas fired power plants[31]. To reduce the emissions of CO_2 in coal-fired power plants in the short and medium term, post-combustion technology is considered as the most suitable among the CCS technologies because its implementation does not involve modifications in the configuration of the plant[41].

Within the post-combustion technology, the main methods are solvent absorption, adsorption using solid sorbents and membrane separation[15,42]. Solvent absorption has been thoroughly studied, and it is the only method that has been deployed at industrial scale[8,10,43]. The most common solvent is monoethanolamine. Other compounds that are often considered as potential alternatives to monoethanolamine are 2-amino-2-methyl-1-propanol, secondary amines such as diethanolamine, and tertiary amines such as methyldiethanolamine[15,32,44,45]. The most important reactions between these compounds and CO_2 are, 1) formation of a carbamate (2-1), 2) reversion of the carbamate to bicarbonate (2-2), 3) formation of bicarbonate (2-3). These reactions are valid for primary and secondary amines, but for tertiary amines the mechanism is

rather different. Tertiary amines are considered to act as a base that catalyzes the hydration of CO_2 (2-4)[32].

$$CO_2 + 2R_1R_2NH \leftrightarrow [R_1R_2NCO_2^- + R_1R_2NH_2^+] \quad (2\text{-}1)$$

$$R_1R_2NCO_2^- + H_2O \leftrightarrow R_1R_2NH + HCO_3^- \quad (2\text{-}2)$$

$$CO_2 + OH^- \leftrightarrow HCO_3^- \quad (2\text{-}3)$$

$$CO_2 + H_2O + R_1R_2R_3N \leftrightarrow R_1R_2R_3NH^+ + HCO_3^- \quad (2\text{-}4)$$

Although these solvents are currently used at commercial scale (a diagram of the process is illustrated in Figure 2.4), there are a number of issues associated with them. These amines suffer from degradation in the presence of O_2, SO_2 and NO_x because of irreversible reactions between the amines and these pollutants[12,41,45,46]. In addition to the presence of pollutants, the temperature cannot be high because amines thermally degrade[47,48]. Also, the regeneration of the solvent (2-2) requires an energy input, which remains as one of the major drawbacks of the amine solvents[44]. Furthermore, environmental and health concerns are associated with the use and handling of the degradation products, such as nitroamines, which are carcinogenic, toxic and mutagenic compounds[15,45].

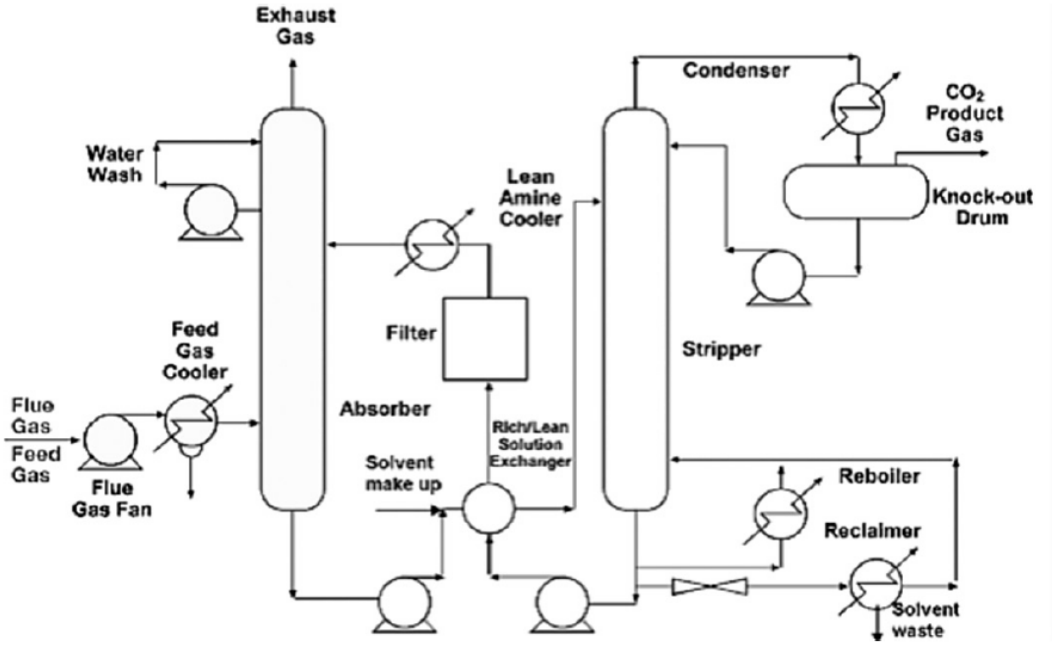

Figure 2.4. Post-combustion capture of CO_2 using amine solvent method[41]. (Reproduced with permission from the publisher, Elsevier. A copy of the copyright permission is provided in Appendix A.3).

The next main method of post-combustion capture uses solid sorbents. Although a number of solid sorbents were developed[49], only two main types of sorbents are considered, namely, amine-based and alkali metal-based sorbents. The amine based-sorbents have the advantage of requiring less energy for their regeneration than the liquid amine solvents. In contrast, the mechanical and thermal stability showed by the amine based-sorbents are poor[15]. As for the alkali based-sorbents, multiple compounds, such as magnesium oxide (MgO) and calcium oxide (CaO), have been studied[15,50]. These compounds can react with CO_2 to form the corresponding carbonate, and then be regenerated by heating the carbonate. For instance, at temperatures between 873 K and 923 K, the CaO reacts with CO_2 to form calcium carbonate

($CaCO_3$) (2-5). Then, the $CaCO_3$ is heated to 1173 – 1223 K to carry out the reverse reaction (2-6), which results in the regeneration of the sorbent and release of CO_2.

$$CaO_{(s)} + CO_{2(g)} \rightarrow CaCO_{3(s)} \quad (2\text{-}5)$$

$$CaCO_{3(s)} \rightarrow CaO_{(s)} + CO_{2(g)} \quad (2\text{-}6)$$

This cycle is normally referred to as calcium looping (CaL), in which the first reaction (2-5) is named carbonation and the second reaction (2-6) calcination. The carbonation is exothermic ($\Delta H_{r,298K}$ = -178 kJ/mol)[47], and it is characterized by an initial rapid rate followed by an abrupt transition to a slow reaction rate, i.e., initially kinetics is the controlling mechanism, but then diffusional limitations control the process[51,52]. This shift of reaction rate is because of the carbonate layer that is formed on the surface of the particles during the carbonation, which hinders the diffusion of the CO_2 molecules. The calcination is endothermic ($\Delta H_{r,298K}$ = +178 kJ/mol), and rapidly reaches completion under a wide range of conditions[47].

The use of CaO as a sorbent presents a number of advantages. The process is performed at high temperatures, which enables the recovery of heat to provide additional energy, to drive a steam cycle for example, and decrease the energy penalty of the process. In addition, the sorbent is widely available and inexpensive, and the waste materials resulting from the process have potential uses in other industrial processes, such as the cement industry[12].

There are, however, two main drawbacks related to the use of CaO as a sorbent, which are the energy input required to carry out the calcination reaction, and the decrease of the capacity to capture CO_2 over cycles. The energy input, as depicted in Figure 2.5, could be provided through the combustion of a fuel using oxygen of high purity, as in the oxy-fuel

combustion process, but that involves an energy penalty and the costs derived for the air separation unit.

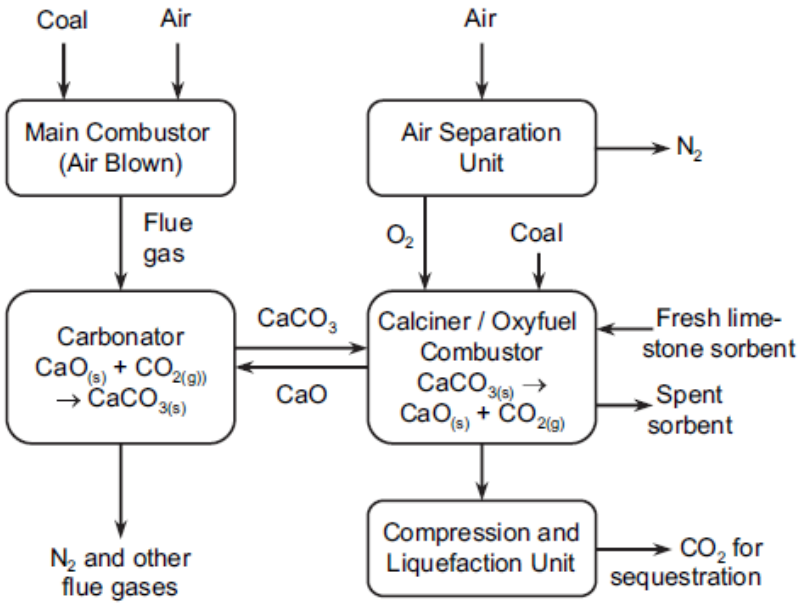

Figure 2.5. Diagram of a theoretical coal-fired process with implementation of calcium looping. (Reproduced with permission from the publisher, Elsevier. A copy of the copyright permission is provided in Appendix A.4).

For this thesis, the decay in capacity is defined as the reduction of the CO_2 uptake of the pellets after multiple cycles. This decay is likely due to sintering, which reduces the pore volume and available surface area of the CaO[14,47,53]. In this regard, multiple approaches have been taken in order to address this problem and minimize the effect of sintering. Ridha et al. modified CaO-based sorbents with formic acid, and after 20 cycles, the capacity was 67% higher[54]; Li et al. used acetic acid, achieving 50% of conversion of the modified CaO-based sorbents after 20 cycles, which was significantly higher than the 15% conversion of the original sorbent[55]. Other approaches have been oriented to the preparation process, or focused on doping the sorbent[56,57].

Although most of them have succeeded in enhancing the capacity of CaO sorbents over cycles, there is still scope for more improvement.

The final method is membrane separation. The use of selective membranes to separate components from flue gas streams is a relatively new concept[31]. Although there are different types of membranes (organic or inorganic, porous or non-porous) and mechanisms of separation (solution/diffusion, adsorption/diffusion, molecular sieve and ionic transport), for CO_2 capture, the membrane processes are narrowed to two types, namely, gas separation membrane, and gas absorption membrane. The first is based on the principle of preferential permeation, which takes advantages of the fact that one of the compounds present in a mixture of gases diffuses faster through the membrane, thus allowing its separation from the rest of compounds present in the mixture. On the other hand, the gas absorption membrane consists of a micro porous solid membrane used as contacting device between the gas and a solvent. The gas flows on one side of the membrane while the solvent flows on the other side. The solid membrane absorbs the CO_2 from the gas providing a sink from which the solvent then can absorb the CO_2.

Some of the disadvantages of the membrane separation process are the low efficiency with streams with low fractions of CO_2 (below 20%). Also, the membranes are highly sensitive to contaminants, such as sulfur compounds[31]. This method could be considered as a complement to other technologies, to refine the final stream to high levels of purity.

2.1.4 Chemical Looping Combustion

The chemical looping combustion (CLC) technology is based on the use of metal oxides that act as oxygen carriers, which transfer the oxygen from the air to the fuel, thus avoiding the direct contact between them[58]. As a result, inherent separation of CO_2 is achieved, which in turn

avoids the energy penalties inherent with other technologies[59]. Once the combustion reaction (2-7) is completed, the oxygen carrier is regenerated by exposure to air (2-8).

$$C_nH_{2m} + (2n+m)Me_xO_y \leftrightarrow nCO_2 + mH_2O + (2n+m)Me_xO_{y-1} \quad (2\text{-}7)$$

$$O_2 + 2Me_xO_{y-1} \leftrightarrow 2Me_xO_y \quad (2\text{-}8)$$

Consequently, the stream obtained after the combustion of the fuel contains mainly CO_2 and steam. The latter can be separated by condensation, thus obtaining a stream of pure CO_2, which can be subsequently compressed and transported for storage[60]. This process is depicted in Figure 2.6. Additionally, the use of oxygen carriers enables the reduction of the emissions of NO_x[31,61].

The CLC technology can be applied to both gas fuels, such as natural gas, and solid fuels, such as coal and biomass. For gas fuels the combustion is carried out by direct contact between the oxygen carrier and the fuel. On the other hand, for solid fuels there are several options considered. For instance, one of the possibilities is to gasify the fuel prior to its combustion[60]. This option is known as syngas-CLC process. Other options are the in-situ gasification CLC (iG-CLC), and chemical looping with oxygen uncoupling (CLOU). In the iG-CLC, the fuel is gasified in the fuel reactor, where the gasification products react with the oxygen provided by the metal oxides[13]. In the CLOU process, the oxygen carrier has the property of releasing gaseous oxygen, which avoids the need of gasifying the fuel[62].

In addition to combustion processes, oxygen carriers are also used in the production of H_2 and some of the processes are steam reforming integrated with chemical looping combustion and

auto-thermal chemical looping reforming. These processes are not considered for discussion in this thesis, and more information can be found elsewhere[13,63]

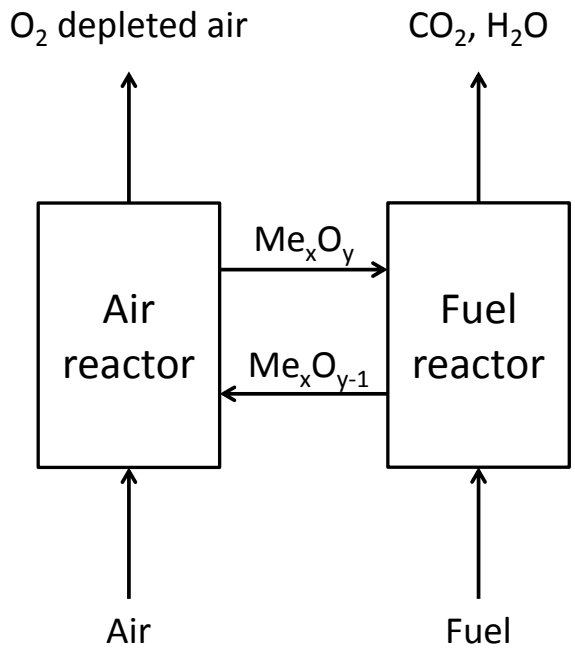

Figure 2.6. Concept of chemical looping combustion process.

The metal oxides for CLC have been extensively studied, with more than 700 compounds tested. Although some minerals, such as iron ore, ilmenite and manganese ore have been tried, most of the oxygen carriers are synthetic materials in which an active metal oxide is supported on an inert material, such as Al_2O_3, SiO_2, TiO_2, ZrO_2 or $MgAl_2O_4$. Some of the metal oxides used as oxygen carriers are NiO, CuO, Fe_2O_3, Mn_3O_4 and $CaSO_4$[13,58,64–66].

2.2 Chapter summary

In this chapter, a general overview of the CCS technologies has been provided. The pre-combustion technology is normally associated with IGCC plants because of the inherent

formation of syngas. However, the implementation of this technology to existing coal-fired power plants is not feasible because it involves multiple modifications in the configuration of the plant. The oxy-fuel combustion is one of the most promising technologies, but it involves important energy penalties associated with the air separation unit needed to produce oxygen of high purity (>95%). Likewise, this technology is not the most suitable for existing coal-fired power plants because of the impact that it would have in the configuration of the plant. Post-combustion is currently the only technology that has been deployed at commercial scale. However, the industrial processes are based on the use of amine based-solvents, which have a number of drawbacks, such as degradation in the presence of oxygen, SO_2 and NO_x, environmental and health concerns, and energy penalty derived from the regeneration of the solvent. Therefore, alternative technologies have been developed to replace the amine-based processes. In this regards, calcium looping arises as one of the most promising alternatives. Last, chemical looping combustion has an important advantage with respect to the rest of the technologies, which is the inherent CO_2 separation due to the use of oxygen carriers that avoid the need of using air. Furthermore, the absence of air during the combustion of the fuel results in lower NO_x emissions. Also, the regeneration of the oxygen carriers requires less energy than the regeneration of absorbents or adsorbents used in other processes.

Chapter Three - Experimental Methods

The preparation of the pellets studied in this thesis was performed by a former collaborator in the project at the facilities of Canmet in Ottawa, Ryad Rahman. Therefore, it is important to remark that the preparation of the pellets was not part of this thesis. The procedure to make the pellets is described elsewhere[14]. The pellets received were first characterized and studied without performing any sort of treatment on them. The characterization of pellets involved different techniques, namely N_2 adsorption analysis to determine the surface area and pore volume distribution, scanning electron microscopy (SEM), energy dispersive X-ray spectrometry (EDX or EDS), X-Ray diffraction (XRD) and thermogravimetric analysis (TGA). Afterwards, some compositions of pellets were treated by different methods with the purpose of enhancing their stability and capacity to capture CO_2 over multiple calcium looping and chemical looping combustion cycles.

In this chapter, the properties of the raw pellets, treatments applied to enhance their capacity to capture CO_2, and techniques to characterize them and study their performance are presented.

3.1 Raw pellets

The pellets received from Canmet had different sizes, configurations and compositions. The first batch of pellets ranged from 0.425 – 1.425 mm, and they had two different configurations, heterogeneous, or core-in-shell, and homogeneous[14,20]. The heterogeneous configuration consisted of two different parts, the inner part or core, which contained a mixture of CuO and CaO, and the outer part or shell, which contained a mixture of cement (CE) and

CaO. The homogeneous configuration was simply the mixture of the three compounds, without the core-in-shell structure. Schemes for both configurations are illustrated in Figure 3-1.

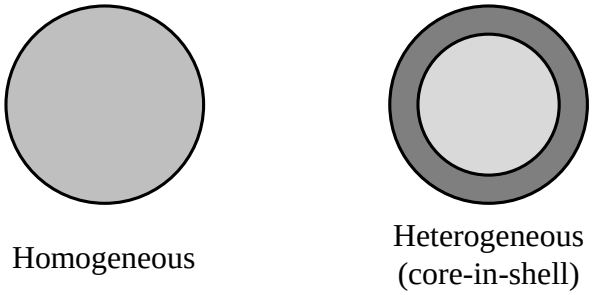

Figure 3.1. Schematic of configurations of pellets prepared at CanmetENERGY.

As for the compositions, in total three compositions were studied and the nomenclature used to name them is explained with one example. One of the compositions contained 50% CuO, 40% CaO and 10% CE (wt%), and it is referred to as 50/40/10. Therefore, the composition is named so that the first number refers to the wt% of CuO, the second number to the wt% of CaO and the third number to the wt% of CE. Also, some compositions of pellets only contained two compounds, and in those cases only two numbers are provided. The compositions studied are summarized in Table 3.1.

Table 3.1. Summary of configurations, sizes and compositions of pellets.

Configuration	Size (mm)	Composition (wt%)	Name
Heterogeneous (core-in-shell)	0.425 – 1.425	50% CuO 40% CaO 10% CE	CS-50/40/10
Homogeneous	0.425 – 1.425	50% CuO 40% CaO 10% CE	50/40/10(L)[a]
	0.250 – 0.600	50% CuO 40% CaO 10% CE	50/40/10
		50% CuO 50% CE	50/50
		90% CaO 10% CE	90/10

[a]L=large homogeneous pellets. There are two sizes of 50/40/10 homogeneous pellets.

3.2 Pre-treated samples

One of the goals of this thesis was to achieve a better stability in terms of maintaining CO_2 capacity over multiple cycles. The loss of capacity was defined as the reduction of the CO_2 uptake of the pellets after multiple cycles. As it will be discussed in subsequent sections, the capacity of the pellets to capture CO_2 decreases dramatically after a few cycles, and most likely the cause for this decay is sintering of CaO, which decreases the surface area and consequently the number of active sites to react with the CO_2 molecules. This effect has been widely studied, and there are a number of publications that cover this issue[53,67]. To address this problem, two

different pre-treatments were applied, namely a thermal pre-treatment and impregnation with potassium, which are explained next.

3.2.1 Thermally treated pellets

The first approach consisted of subjecting the 90/10 pellets to a thermal pre-treatment to give the CaO a certain structure with more thermal stability. This treatment was only performed on this type of pellets because it was the most suitable to study the effect of sintering. The treatment involved heating the pellets up to 1173 K under N_2 (Praxair, 99.999%) atmosphere (50 ml/min) with a heating rate of 1.5 K/min, which was 10 times smaller than the heating rate for the calcium looping experiments (15 K/min). Once 1173 K was reached, it was kept constant for 2 h. The idea was to heat the pellets up to a temperature similar to the maximum temperature used in the actual process, but using a much slower heating rate, so that the CaO could develop a more stable to sintering structure. The hypothesis was that when the heating rate was fast, the CaO did not have time to develop a stable structure and, consequently, it became less resistant to sintering. In terms of thermal stability, this same idea is common in glass production, where, in order to achieve a resistant and strong glass, the mixture is slowly cooled once it comes out of the furnace (annealing)[68]. Otherwise, the glass obtained is fragile and little resistant to sudden temperature changes.

Additionally, the same treatment was performed under air (50 ml/min) in order to test the influence of the gas used. Air is cheaper and more available than N_2. The presence of oxygen was taken into consideration, and based on experiments performed on pellets with CaO present, it was expected to have no negative effect. Moreover, it was believed that because of the high

temperature reached during the treatment, it could enhance the removal of impurities present on the pellets.

In addition to the aforementioned thermal treatments, a third treatment was tried. In this case, N_2 was the carrier gas, but the heating rate was increased to 7.5 K/min. The final temperature was also 1173 K and the pellets were kept at that temperature for 2 h as well.

For these samples, the nomenclature will be TT1.5N-90/10 for those thermally treated (TT) under N_2 using the 1.5 K/min ramp, TT1.5A-90/10 for those treated under air and with a heating rate of 1.5 K/min and TT7.5N-90/10 for those treated under N_2 and using 7.5 K/min as the heating rate.

3.2.2 Impregnation of pellets with potassium hydroxide

The impregnation of the pellets with potassium hydroxide was taken as a second approach to improve the performance of the pellets. As with the thermal treatment, this approach was performed exclusively with the 90/10 pellets. The hypothesis in this case was based on obtaining a highly mobile form of potassium in the pellets and test whether the high mobility of this species, previously reported by other authors[69] could prevent some pores from closing. Consequently, the activity to capture CO_2 could remain high for more cycles. In addition, different potassium-based compounds have been applied for CO_2 capture[70–72]. Thus, by adding potassium hydroxide, there was the possibility of increasing the capacity to capture CO_2. Also, other types of sorbents, such as carbon-based sorbents, have been treated with KOH to enhance their capacity[73].

Two different cases were tested; for the first case an addition of 20% of K (wt%) with regards to the amount of CaO, taking KOH as the precursor of K, was performed. In the second

case, the amount of potassium was reduced to 5%. The impregnation method was chosen based on several references[74,75]. The most common method used for CaO compounds was wet impregnation; the required amount of KOH was dissolved in 50 ml of deionized water and then, the pellets were added to the solution. An example of the calculations performed to obtain the amount of KOH is included in Appendix B.1.

Next, the solution with pellets was left in the rotary evaporator, at a temperature of 343 K, under vacuum, and at a speed between 7 – 12 rpm. Figure 3.2 depicts this system. The rotation was stopped once the solution was completely evaporated, which took approximately 90 min. The vacuum and heating were kept for 3 h more to ensure a good level of drying before removing the sample from the rotary evaporator. Then, the pellets were left drying at 393 K for 24 h and, last, they were subjected to the slow thermal treatment (1.5 K/min until 1173 K and kept for 2 h) under N_2 atmosphere. For these samples, the naming will be 20K-90/10 (20% of K) and 5K-90/10 (5% of K). The naming does not make reference to the thermal treatment since the treatment was the same.

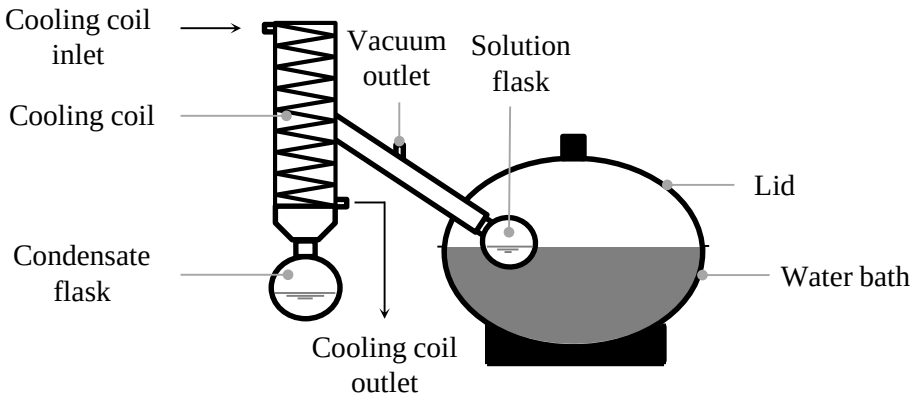

Figure 3.2. Schematic of rotary evaporator system.

3.3 Workflow of samples

The workflow depicted in Figure 3.3 provides a summary of the samples studied as well as the treatments performed to enhance the capacity of the pellets to capture CO_2.

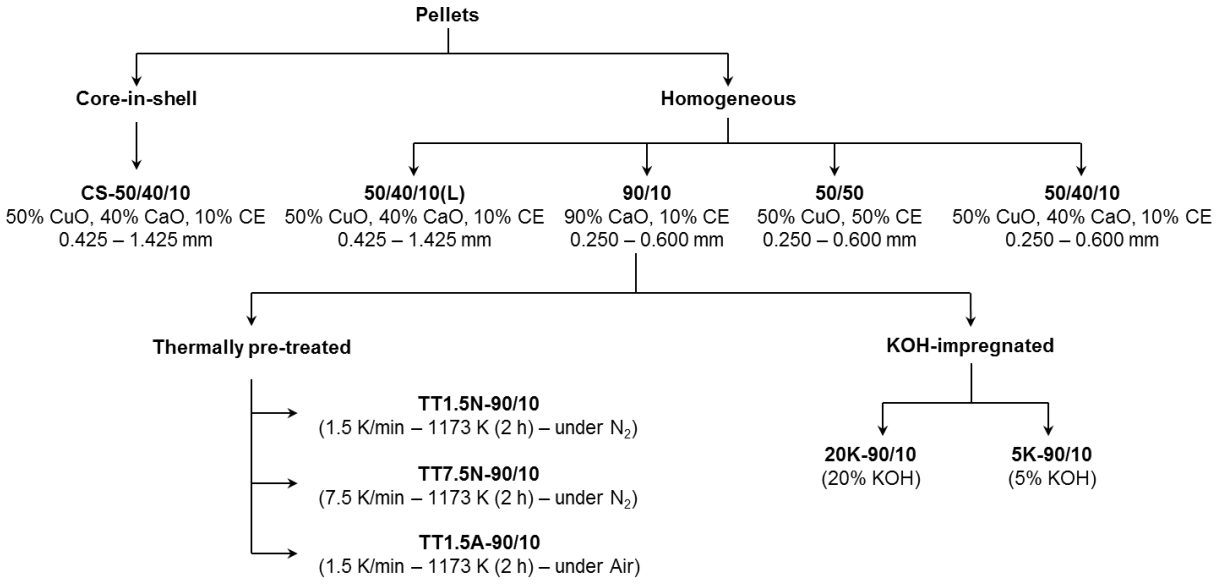

Figure 3.3. Summary of the pellets tested and modified.

3.4 Characterization Methods

3.4.1 N_2 adsorption

The surface area and pore volume distribution of some compositions of pellets were determined by N_2 adsorption in the Micromeritics Tristar 3000 instrument. The physisorption analysis was carried out at 77 K, which is the boiling temperature for N_2. Prior to the analysis, the samples were degassed in a separate unit to remove any adsorbed species (e.g. moisture). The degassing procedure involved heating the samples up to 573 K, under vacuum, and to keep them in those conditions for three hours. Although different conditions were reported in the literature, for instance 18 h at 473 K[76], the limited availability of the Tristar instrument required to use

different conditions. In addition, these conditions were compared to the conditions used for other samples, such as petroleum coke or activated carbon, which because of their nature were more likely to have more adsorbed species. For those samples, the outgassing normally did not take longer than four or five hours, and the temperature for outgassing was lower[77]. In this regard, the temperature used for the outgassing of pellets was chosen so that it did not affect any of the compounds present in the pellets.

Also, for outgassing it is required that the pressure be at most 100 – 120 mmHg at the end of the treatment to consider the sample properly degassed. For the samples that were analyzed, that range of pressure was achieved, which supported the use of the established conditions for degassing. The limit of the pump is approximately 100 mmHg, and that is the reason to establish the aforementioned range. However, sometimes it can be difficult to remove all the moisture because of the temperature that would be required, which could involve the decomposition of the sample or loss of its structure, or it could be that the equipment cannot reach that temperature. Therefore, it is important to know the sample and its properties thoroughly to find the balance to achieve the best conditions for outgassing.

Another important parameter is the mass of sample, which can vary depending on the surface area that could be expected. The lower limit of detection for the Tristar is approximately 10 m^2/g, which means that the amount of sample for the analysis must provide at least that surface area in order to obtain valid results[78]. For instance, for a sample with a high surface area, such as 1000 m^2/g, it would be necessary to put at least 0.01 g (10 mg). The samples that were analyzed in this work had small surface areas, requiring larger sample masses. Initially, the surface area of the pellets was unknown and preliminary experiments were performed in order to

estimate the mass that was required to obtain valid results. The minimum mass to ensure sufficient surface area was set at 1 g.

For the definitive analyses, three samples of each composition of pellets were examined in the Tristar to obtain an average of each parameter, and perform the study of errors. In this study, the confidence interval was calculated by means of Eqn. 3-1:

$$\mu = \bar{x} \pm z\frac{s}{\sqrt{n}} \tag{3-1}$$

where $\bar{x}$ is the mean, z is the statistical value corresponding to a level of confidence of 95% for three runs in a standard normal distribution (Appendix B.2), s is the sample standard deviation, and n is the number of runs, which was three.

Prior to performing the degassing and physisorption analysis, every sample had to be weighed. Determining the dry mass of sample is critical in this analysis, and because of that, a number of measurements were necessary to obtain an accurate value. The following masses were measured using the Mettler Toledo scale:

1. Mass of empty cell, [C]
2. Mass of cell + sample before degassing, [CS]
3. Mass of cell + sample before degassing + quartz wool, [CSW]
4. Mass of cell + sample after analysis + quartz wool, [CSWA]

The dry mass of sample [D] placed in the Tristar was calculated using Eqn. 3-2. In Appendix B.3 it is shown how this equation was developed.

$$[D] = [CSWA] - [CSW] + [CS] - [C] \tag{3-2}$$

After weighing and degassing, it was possible to place the samples in the Tristar to perform N_2 adsorption. For this analysis, a 2.5 L Dewar flask was filled with liquid nitrogen, and the flask was positioned in the Tristar stand. The test parameters were entered into the Tristar software interface. Once the experiment was initiated, the air inside the cells was evacuated via a vacuum pump to reduce the pressure down to 0.01 mmHg and held for a leak test. This test evaluated if the cells were well sealed, which is vital for the analysis. If the test showed that the leak rate was less than the target value (0.01 mmHg per 2 s), the Dewar flask was then raised to immerse the cells into the liquid nitrogen. The N_2 adsorption isotherms were measured, on average, at 86 different relative partial pressures (p/p_0) between 0.01 and 0.99. The reported values of total surface area, and total pore volume were determined from N_2 adsorption. The analysis of micropores using CO_2 adsorption at 273 K was ruled out because of the low values of surface area and pore volume that were obtained, which are shown and discussed in Chapter Five. The pore size distribution was plotted using the data obtained from the Barret-Joyner-Halenda (BJH) method. This method assumes 1) pores have cylindrical shape, 2) the amount of adsorbate in equilibrium with the gas phase is retained by the adsorbent by physical adsorption on the pore walls and capillary condensation in the inner capillary volume, and 3) the radius of the pore is the sum of the thickness of the gas layer and the radius calculated from the classical Kelvin equation, Eqn. (3-3);

$$\log\left(\frac{p}{p_0}\right) = -\frac{2\sigma V}{RTr_k} = -\frac{4.14}{r_k} \qquad (3\text{-}3)$$

where p is the vapor pressure, p_0 is the saturated vapor pressure , σ is the surface tension of liquid N_2, V is the molar volume of liquid N_2, R is the gas constant, T the absolute temperature and r_k the pore radius.

The Brunauer-Emmett-Teller (BET) model was used as a standard method to evaluate surface area from gas adsorption. The BET linearized equation is defined as the following[78]:

$$\frac{p}{v[p_0 - p]} = \frac{1}{v_m c} + \frac{c-1}{v_m c}\left(\frac{p}{p_0}\right) \quad (3\text{-}4)$$

where v is the volume adsorbed, v_m the monolayer volume, p is the adsorbate equilibrium pressure, p_0 is the saturation pressure of the adsorbate, and c is the BET constant. The main assumptions for the BET model are as follows: 1) the heat of adsorption of the successive layers (except for the first layer) is equivalent to the heat of condensation of gas molecules on the adsorbent, 2) energetically homogeneous surface, 3) no lateral interaction between the infinite number of adsorbed layers of molecules, and 4) constant quantity of gas molecules in each adsorption layer.

The linear range of the isotherm varied for some samples, which was usually apparent by a negative constant c. This issue could be addressed by removing the last points (two or three) of the isotherm, which resulted in the constant c having a positive number (essential requirement).

The total pore volume V_{total} of each sample was determined at a relative pressure p/p_0 = 0.98, under the assumption that the volume of vapour adsorbed condenses within the walls of the pores. The molar quantity of vapour adsorbed at p/p_0 = 0.98 was converted to liquid volume by Eqn. 3-5:

$$V_{total} = \frac{Q_{molar} MW_{N2}}{\rho_L} \quad (3\text{-}5)$$

where, Q_{molar} is the molar quantity of vapour adsorbed at p/p_0 = 0.98, MW_{N2} is the molecular weight of N_2 molecules (28 mg/mmol), and ρ_L is the density of liquid nitrogen (808 mg/cm^3).

3.4.2 Scanning electron microscopy (SEM)

SEM analysis was performed using an environmental SEM (Philips XL-30 ESEM, located at the Microscopy and Imaging Facility at the Health Science Center, University of Calgary) with the assistance of Dr. Michael Schoel (Research Associate, Department of Cell Biology & Anatomy). SEM is a technique to characterize the morphology of a solid surface. During SEM, the sample is impacted with a beam of focused electrons (energies up to 40 keV) that scans along a pattern of parallel lines, resulting in the generation of various signals consisting of mainly secondary electrons (>50 eV), high energy backscattered electrons and characteristic X-rays. These signals are collected to form images. The low-energy secondary electrons are used to generate the topography of the sample. The backscattered electrons are used to differentiate various elements on the surface of the sample based on their atomic numbers. Higher atomic number elements will emit a higher number of backscattered electrons thus appearing brighter than elements with lower atomic number.

Prior to analyzing the sample in the SEM, the samples were mounted on standard SEM stages and then coated with a layer of ~2 nm of a mixture of gold and palladium (60:40) to prevent electrostatic charges that may affect the image quality. The coating was performed at very low pressure, 30 mmHg, to avoid as much as possible any interference with particles and molecules present in the ambient environment. The micrographs in this thesis were obtained at magnification ranges of 50X to 30,000X with an electron beam of 20 kV.

3.4.3 Energy dispersion X-ray spectrometry (EDS)

Electron dispersive X-ray spectrometry (EDX or EDS) is an additional analytical technique available on the SEM equipment and used for elemental composition analysis of a

sample based on the emitted X-ray signal from the electron-surface interaction. The core-in-shell pellets were analyzed using this technique to determine whether the two layers, core and shell, were distinct or mixed. By comparing the atomic compositions of the inner and outer parts of the pellets, it could be inferred if the ratio of elements corresponded to the theoretical mass ratio of CuO and CaO. In this regard, it is important to mention that the information drawn from the EDS analysis was always considered complementary to the images obtained from the SEM analysis. In the SEM images the differentiation of the two layers could be complicated and thus, the EDS analysis could provide valuable information to determine if the core-in-shell structure was well formed or not.

3.4.4 X-Ray Diffraction (XRD)

XRD analysis was performed to determine the compounds present in the pellets and the mass fraction of each compound. XRD powder patterns were obtained using a Rigaku Ultima IV X-ray diffraction system at 40 kV tube voltage and 20 mA tube current with a scan rate of 2°/min over 5° to 80° 2θ. The analyses were performed by Valerie Omatsu-Baas, analytical chemist at CanmetENERGY-Ottawa.

Generally, in an XRD measurement, the sample is mounted on a goniometer and irradiated with a monochromatic beam of X-rays at an angle, θ, at which the beam is partially scattered by the first and subsequent layer of atoms. The collective intensity of the X-rays scattering from regularly spaced spots of a crystal is known as X-ray diffraction and can be captured by an X-ray detector and recorded as a function of angle. The intensity of X-rays diffracted from a crystal depends on the constructive and destructive interference among the scattered beams. The diffracted X-ray is detectable only if Bragg's Law is satisfied:

$$n\lambda = 2d\ sin\theta \quad (3\text{-}6)$$

where n is the order of reflection, λ is the wavelength of the incident beam, and d is the interplanar distance of the crystal[79]. The quantification of the compounds present in the samples analyzed was performed using the Rietveld method.

In this thesis, the pellets analyzed by XRD contained 90% CaO and 10% cement. The purpose of the XRD analysis was to determine whether compounds, such as mayenite, are formed when the pellets are subjected to high temperatures and/or multiple cycles of calcium looping. The formation of such compounds may have some influence in the capacity to capture CO_2.

3.5 Thermogravimetric Analysis (TGA)

This section, in addition to presenting information about thermogravimetric analysis (TGA), includes two more subsections (3.4.2 and 3.4.3) that show certain modifications that were needed on the TGA setup.

3.5.1 Experimental conditions

The calcium looping and/or chemical looping combustion experiments were conducted in a TGA instrument (Cahn Thermax 500, Thermo Scientific). This instrument enables high-sensitive measurements of mass change in real time; on the order of 0.1 μg for small samples and 1 μg for large samples (up to 100 g of sample). The user can set the frequency to collect the mass changes, otherwise the software establishes the frequency as one second by default. Also, the TGA has the capability of reaching temperatures as high as 1373 K, although it is recommended to operate below that limit. The operational limit was set at 1273 K. In addition, this model

allows the user to work at high pressures, up to 100 bar. As per the flowrates of gases, this instrument allows a maximum flowrate of 400 ml/min and minimum of 100 ml/min, per gas[80].

For this thesis, the amount of sample typically ranged from 25 – 30 mg, and the flowrates were set to 300 ml/min, except for the purge gas, which was set to 330 ml/min. This exception is explained in further detail in the subsequent section (Section 3.4.2). The gases used were a mixture of 20% CO_2, balance N_2 (Praxair), for carbonation, methane (Praxair, 99.97%) for calcination/reduction and air (Praxair) for oxidation. The temperatures were different depending on the step to be performed, and they were modified throughout the research process based on calculations and energy balances performed by our collaborators at CanmetENERGY – Ottawa and University of Ottawa[21].

Initially, the conditions for calcium looping were chosen based on the literature; the temperature for carbonation was 873 K, while the temperature for calcination was 1073 K. The same temperatures were used for the chemical looping combustion; 873 K for oxidation and 1073 K for reduction[14,20]. The heating rate was 15 K/min and the cooling rate was 10 K/min.

The operation temperatures were changed afterwards based on energy balances performed by our collaborators at the University of Ottawa, and also due to partial pressure limitations[21,47]. For the carbonation, the temperature was set to 923 K, and for the calcination/reduction the temperature was fixed based on a range of temperatures given, namely 1140 K to 1187 K, with the final value set to 1148 K. In this case, the reason that supported the change of temperature was the partial pressure of CO_2; in the actual process, part of the stream of pure CO_2 would be recirculated to the calciner as fluidization gas, thus increasing the concentration of CO_2 and requiring a higher temperature to overcome the equilibrium concentration (Le Chatelieur's principle). At 1073 K, the equilibrium partial pressure of CO_2 is

~0.22 atm, while at 1148 K is ~0.70 atm (see Appendix B.4 for calculations), which proves the benefit of working at a higher temperature. Regarding the temperature for the oxidation, it was determined by the energy balance[21] that this temperature should be between 10 and 50 degrees higher than the calcination/reduction temperature. According to this condition, the temperature for the oxidation was set to 1173 K, which was 25 degrees higher than the temperature for calcination/reduction.

Thus, summarizing, the carbonation temperature was changed from 873 K to 923 K, the calcination/reduction temperature from 1073 K to 1148 K and the oxidation temperature from 873 K to 1173 K. The composition of gases and flowrates remained unchanged, i.e., 20% CO_2 balance nitrogen for carbonation, 99.97% CH_4 for calcination/reduction, air for oxidation, and 300 ml/min as the flowrates.

3.5.2 Thermogravimetric Analysis (TGA) Apparatus – Initial setup

The Thermogravimetric Analysis instrument (TGA) was used to study the performance of the pellets developed for this project. The initial configuration for this instrument is depicted in Figure 3.4. The cylinders used for this instrument are directly connected to the control box by means of flexible hoses. Through each connection the gases are sent to the mass flow controller (MFC), which allows selection of the flowrate for each gas. Afterwards, the gases leave the control box and they are sent to the high-pressure reactor and high-sensitivity balance of the TGA. The high-pressure reactor and balance are located on the right part of Figure 3.4. The balance is at the top of the instrument and supported by three legs.

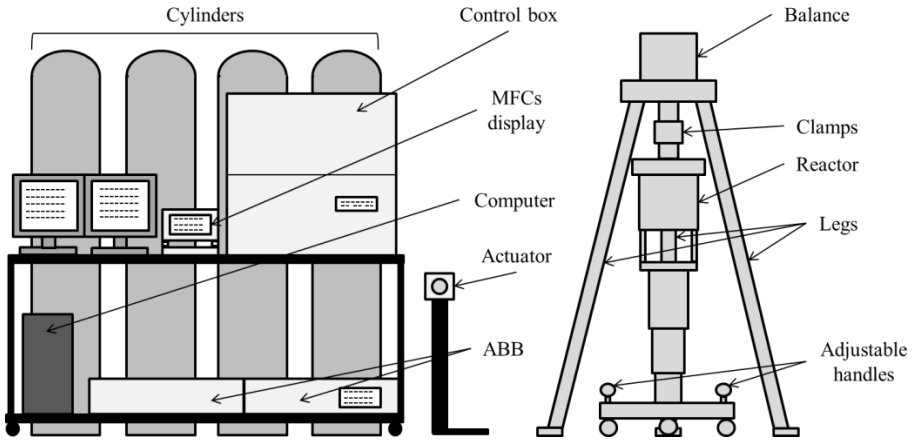

Figure 3.4. Thermogravimetric analysis apparatus setup.

From the balance hangs a wire on which the crucible that contains the sample to be studied is placed. The crucible is made of quartz, and non-porous, which forces the gas to flow around it. Figure 3.5 shows a schematic of the crucible and the way that the gases must follow in order to reach the sample.

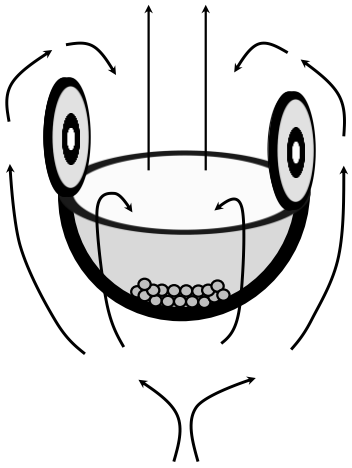

Figure 3.5. Crucible with sample, and flow of gas around it.

The reactor is located below the balance and it has a mechanism that enables it to move upwards and downwards. Also, the reactor has three adjustable handles to regulate the height and slant of the reactor so that it matches with the lower part of the balance. This adjustment is crucial since it is important that the hanging-wire and the baffle that surrounds it enter the reactor smoothly, avoiding as much as possible any contact between the baffle and the reactor. Also, it is essential that the lower part of the balance and the reactor get close enough to join them with the clamps, but not too close because then the reactor can bump the balance, which may cause damage to both the balance and the reactor. Figure 3.6 is a schematic of the system from inside when both parts are joined and closed by the clamps.

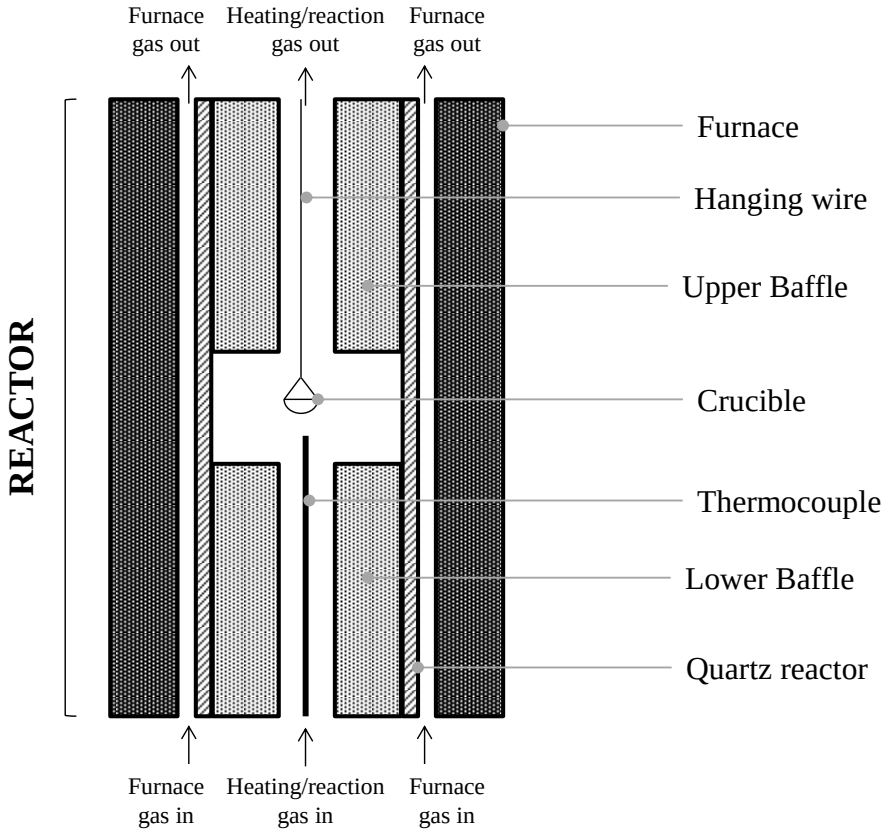

Figure 3.6. Schematic of system with reactor closed.

To the balance, as it can be observed in Figure 3.7, there is one hose connected (purge gas), through which N_2 (Praxair 99.999%) is fed in order to avoid any kind of deposit on the balance, such as dust, that will affect its reading, and also prevent the gases that are fed to the reactor, or generated inside it, to reach the balance.

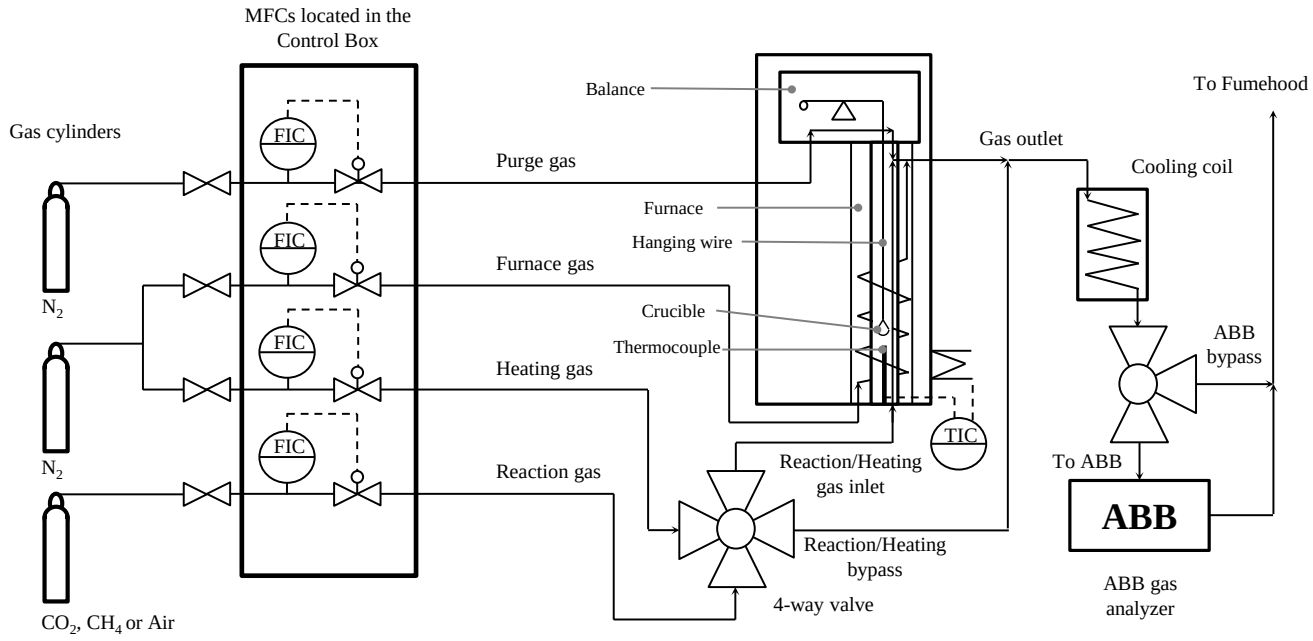

Figure 3.7. Schematic of TGA gases connections.

To the reactor there are two hoses connected; one of them connects to the outer part of the quartz reactor. The gas that is fed through this hose is named furnace gas and it is also N_2 (Praxair 99.999%). Its purpose is to keep the pressure outside the reactor equal to the pressure inside, so that the reactor does not break apart. Also, it helps to have a more efficient transfer of the heat from the high temperature furnace to the centre of the reactor. The second hose connects to the inner part of the quartz reactor, where the crucible with the sample is placed. The gas fed

through this hose is named either heating gas (N_2) or reaction gas (CH_4, CO_2 or air), depending on the gas that is fed into the reactor. If the gas is N_2 (Praxair 99.999%), then it is assumed that the gas only has heating and cooling purposes, and it will not influence the reaction(s) that may take place in the process whatsoever. In order to switch between heating and reaction gases, their primary hoses are connected to a 4-way valve (see bottom of Figure 3.7). This 4-way valve is mounted with an actuator that allows precise and fast switching. The actuator (VICI Universal Electric Actuator, model EUH) is programmed by the user to have only two positions, which for this case are named A and B: at position A the reaction gas goes into the reactor, while at position B the heating gas is fed to the reactor. Additionally, the actuator can be either controlled through a display or the Thermal Acquisition software that came along with the TGA.

As per the requirements of the flowrates for each connection, and in order to prevent the gas from the reactor to go into the balance, the flowrate of the purge gas must be 10% larger than the flowrate of the heating/reaction gas. Thus, the flowrate of purge gas was 330 ml/min and the other flowrates were 300 ml/min. The furnace gas flows through a different part of the reactor, and it cannot reach the balance unless the purge gas and the heating/reaction gas are turned off.

In the end, the purge gas and the heating/reaction gas leave the reactor through the same outlet, and then they merge with the furnace gas. Next, they are sent to a cooling coil. Afterwards, the gases can be sent either to the fumehood or to the ABB gas analyzer (AO2020 Series Gas Analyzer). This instrument is provided with three different detectors, namely two Uras 26, and one Caldos 27. One of the Uras 26 detectors enables the analysis of methane (CH_4) within the range of 0 – 5000 ppm, while the other Uras 26 enables the analysis of carbon monoxide (CO) and carbon dioxide (CO_2), also within the range of 0 – 5000 ppm. The Uras 26 set for CO and CO_2 also provides the option of obtaining the volume percent (vol%). The Caldos

27 detector can detect hydrogen (H_2) and offers two ranges of detection, from 0 – 0.5 vol% and from 0 – 10 vol%.

As it has been mentioned, the flowrates are controlled by means of a mass flow controller (MFC) located inside the control box of the TGA. This MFC can be controlled through the display or through a LabVIEW interface created by a former member of the LECA group (Dr. Benjamin Feist). The LabVIEW interface is shown in Figure B.1, in Appendix B.5, and it provides several options.

First it enables the user to connect to the COM port through which the MFC can be controlled. Second, it provides the option of choosing the frequency at which the information displayed on the interface is updated. Third, it allows collection of the data displayed on the interface for future references or reviews. Also, it provides four boxes (SP boxes) in which the user can enter the desired flowrate for each gas, in percent (%) units. Calibrations for each gas were performed in order to know the flowrate fed into the TGA in (ml/min) units. Adjacent to each of the SP boxes there is another box that shows the actual flowrate, also in (%) units. Finally, the interface has the option of setting up two set points that would change the flowrates to different values, to be set by the user, after a certain time. For instance, if our experiment lasts one hour, after that the TGA starts to cool to room temperature. Usually after four hours the TGA is already at room temperature, and it is no longer necessary to be feeding heating and/or reaction gas and furnace gas, which in turn allows us to reduce the flowrate of purge gas. Thus, one of the set points can be set to change the flowrates of gases to zero for the heating and/or reaction and furnace gases, and a smaller number for the purge gas. This way, it is not necessary to be present at the time at which this change is made.

3.5.3 Thermogravimetric Analysis (TGA) Apparatus – Modifications to the initial setup

The initial setup of the TGA was suitable for other types of experiments, such as gasification. However, in order to perform cycles of calcium looping and chemical looping combustion efficiently and safely, it was limited. As commented before, the initial configuration allowed one to switch between heating and reaction gas, controlling this action through the Thermal Acquisition software that came along with the TGA. However, for the CaL and CLC cycles, it was necessary to switch between three different reaction gases, namely CH_4, air and the mixture of 20% CO_2 and N_2, and the heating gas (N_2). Therefore, every time the reaction gas needed to be changed, it was necessary to change the reaction gas cylinder, which involved disconnecting and connecting the reaction gas hose from cylinder to cylinder and checking for leaks to ensure the connection was well made. These steps made the process much longer, inefficient and tedious. It also involved the wearing of the connections due to the continuous disconnecting and connecting. Another disadvantage was the limitation in the number of cycles that could be performed, being five cycles the maximum achieved in one day. Therefore, in order to address the problems that were hampering the performance of the experiments and to make the process more efficient, safer, less tedious and less limited, certain modifications were made. In first place, the problem to switch between the different reaction gases was set as the priority. To solve it, two 3-way solenoid valves (Parker, Series 99) were implemented; these two solenoid valves would allow to choose between the three different reaction gases that have been mentioned before, as Figure 3.8 illustrates. The first solenoid valve (SV1) allows only one gas, either the CO_2/N_2 mixture or air to go to the second solenoid valve (SV2), which in turn allows either CH_4 or the gas coming from SV1 to move forward to the 4-way valve.

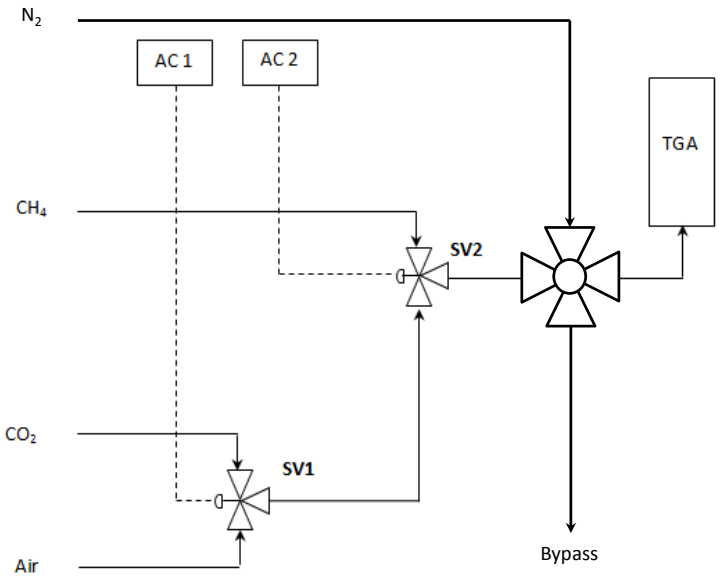

Figure 3.8. Schematic of solenoid valves configuration.

However, this modification involved losing the capacity to switch between reaction and heating gas since the TGA software only allowed control of up to two external devices. This resulting drawback was overcome by modifying the LabVIEW interface that had been first designed to control the flowrates of gases. The modifications included the addition of a number of extra set points that would change the flowrates of gases upon termination of a timer. Initially there were only two set points, and it was determined that the number of set points that would be needed for the calcium looping and chemical looping combustion experiments was six. Hence, four extra set points were added. In addition, since the capacity to switch between heating and reaction gas had been lost when the solenoid valves were installed, a controller was introduced in the new LabVIEW interface so that it was possible to manipulate the actuator that switched between heating and reaction gas without any manual operation. Also, since each set point would require either heating or reaction gas, the option of choosing the position of the actuator for each

set point was introduced. Last, an option that would automatically reset the time once all the timers came to zero was added. This permitted repetition of the conditions entered on the set points indefinitely, or until the user decided to stop the experiment, which meant that now it was up to the user to choose the number of cycles to be performed. Later on it was found that the maximum number of cycles to be performed was 20 because of the TGA software, but still, the maximum number of cycles in one day had been increased from 5 to 20.

Summarizing, by introducing the solenoid valves and modifying the LabVIEW interface, the TGA setup was upgraded in such a way that it was possible to choose between three different reaction gases through the Thermal Acquisition software and between heating and reaction gas through the LabVIEW interface. Also, an autoreset-time option was added so that the set points conditions would be repeated. Figure B.2 (Appendix B.5) shows the final interface.

3.6 Preliminary experiments

The first batch of pellets (first two rows of Table 3.1) contained the two initial configurations that have been mentioned, core-in-shell and homogeneous, the size ranged from 0.425 to 1.425 mm and the composition was 50% CuO, 40% CaO and 10% cement (50/40/10). Between these two configurations, the core-in-shell was chosen first to carry out preliminary experiments in the TGA, and also preliminary analyses of N_2 adsorption and SEM/EDS. The results from these preliminary analyses are provided in this section.

3.6.1 Determining experimental times for complete conversion for each stage in the TGA

The first experiments were oriented to provide basic information regarding the reactions that were to be carried out, that is, carbonation, calcination, reduction and oxidation. For the

experiments that are contained in this section, the TGA setup did not have the modifications described in Section 3.4.3.

Prior to any experiment, the pellets were always heated to 1073 K to decompose the calcium carbonate that could be present, and remove moisture. Figure 3.9 illustrates the changes in the mass, each of them corresponding to a specific compound(s). When 1073 K was reached, CH_4 was fed into the reactor to reduce the CuO to Cu. The heating rate was 15 K/min, and the pellets were held at 1073 K for 10 min.

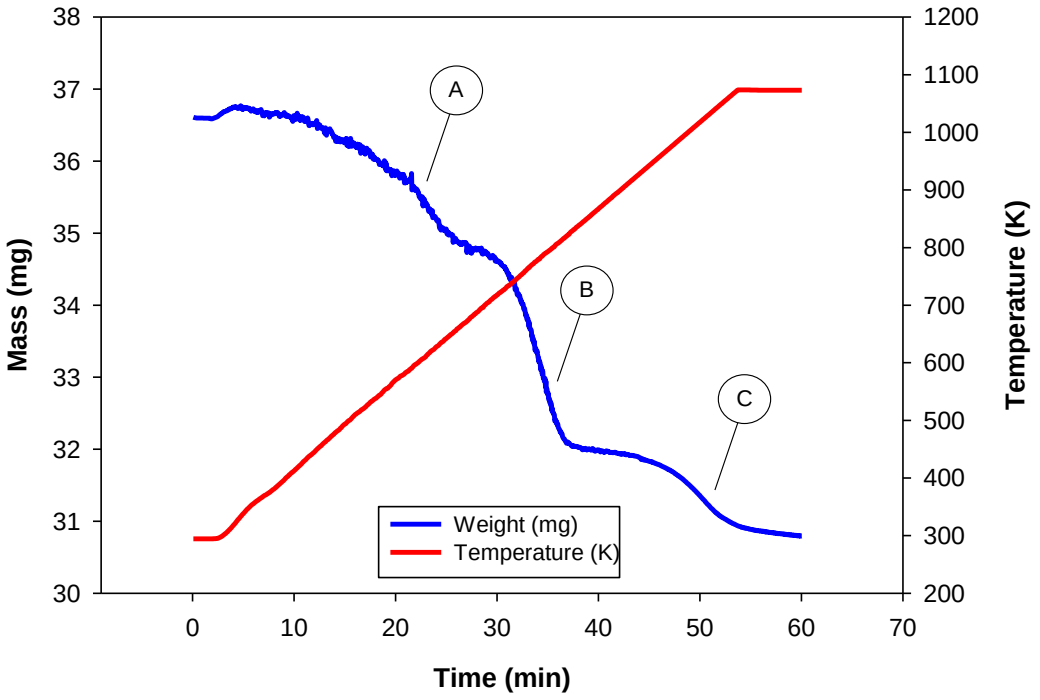

Figure 3.9. Initial step prior to any experiment in the TGA. (A) Removal of adsorbed water and dehydration of some hydrates; (B) decomposition of $Ca(OH)_2$; and (C) decomposition of $CaCO_3$.

The order of the reactions was 1) oxidation, 2) carbonation, and 3) calcination/reduction. This order was chosen based on the literature[20], where three different configurations were proposed:

(a) Carbonation → Calcination → Oxidation → Carbonation

(b) Carbonation → Calcination → Carbonation

(c) Carbonation → Oxidation → Calcination

Among these options, the carbonation-calcination-oxidation was chosen as the most suitable for several reasons. First, option (b) would be suitable only for cases where the ratio of O_2/CO_2 in the flue gases would be high, since the oxidation of the reduced Cu could be performed at the same time as the carbonation takes place. Otherwise, this option limits the regeneration of Cu and, in turn, the possibility of providing the heat for the decomposition of $CaCO_3$. Option (c) requires strict control of the temperature to prevent partial decomposition of the $CaCO_3$ in the air reactor, which would diminish the effectiveness of the process in capturing CO_2. Therefore, option (a) was selected because, even though option (b) was the simplest, and it would not require a third reactor, high ratios of O_2/CO_2 may occur in very specific situations but not generally; also, because as opposed to option (c), option (a) did not involve issues with partial decomposition of carbonate while oxidizing Cu.

Hence, after the first step, the oxidation reaction was performed, followed by the carbonation, and finally, the calcination/reduction, which returned the pellets to the initial state. For the oxidation, the temperature needed to be decreased to 873 K, the reaction gas was air, and this reaction took approximately 450 min to reach complete conversion of Cu. However, it is significant that almost 80% of conversion was achieved in the first 20 – 25 min. The change in the reaction rate with time suggests kinetics control (Figure 3.10) initially, up to ~25 min, and

then diffusional control. After this reaction the composition of pellets was 50% CuO, 40% CaO and 10% CE.

Then the carbonation was performed, at the same temperature, with 20% CO_2/N_2 balance as reaction gas, but in this case it was not possible to achieve complete conversion. After 20 hours, only 70% conversion was reached, which was attributed to the blockage of pores due to the larger volume of the resultant carbonate versus the calcium oxide. In this reaction, the conversion versus time curve has a shape similar to that of the oxidation reaction, with an initial part where the kinetics seems to control the process, and then the diffusional mechanism takes over to slow down the reaction rate. This fact has been reported by other authors as well[12,53,54]. For this reaction, approximately 60% of conversion could be achieved before the kinetics stopped controlling the process.

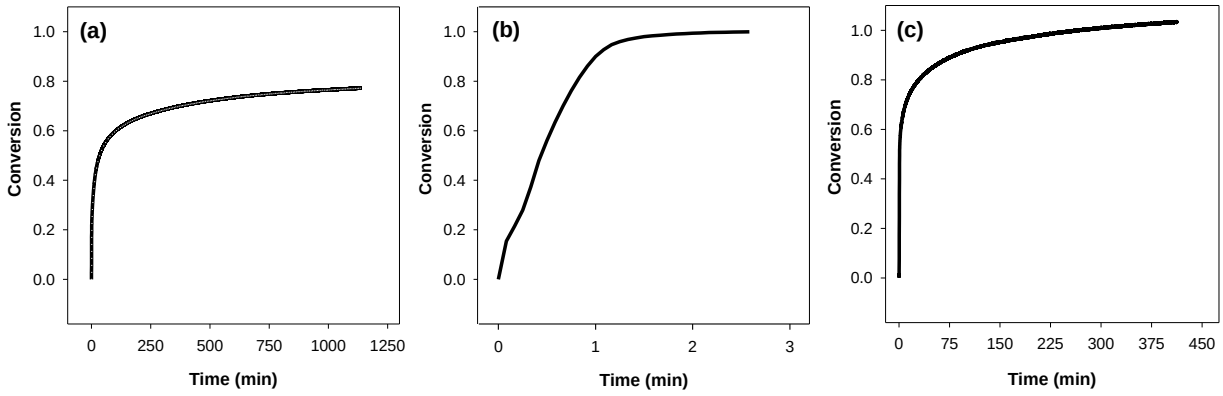

Figure 3.10. Conversion vs time curves for (a) carbonation, (b) calcination/reduction, (c) oxidation.

Last, the calcination/reduction stage was carried out; the temperature for this reaction was increased to 1073 K, and the reaction gas was methane. This reaction was very fast and it took

approximately 3 min to reach complete reduction of CuO and decomposition of $CaCO_3$. However, in this stage, as it will be discussed in the next chapter, by the time 1073 K was reached, almost complete decomposition of the carbonate was achieved due to the high temperature.

Therefore, these results showed that both oxidation and carbonation had the same behaviour, with initial control by the kinetics of the reactions, and subsequent diffusional control. Complete conversion, although possible, was not feasible for any of these reactions. For the calcination/reduction, the reaction was controlled by the kinetics at all times.

3.6.2 Cycles of Calcium Looping and Chemical Looping Combustion

The combination of calcium looping and chemical looping combustion was initially studied with the core-in-shell pellets. The conditions used for this part of the preliminary experimentation are those that have been described before, and the number of cycles of oxidation/carbonation/calcination/reduction was five. The setup of the TGA for these experiments was not upgraded yet, which limited the number of cycles that could be performed. Still, five cycles took approximately eight hours since it was necessary to connect and disconnect hoses continuously; the theoretical time for the experiment was less than seven hours.

The result obtained after five cycles is depicted in Figure 3.11. The initial part is similar to that shown in Figure 3.9 (Section 3.5.1). After the initial calcination, the temperature was lowered to 873 K and air was fed into the reactor for 10 min. Next, the air flow was stopped and its cylinder connection to the TGA was changed to that of the 20% CO_2/N_2 balance mixture. The temperature was not changed, and the mixture was fed for 15 min. Afterwards, the temperature was increased to 1073 K, and in the meantime the connection of the 20% CO_2/N_2 mixture was

changed to pure CH_4. At 1073 K, methane was fed into the reactor for 10 min and then a new cycle started.

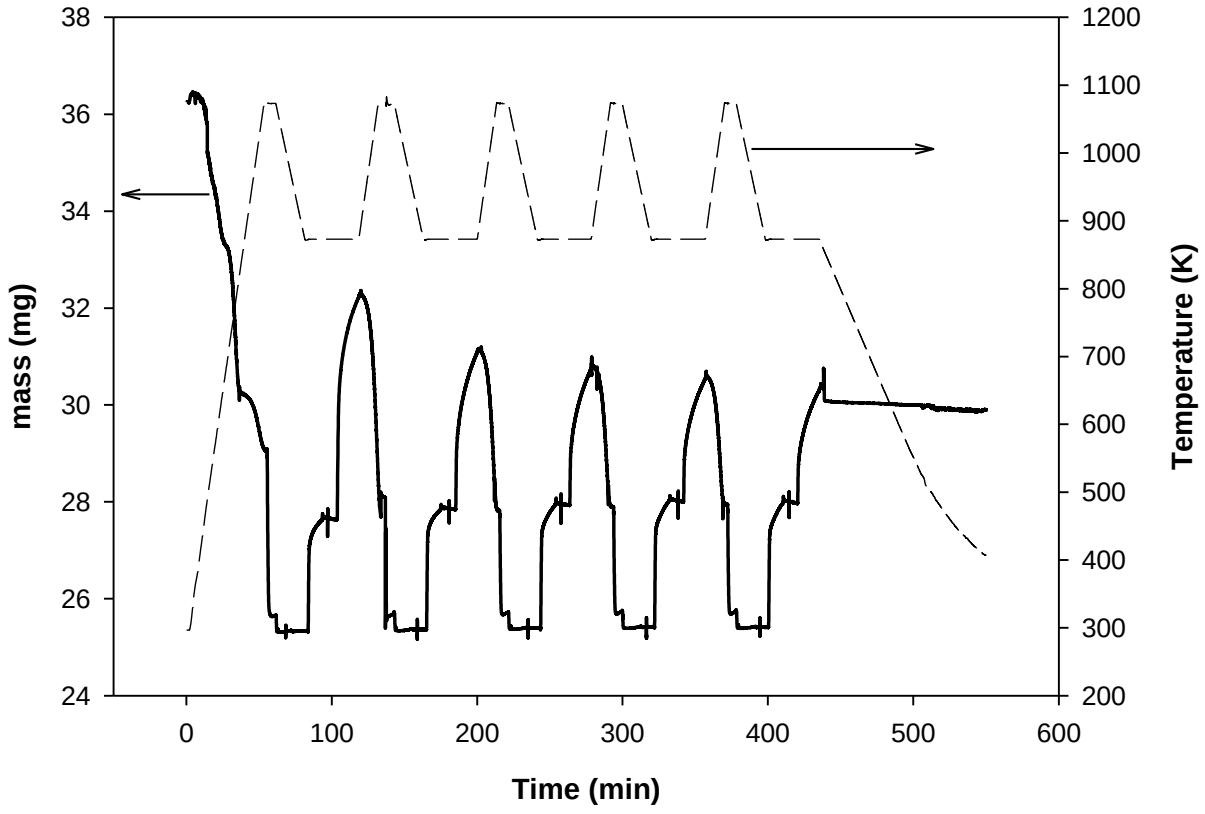

Figure 3.11. Five cycles of oxidation/carbonation/calcination/reduction with core-in-shell pellets.

After the five cycles, the experiment was stopped and cooled. The experiment was repeated two more times to perform the study of errors, and the results are summarized in Table 3.2. In this table, the properties shown are 1) conversion for carbonation, 2) conversion for oxidation, 3) CO_2 capacity, CC (gCO_2/gPellets), 4) O_2 capacity, OC (gO_2/gPellets), 5) CO_2 capacity loss, CCL (%), and 6) O_2 capacity loss, OCL (%), and the calculation methodology is provided in Appendix B.6. After five cycles, the capacity to capture CO_2 decreased by 50%,

which means that in the fifth cycle the amount of CO_2 captured was half the amount captured in the first cycle. On a mass basis the capacity decreased from 0.147 to 0.074 gCO_2/gPellets. On the contrary, the oxidation capacity remained constant, reaching conversions up to 68.5%.

Table 3.2. Five cycles oxidation/carbonation/calcination/oxidation with core-in-shell pellets.

Cycle	$\chi_{carbonation}$ (%)	$\chi_{oxidation}$ (%)	CO_2 Capacity (gCO_2/gPellets)	O_2 Capacity (gO_2/gPellets)	CCL (%)	OCL (%)
1	46.9 ± 3.0	66.8 ± 2.8	0.147 ± 0.009	0.084 ± 0.003	N/A	N/A
2	35.8 ± 2.2	67.9 ± 3.3	0.112 ± 0.007	0.085 ± 0.004	23.6 ± 1.0	-1.6 ± 1.8
3	29.4 ± 2.0	66.5 ± 3.4	0.092 ± 0.006	0.084 ± 0.004	37.3 ± 1.6	0.4 ± 2.4
4	25.7 ± 1.3	68.5 ± 4.0	0.081 ± 0.004	0.086 ± 0.005	45.2 ± 0.8	-2.6 ± 2.5
5	23.4 ± 0.9	68.2 ± 3.3	0.074 ± 0.003	0.086 ± 0.004	50.0 ± 1.1	-2.2 ± 1.9

a. CCL ≡ CO_2 Capacity Loss
b. OCL ≡ O_2 Capacity Loss

3.6.3 N_2 Adsorption

As part of the initial characterization of the pellets that were to be studied, N_2 adsorption analyses were performed. Some trial and error was required to determine the appropriate analysis procedures. The shape of the Langmuir isotherm (see Figure 3.12) for the initial test had an unconventional shape, and negative values of adsorbed amount of nitrogen, which indicated that the analysis was not correct. This issue was overcome by increasing the mass of pellets to enable an accurate analysis. The difference between the isotherms is evident in Figure 3.12.

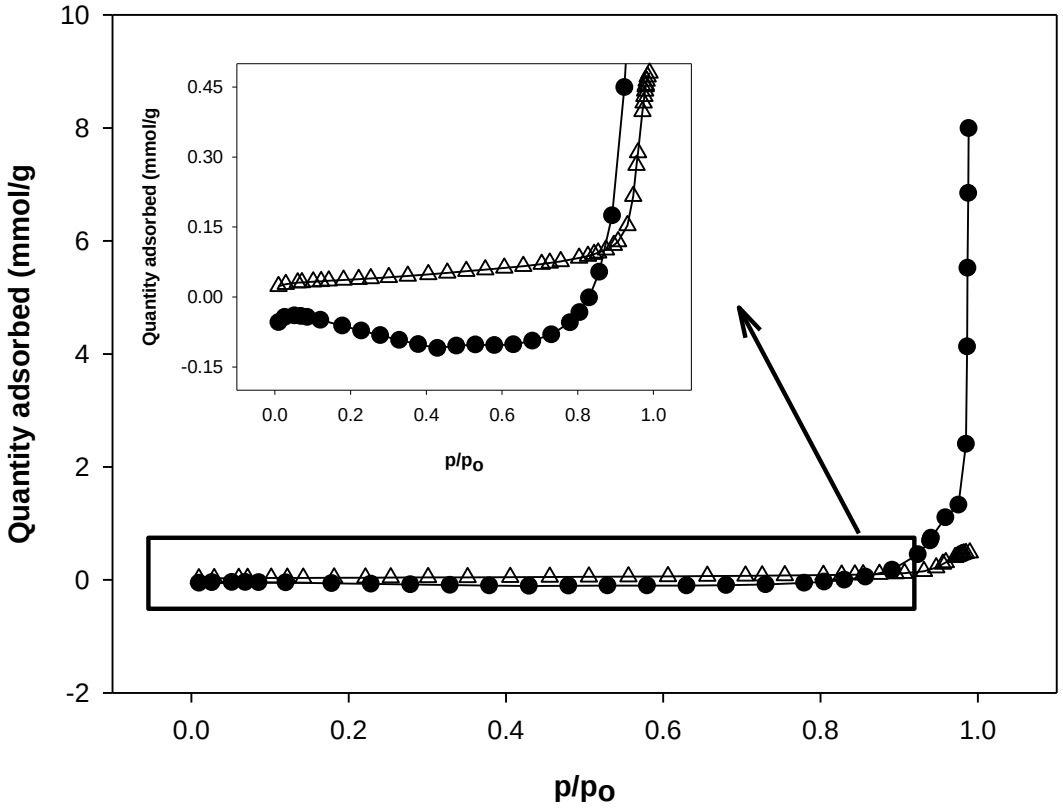

Figure 3.12. Isotherms of N_2 adsorption analyses with large and small amounts of pellets.

Isotherm with too low a mass of pellets, Isotherm with larger mass of pellets.

For the correct analysis, the surface area was 3.1 m^2/g, and the pore volume, at p/p_o = 0.98, was 0.013 cm^3/g. The pore size distribution is shown in Figure 3.13; the majority of the pores are in the range of 200 Å to 1200 Å, i.e., mesopores and macropores[81] but some pores are in the range of 20 to 50 Å. This result was not duplicated because the purpose of the analysis was to obtain an accurate estimation of the surface area of the pellets, so that subsequent analyses could be performed correctly. In addition, the first batch of pellets was discarded because of their size, which was unsuitable for use in a fluidized bed. The eventual application of these pellets

would be in a fluidized bed, and the preliminary experiments of the collaborators at the École Polytechnique de Montréal determined that the pellets should be smaller in order to use them in such reactor. Therefore, the surface area, pore volume and pore volume distribution were studied only for the homogeneous pellets whose size was in the range of 0.250 to 0.600 mm (second batch), and those analyses were indeed duplicated two times, so that the analysis of errors could be performed. The results can be found in Chapter Five.

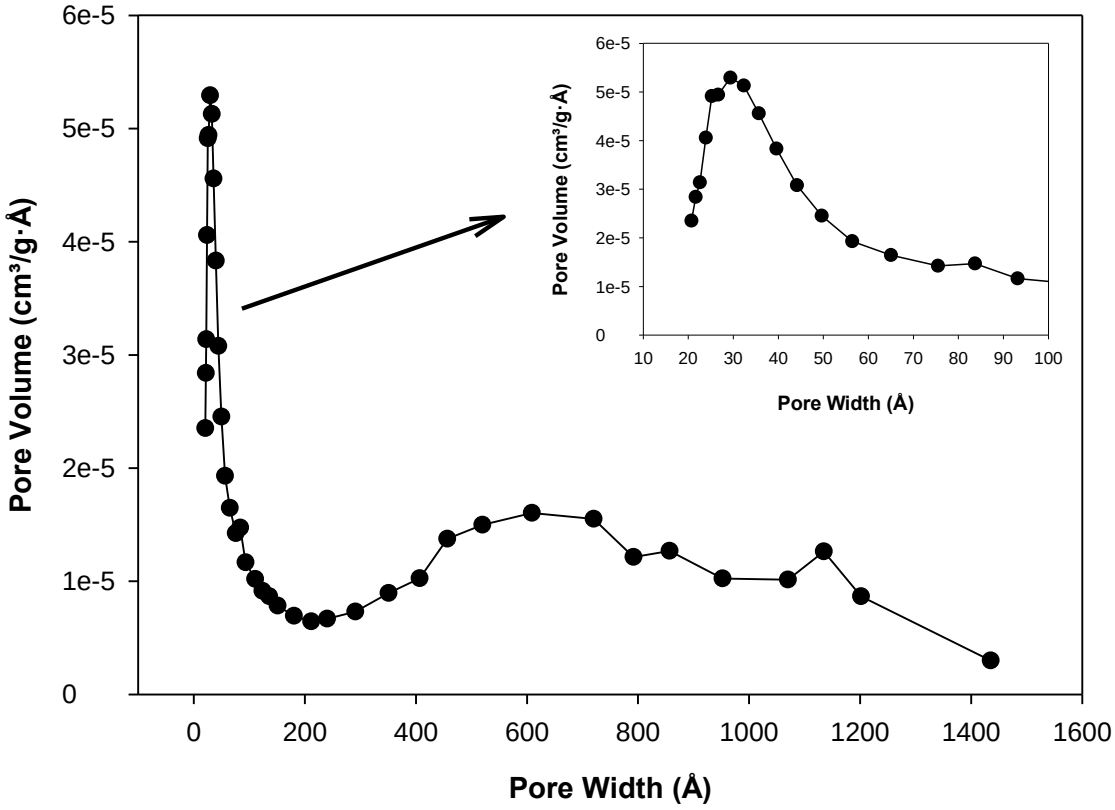

Figure 3.13. Pore size distribution of the core-in-shell pellets.

3.6.4 SEM and EDS analyses

The last techniques used as part of the characterization of the pellets were scanning electron microscopy (SEM) and energy dispersion X-ray spectrometry (EDS or EDX). These

techniques were applied to study the external and internal structure of the pellets and especially to determine the existence of the core-in-shell structure. Also, the EDS helped to determine whether the composition of pellets was similar to the theoretical composition or not. These techniques were applied to both configurations of pellets, core-in-shell and homogeneous, but to be consistent with the results provided for previous analyses (TGA and N_2 adsorption), only the results of core-in-shell are provided in this section. Images of the homogeneous configuration can be found in the Appendix B.7.

For raw and calcined (heated to 1073 K) core-in-shell pellets, images of the surface at 5000X magnification were obtained, and are illustrated in Figures 3.14 and 3.15. In these images it is possible to appreciate that the surface structure changes after calcination, becoming smoother and even showing some cracks, which make the structure of the pellet more fragile. The smoothing of the surface can be due to sintering and the cracks could be a result of the calcination, which would mean poor thermal stability of the pellets.

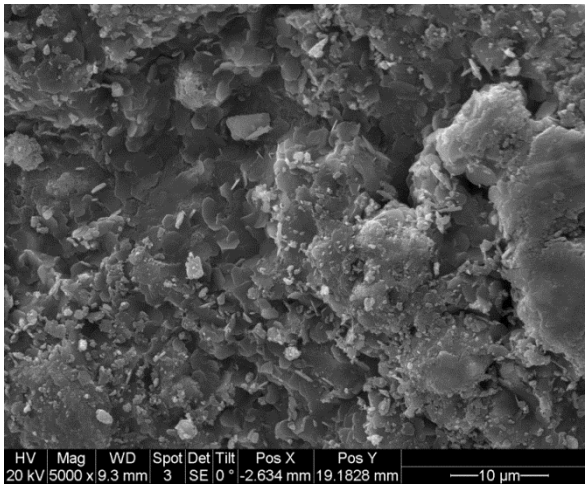

Figure 3.14. Raw core-in-shell pellet surface.

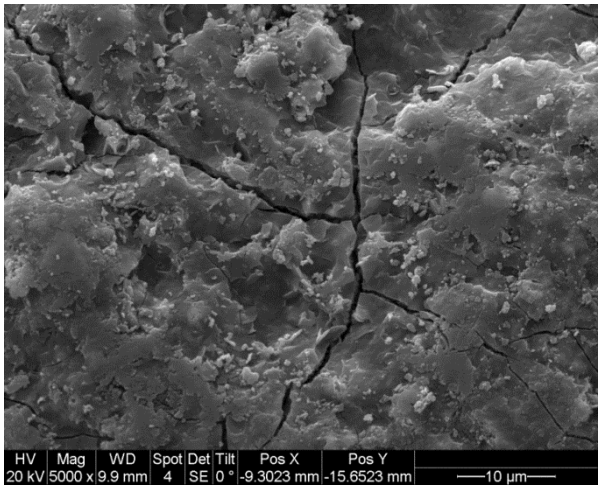

Figure 3.15. Calcined core-in-shell pellet surface.

Also, images of the internal part of the pellets were captured before and after calcination at different magnifications. In this section, images at 250X magnification are shown in Figures 3.16 and 3.17. Figure 3.17 (calcined) shows the internal part of the pellet and also some part of the surface because of its position. The calcined pellet shows a more porous structure than the raw pellet, which is explained by the smaller volume of CaO versus the volume of $CaCO_3$, as well as Cu versus CuO.

The EDS analysis was performed on the pellet that is shown in Figure 3.18. The outer and inner parts of the pellets were analyzed separately in order to determine the composition of each part. The results should show different ratios of copper, calcium, oxygen and aluminum for each case. In Figure 3.18 are illustrated the spectra obtained for each part, as well as the identification for each element.

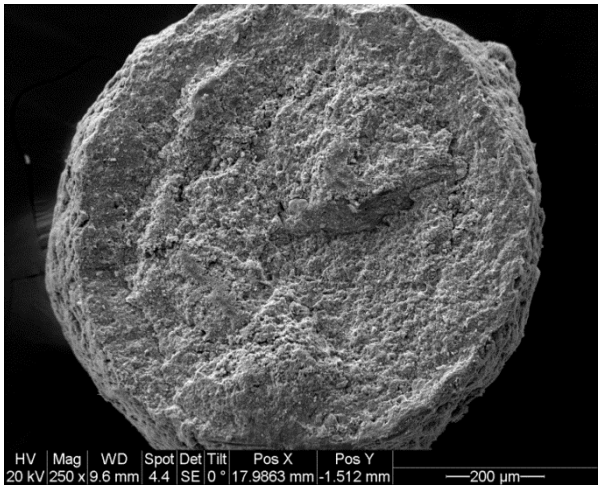

Figure 3.16. Raw core-in-shell pellet cross-section.

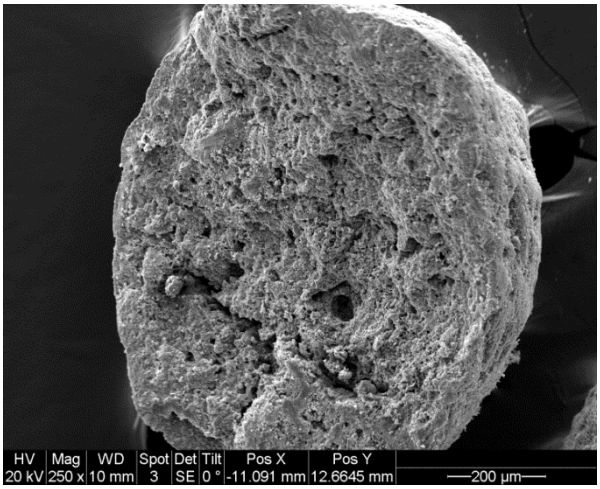

Figure 3.17. Calcined core-in-shell pellet cross-section.

As per the spectra, the core contains copper, little aluminum, calcium and oxygen. This is in agreement with the theoretical composition of the core, which should be mainly CuO and CaO. Regarding the shell, the peak for copper is barely noticed, while the peak for aluminum is well defined. There is also calcium and oxygen as the shell should contain Al_2O_3 and CaO. Therefore, according to these results, it seems that the pellet was made of a core that contained copper, calcium and oxygen mainly, and a shell that contained aluminum, calcium and oxygen. Note that the presence of gold and palladium is due to the coating layer.

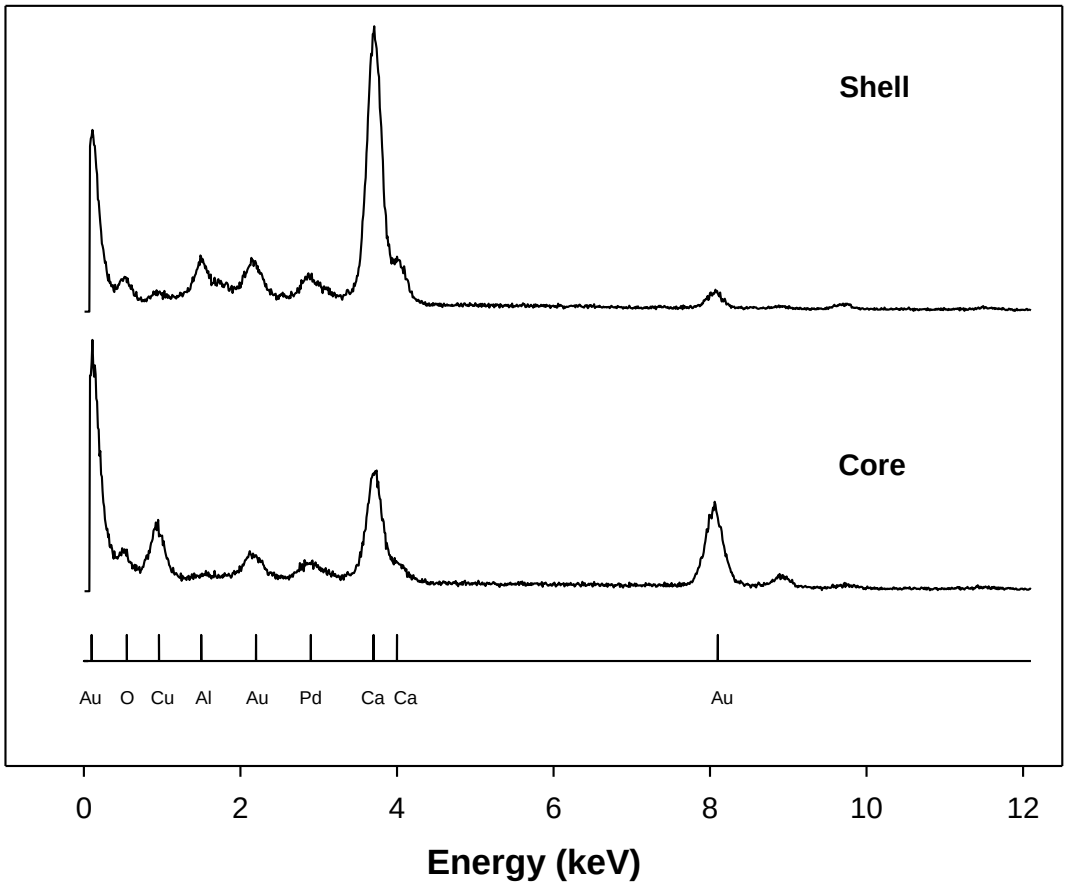

Figure 3.18. EDS spectra for core and shell respectively; shell spectrum on top, core in the middle and key to identify elements on bottom.

3.7 Chapter summary

In this chapter it has been introduced the compositions, configurations and sizes of the pellets that have been used for this thesis. In total, two configurations (core-in-shell and homogeneous), three different compositions (50% CuO, 40% CaO and 10% cement, 50% CuO and 50% cement, and 90% CaO and 10% cement) and two ranges of size of pellets (0.450 – 1.425 mm and 0.250 – 0.600 mm) were tested. Also, with the purpose of enhancing the capacity of the pellets to capture CO_2 over cycles, which decays dramatically after 4 – 5 cycles (~50%), two different approaches, thermal treatment and impregnation with potassium were taken, and the procedure followed for each approach has been thoroughly explained. Additionally, the techniques used to characterize the pellets have been explained in detail, namely N_2 physisorption, scanning electron microscopy, energy dispersion X-ray spectrometry, X-ray diffraction and thermogravimetric analysis. With regards to the thermogravimetric analysis, it has been commented the modifications performed on the setup to address the limitations of the previous setup and enable multiple cycles of carbonation, oxidation, calcination and reduction.

Preliminary experiments were performed with the core-in-shell configuration of pellets and the results have been provided. It was determined that the pellets had low surface area, which indicated that, to obtain valid results, large amounts of pellets for the physisorption analysis would be required. The minimum was set at 1 g. The thermogravimetric analysis determined that the capacity of the core-in-shell pellets decayed approximately 50% after 5 cycles, while the oxidation capacity remained stable after 5 cycles. Last, the SEM images enabled the study of the internal and external parts of the pellets, and the EDS analysis suggested that the core-in-shell pellets had indeed the core-in-shell structure.

Chapter Four – Heat transfer model

The results presented in Chapter Three showed that the capacity of the pellets to capture CO_2 decreased dramatically after 5 cycles (50%). This decay, according to the literature, is due to sintering, which reduces the number of pores and, in turn, the surface area on which CO_2 can adsorb[14,54,82]. Sintering is a kinetic phenomenon that depends on the material properties, such melting point temperature, particle size, and porosity, as well as the heating rate, atmosphere, and temperature[83]. Since the reactions involved in the calcium looping-chemical looping combustion process are all exothermic, except for the calcination, it is expected that if the particles experience high temperatures during one or more of the stages of the process, the kinetics of the sintering process can be significantly enhanced. Thus, significant insight can be gained from a transient model for heat and mass transfer coupled with reaction kinetics that can predict the temperature distribution within the pellets.

$$CaO + CO_2 \rightarrow CaCO_3 \qquad \Delta H_R = -174.7\ kJ/mol \qquad (4\text{-}1)$$

$$4\ Cu + 2\ O_2 \rightarrow 4\ CuO \qquad \Delta H_R = -144.0\ kJ/mol \qquad (4\text{-}2)$$

$$4\ CuO + CH_4 \rightarrow CO_2 + 4\ Cu + 2\ H_2O \qquad \Delta H_R = -234.7\ kJ/mol \qquad (4\text{-}3)$$

$$CaCO_3 \rightarrow CaO + CO_2 \qquad \Delta H_R = 174.7\ kJ/mol \qquad (4\text{-}4)$$

The study of the system is complicated because the reaction front, and thereby the heat source/sink, during each of the stages moves. Thus, the phenomenon belongs to the class of the moving boundary / moving heat source problems. Although similar types of problems have been studied[84–89], due to the complexity involved and to the different approaches taken to model the

moving boundary, no general solution has been provided. Some studies involved the freezing or drying of food in which the phase transition of the water present in the food creates a moving boundary problem[84,85]. A numerical method was applied to solve the set of differential equations, namely the variable space network (VSN). More related to the present work is the study of the reduction of an iron ore-coal composite pellet, which takes into consideration the shrinkage and swelling of the pellet and was solved using control volume scheme discretization[86]. Another work involved the study of a reaction-diffusion system with a moving heat source, which led to a Green's function type of problem solved by a numerical solution using the Galerkin finite element method[87]. More approaches to problems where heat transfer and a moving boundary can be found elsewhere[88,89]. The common approach for all the aforementioned studies is the use of numerical methods to solve the set of differential equations.

In this chapter, the heat and mass transfer within the pellets is studied with the purpose of providing an analytical solution for the heat transfer problem and, ultimately, estimate whether the temperature reached in the pellets is higher than expected. The temperatures set for the preliminary experiments were 873 K for carbonation and oxidation and 1073 K for calcination and reduction. To support the study, experiments designed based on the results obtained from the study were conducted. Also, a parametric study of some of the key variables, namely particle size, heat of reaction, thermal conductivity and time of reaction, is provided in Appendix C.

Last, the core-in-shell pellets were chosen as the base case because the preliminary experiments had been conducted with this configuration of pellets. The results obtained from the characterization, particularly SEM images and N_2 physisorption, as well as the conditions used for the TGA experiments (flowrate, temperatures and composition of gases) are used for this study.

4.1 Model Development

A mathematical model describing the pertinent transport phenomena for a single spherical pellet is developed here. The primary aim is to predict the spatio-temporal distribution of the temperature within the pellet during the various stages of the Calcium Looping (CaL) process. The thermal model requires a source/sink term for the heat, i.e. the rate of heat generated/consumed during each stage of the CaL process.

In absence of intrinsic kinetics of each of the stages of the CaL process, in this study, the rate of reaction is assumed to be mass transport limited. This assumption, the validity for which is examined subsequently, permits us to relate the diffusion rate to the rate of reaction and, thereby, to the quantification of heat source/sink term.

4.1.1 Mass transport model

The mass transport during the oxidation, carbonation and reduction reactions was described using the shrinking core model. This model was originally developed for particles that go through a combustion process, e.g. carbon particles. In the current study, the process that takes place inside the pellet can be assumed to follow similar mass transport/reaction mechanism, i.e., the gas molecules diffuse through the outer non-reacting shell, and then through the reacted core, ultimately arriving at the unreacted/reacted material interface. The reacting gas is considered to react instantaneously upon reaching this interface but resulting in a finite amount of consumption/reaction of the core. This process continues until the whole core has reacted. Thus, the reacting interface moves to the interior with time. This situation represents a *moving boundary* problem. It is recognized that as the reaction proceeds, the porosity and the

composition as well as all properties that depend on these two variables continuously change. Figure 4.1 illustrates this mechanism.

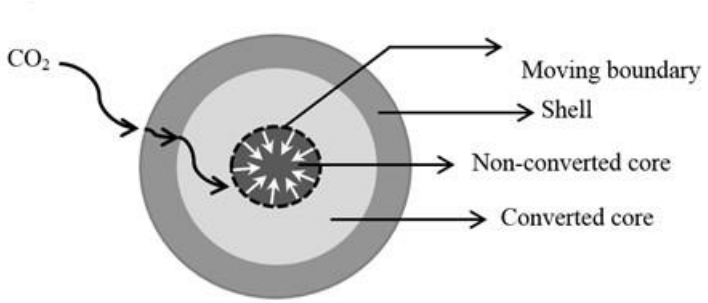

Figure 4.1. Schematic of the pellet structure and shrinking core model mechanism.

Since the reaction is considered to be instantaneous, the rate of reaction becomes diffusive mass transport limited. Under this assumption, the shrinking core model can be applied to relate the extent of non-dimensional non-converted radius (X) for a spherical particle as a function of time (*t*).

$$t = a_1[1 - 3X^2 + 2X^3] \tag{4-5}$$

Here, a_1 and X are:

$$a_1 = \frac{\rho_s \phi R_{core}^2}{6 D_e C_{g,bulk}} \quad \text{(4-5a)} \qquad X = \frac{r_{non}}{R_{core}} \quad \text{(4-5b)}$$

where, ρ_s is the density of the unreacted solid, ϕ is the volume fraction of the component that reacts, R_{core} is the original radius of the core, D_e is the effective diffusivity, $C_{g,bulk}$ is the concentration of the gas in the particle and r_{non} is the radius of the non-converted core, and its value ranges from zero to R_{core} [90,91].

A number of parameters are needed to relate the conversion (X) to the reaction time (t). The structural parameters of the pellet (R_{core} and ϕ) were obtained from images obtained by

scanning electron microscopy (SEM) and from the mass ratio respectively. The effective density of the pellet was calculated as the average of densities based on the mass ratio of the compounds present in the pellet. The transport coefficient, i.e. the effective diffusivity can be calculated following the Bosanquet formula (4-6) considering both Knudsen and molecular diffusivities.

$$\frac{1}{D_e} = \frac{\varepsilon}{\tau}\left(\frac{1}{D_K} + \frac{1}{D_A}\right) \tag{4-6}$$

where, ε refers to the porosity of the pellet, τ is the tortuosity and D_K and D_A are the Knudsen and molecular diffusivities respectively[92]. Since the average pore size (223Å) that was obtained by N_2 adsorption analyses was smaller than the mean free path of the molecules (>1000Å), the Knudsen diffusion rate was much slower than the molecular diffusion rate. Therefore, the latter was neglected and only the Knudsen diffusion was taken into consideration with its value determined by Eqn. (4-7). In this regard, note that the average pore size is significantly smaller than the size of pore that would be required to take into consideration the molecular diffusivity. That means that, although the pore size changes throughout the reactions, most likely it would not become similar or larger than that at which molecular diffusion competes with Knudsen diffusion. Nevertheless, considering only Knudsen diffusion, a larger average pore size would result in a faster Knudsen diffusion rate, which in turn would result in the gas molecules reaching the active sites faster, i.e., shorter times of reaction. On the contrary, a smaller average pore size would result in slower Knudsen diffusion rates, and longer times of reaction.

$$D_K = 4850 d_p \sqrt{\frac{T}{M_A}} \tag{4-7}$$

Eqn. (4-6) contains a factor for the tortuosity, which is often unknown and must be estimated. In the present study, the tortuosity was calculated as the inverse of the porosity[92], as shown in Eqn. (4-8):

$$\tau = \frac{1}{\varepsilon} \tag{4-8}$$

In addition, the porosity of the particles changes as the reactions proceed, which changes the diffusivity. For instance, while the carbonation takes place, the CO_2 molecules occupy the void space, reducing the porosity and making the path more tortuous. Eqn. (4-9) was used to capture the change in diffusivity[93]:

$$D_e = D_{e,0}\left(\frac{\varepsilon}{\varepsilon_o}\right)^2 \tag{4-9}$$

$D_{e,0}$ and ε_o are the initial values of the diffusivity and porosity respectively, i.e., the values at time zero of the reaction, while D_e and ε are the values at any time after the reaction has started. According to the literature, the exponent of Eqn. (4-9) must be between 2 and 5, so since from the development of the mathematical model, the resulted number is 2, no further modification was considered[93,94].

Since the porosity of the pellet changes with the progression of reaction, the term instantaneous porosity will be used to refer to the porosity at any time while the reaction takes place, ε. It was calculated following Eqn. (4-10) and, in that equation, χ_s is the conversion, V_{non} and V_{con} are the specific volumes of the non-converted and the converted core respectively, and C_{So} is the concentration of solid in the particle.

$$\varepsilon = \varepsilon_o + \chi_s\left(V_{non,s} - V_{con,s}\right)C_{So} \tag{4-10}$$

The conversion is expressed via Eqn. (4-11) below:

$$\chi_s = 1 - \frac{V_{non}}{V_{core}} = 1 - \frac{{r_{non}}^3}{{R_{core}}^3} \tag{4-11}$$

Eqn. (4-12) and (4-13) were used to obtain the concentration of gas and solid in the particle respectively.

$$C_{g,bulk} = \frac{P_i MW_i}{RT} \tag{4-12}$$

$$C_{So} = \frac{m_i}{V_{core}\varepsilon_o} \tag{4-13}$$

4.1.2 Heat transfer model

The spatio-temporal temperature profile can then be obtained by solving the classical heat transfer by conduction problem. The generalized heat conduction equation in spherical coordinates is presented below (4-14). The same equation applies to all three domains – shell, converted core and non-converted core; here, the subscript non, refers to the non-converted core.

$$\frac{1}{\alpha_{eff,non}}\frac{\partial T_{non}}{\partial t} = \frac{1}{r^2}\frac{\partial}{\partial r}\left(r^2\frac{\partial T_{non}}{\partial r}\right) \tag{4-14}$$

The effective thermal diffusivity of the non-converted part of the core was calculated following Eqn. (4-15).

$$\alpha_{eff,non} = \frac{k_{eff,non}}{(\rho C_P)_{eff,non}} = \frac{\left[(1-\varepsilon)\cdot\sum x_{S,i}k_{S,i}\right]_{non} + \left[\varepsilon\cdot\sum y_{g,i}k_{g,i}\right]}{\left[(1-\varepsilon)\cdot\sum x_{S,i}\rho_{S,i}{C_P}_{S,i}\right]_{non} + \left[\varepsilon\cdot\sum y_{g,i}\rho_{g,i}{C_P}_{g,i}\right]} \tag{4-15}$$

Boundary Conditions: The boundary conditions for each domain were as follows.

For the non-converted core, the symmetry condition is applied.

$$At\ r = 0 \qquad \left.\frac{\partial T_{non}}{\partial r}\right|_{r=0} = 0 \tag{BC.1}$$

In addition, the condition at the interface between the non-converted and the converted core must be applied. This condition establishes that the heat generated at the moving source due to the exothermic reactions is distributed between the non-converted and converted cores. The heat that each part will take depends upon their thermal conductivity.

$$\text{At r} = \text{s(t)} \qquad \rho_s q_{reaction} \frac{\partial s}{\partial t} = -\left[k_{non} \frac{\partial T_{non}}{\partial r} + k_{con} \frac{\partial T_{con}}{\partial r}\right] \qquad 0 < \text{t} < \text{t}_{\text{reaction}} \qquad \text{(BC.2)}$$

The parameter *s(t)* is the time-dependent location of the interface, which moves as the reaction takes place. The interface position as a function of time is obtained via equation (4-5). Linear approximation to the non-linear relationship between non-converted radius with time is applied and discussed in more detail in Section 4.2.2

For the converted core, the first boundary condition is also applied at the moving interface. The condition assumes equal temperatures for the non-converted and converted cores. Also, the symmetry condition is applied, but this time only at the time at which the reaction is complete, i.e., the whole core has been converted.

$$At\ r = s(t) \qquad T_{non}\,(s(t), t) = T_{con}\,(s(t), t) \qquad \text{(BC.3)}$$

$$At\ r = 0\ and\ t = t_{reaction} \qquad \left.\frac{\partial T_{non}}{\partial r}\right|_{r=0,\ t=t_{reaction}} = 0 \qquad \text{(BC.4)}$$

Finally, for the shell, the first boundary condition establishes that the temperature at the interface between the converted core and the shell is the same. Regarding the second boundary condition, it states that the heat conducted through the shell is the same as that transferred to the external ambient.

$$At\ r = R_{core} \qquad T_{con}\,(R_{core}, t) = T_{shell}\,(R_{core}, t) \qquad \text{(BC.5)}$$

$$At\ r\ =\ R_o \qquad -k_{shell}\frac{\partial T_{shell}}{\partial r} =\ h(T_{shell} - T_\infty) \tag{BC.6}$$

The heat transfer coefficient *h* was obtained by calculating the Nusselt number through Eqn. (4-16), which is for flows around spheres.

$$Nu\ =\ 2\ +\ \left(0.4Re_D^{1/2}\ +\ 0.06Re_D^{2/3}\right)Pr^{0.4}\left(\frac{\mu}{\mu_S}\right)^{1/4} \tag{4-16}$$

In order to calculate the velocity, to obtain the Reynolds number, we used experimental values of flow rates (300 cm^3/min) and dimensions of the TGA system where the experiments were performed (i.d. 5.6 cm).

$$v\ =\ \frac{F}{A_S} = \frac{F}{\frac{\pi}{4}D^2} \tag{4-17}$$

Initial conditions: The initial conditions used for each part of the pellet are the same. For carbonation (4-1) and oxidation (4-2) reactions the initial temperature was 873 K, while 1073 K was the initial temperature for reactions reduction (4-3) and calcination (4-4).

Model parameters: To calculate the effective properties, the porosity and composition of the pellet had to be taken into consideration. As explained previously, the instantaneous porosity was calculated using Eqn. (4-10). The thermal conductivity, density and heat capacity were taken from the literature[95],[96], and are summarized in Tables 4.1 and 4.2. Note that these properties are temperature-dependent. However, in this work, they were assumed to be constant at the temperatures at which the process was carried out, i.e. 873 K and 1073 K. As mentioned, the chemical composition of the non-converted pellet was 50% CuO, 40% CaO and 10% cement.

Table 4.1. Volumetric heat capacity ($C_P \times \rho$) for solid and gas phase components.

Compound	$C_P \times \rho$ (J/m^3-K)	$C_P \times \rho$ (J/m^3-K)
	873 K	**1073 K**
CaO	3,150,833	3,224,264
Cu	3,914,822	4,110,444
$CaCO_3$	3,388,504	3,467,177
CuO	4,293,395	4,438,119
Al_2O_3	4,723,738	4,893,792
CH_4	-	980
CO_2	723	617
Air	447	-
H_2O	-	472

Table 4.2. Thermal conductivity (k) for solid and gas phase components.

Compound	k (W/(m-K))	k (W/(m-K))
	873 K	**1073 K**
CaO	7.2	7.0
Cu	348.7	334.8
$CaCO_3$	0.6	0.2
CuO	17.9	17.2
Al_2O_3	4.2	3.3
CH_4	-	0.2167
CO_2	0.0621	0.0754
Air	0.0621	-
H_2O	-	0.1076

For the shell, it is important to note that, although it contains CaO, to simplify the problem it is assumed that no reaction takes place within the shell. Therefore, neither the porosity nor the composition changed with time. Consequently, the thermal conductivity, density and heat capacity remained constant for each temperature.

Hence, for the stated partial differential equations with the associated boundary and initial conditions, an analytical solution of the form below was considered:

$$T_{non}(r,t) = A + B\left(1 - \left|erf\left(\frac{r}{2\sqrt{\alpha_{non}t}}\right)\right|\right) \quad (4\text{-}18)$$

$$T_{con}(r,t) = C + D\left(1 - \left|erf\left(\frac{r}{2\sqrt{\alpha_{con}t}}\right)\right|\right) \quad (4\text{-}19)$$

For the shell, since no reaction takes place there, a linear temperature profile was obtained. The mathematical expression is Eqn. (4-20).

$$T_{shell}(r,t) = E + rF \quad (4\text{-}20)$$

4.2 Results and Discussion

4.2.1 Carbonation – Reduction/Calcination – Oxidation cycles

For the model, it was taken into consideration that the calcination step was generally complete before the reduction of CuO started. That is, while the pellets are heated from 873 K to 1073 K, the carbonate decomposed (i.e., the mass decreased). Figure 4.2 depicts three experimental cycles in which this effect is observed.

Therefore, when CH_4 was introduced to reduce CuO, little or no $CaCO_3$ remained such that the heat released during the combustion of CH_4 was not being used to decompose the $CaCO_3$. Hence, it is possible that the temperature inside the pellets during the reduction stage increased significantly, favouring sintering. For this chapter, instead of referring to the reduction/calcination stage, only reduction will be mentioned.

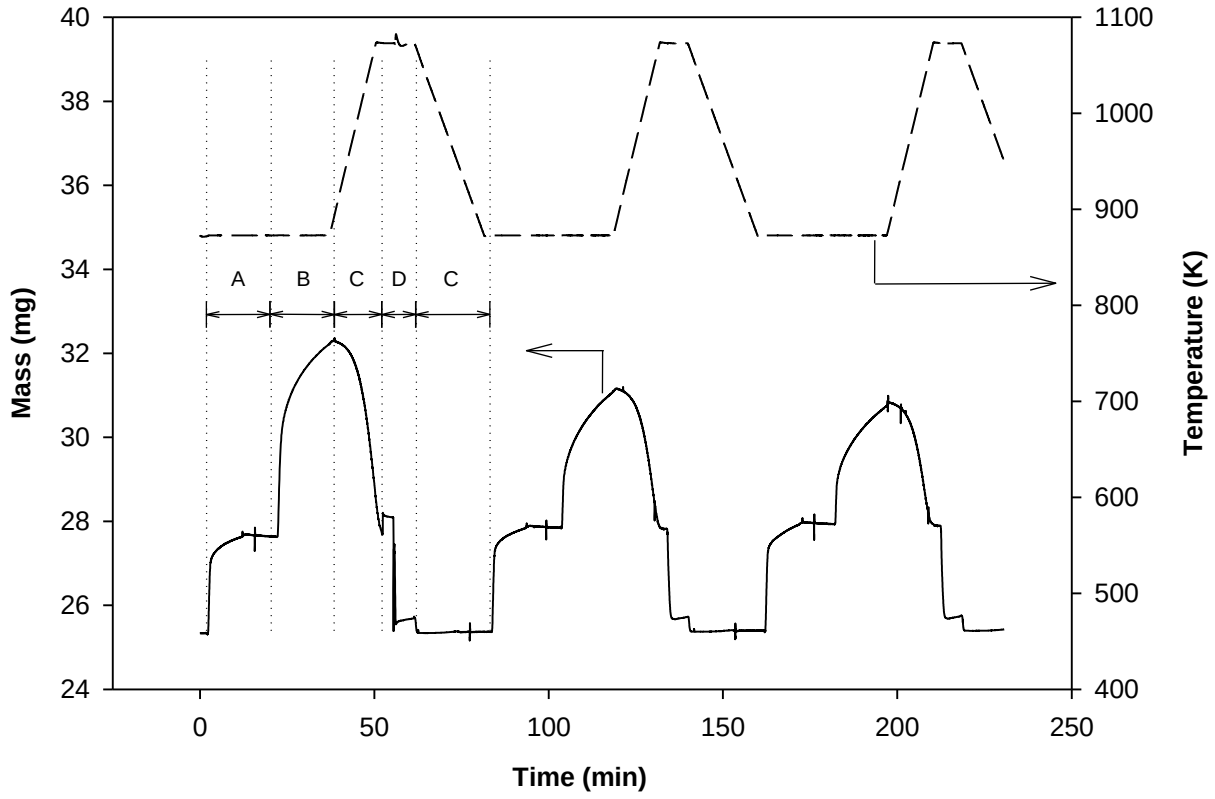

Figure 4.2. Typical experimental cycling of core-in-shell pellets consisting of A: Oxidation with air, B: Carbonation with 20% CO_2/N_2 balance, C: Calcination in N_2, and D: Reduction in CH_4. As shown, the conditions for these cycles were carbonation and oxidation at 873 K, and reduction at 1073 K.

4.2.2 Mass transport

The experimentally observed conversions as a function of time for the carbonation, reduction and oxidation steps are shown and compared with those predicted by the shrinking core model in Figure 4.3. The largest difference is found in the reduction step, while for the oxidation and carbonations steps the differences are smaller. The shrinking core model for the

carbonation step predicts 80% conversion to be achieved in approximately 430 min (~7 h) whereas in TGA experiments this was achieved in ~1200 min (20 h). That is, the model appears to imply faster mass transport than is actually observed. During carbonation, the porosity and pore size are both expected to reduce and some pores may be even blocked, which hinders the access to the inner part of the pellet. Such blockages of pore are not considered in the model.

For the reduction step, the shrinking core model overpredicts the time for complete conversion as 82 min whereas the experimentally observed time is less than 3 min. Since the model assumes mass transport-limited rate of conversion, the experimentally observed rate cannot be attributed to increase in kinetics because a faster kinetics would imply an even more dominant transport limited conversion. From our simple analysis, it would appear that the model considers a significantly reduced diffusivity than that in the real system.

For the oxidation stage, although the shrinking core model is not a good fit to the experimental data, it does follow the same trend and the predicted time for complete conversion compares very well with that observed experimentally. For this step complete conversion was reached in the TGA experiments after approximately 450 min. It is possible that the oxidation is less affected by the reduction of porosity since this reaction is performed when the pellet is calcined and reduced, which means that it is at its highest level of porosity. Unlike the carbonation reaction, for this particular application no study on the kinetics of this reaction has been found in the literature. For the carbonation, it has been reported that the reaction is controlled by the kinetics initially, and subsequently diffusion becomes the controlling mechanism[82]. Based on the similar behaviour during the oxidation stage, the same mechanisms may apply.

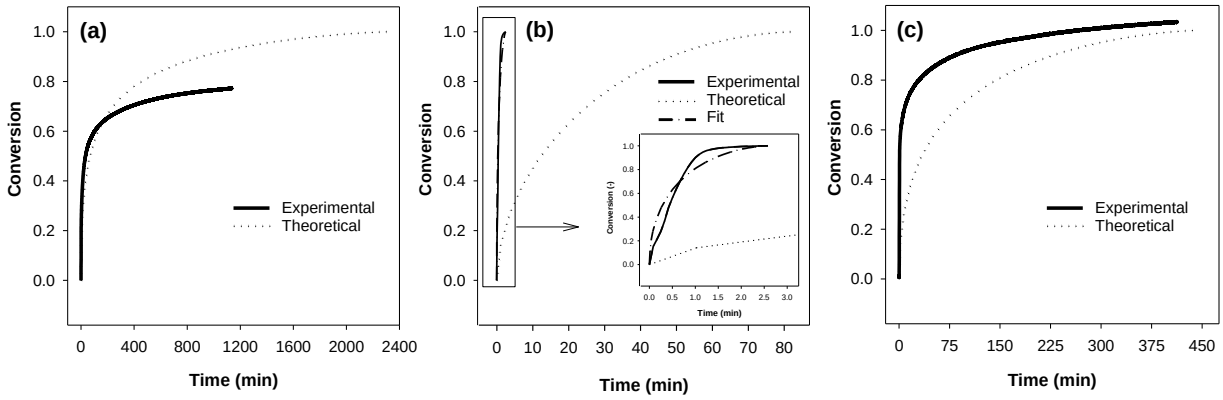

Figure 4.3. Conversion vs time results for each stage with time. Comparison of the experimental results and those provided by shrinking core model - (a) Carbonation reaction (b) Reduction reaction (c) Oxidation reaction.

The differences in the model predictions and experiments point out the need for an improved mass transfer model. For example a two-zone variable diffusivity shrinking core model with expanding product layer[50] may result in a closer match to the experimental data. However, testing different mass transfer models is not trivial. In this study, we have used the conversion versus time obtained from the mass transfer model for carbonation and oxidation stages. For the reduction stage, an empirical fit of the experimentally observed conversion data is employed to determine the heat source term in the heat transfer model. This was accomplished by changing parameter a_1 in equation (4-5). The property/parameter with highest uncertainty in the expression for a_1 (Eqn. 4-5b) is the effective diffusivity. As pointed out, a higher diffusivity would be needed to capture the observed fast conversion. Although the exact reason for the higher diffusivity is not clear, it may be possible that molecular diffusion rather than Knudsen diffusion contributes to the overall diffusivity. Another possibility is that a faster diffusing species, e.g. H_2,

rather than CH_4 serves as the reducing species. Hydrogen could be produced from methane at the copper sites in the converted portion of the pellet.

The evolution of the moving interface with time for each stage, obtained from shrinking core model, is depicted in Figure 4.4 in the form of the ratio R/R_o for each of the three stages. In each of the three stages, the ratio R/R_o follows a linear trend with respect to time except at the beginning and end of the reactions.

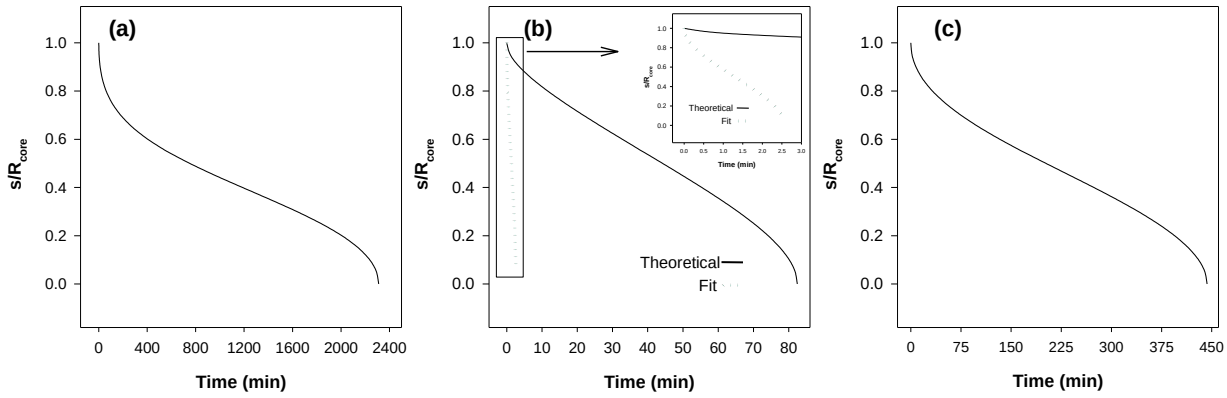

Figure 4.4. Moving boundary (*s(t)*) position relative to pellet's core radius (R_{core}) - (a) Carbonation reaction (b) Reduction reaction (c) Oxidation reaction.

The linearity range for each reaction is different; for carbonation is observed approximately between 400 to 2000 min; for calcination, between 5 to 75 min; and for oxidation between 75 to 375 min. Accordingly, a linear approximation for the R/R_o plots was employed. Again, it must be noted that the mass transport is not the focus of this study and that the results provided by the shrinking core model were used as an input to develop the spatio-temporal temperature profiles. Moreover, based on the results provided by the heat transfer model, we can infer how the results would appear if a more accurate mass transfer model is implemented.

4.3 Heat transfer results

4.3.1 *Temperature evolution with time*

The evolution of the temperature with time for each reaction stage is shown in Figure 4.5. It is important to note that the temperatures shown correspond to the moving boundary, i.e., the point where heat is released. Since each of the reaction stages is exothermic, the temperature at the moving boundary is the maximum temperature reached inside the pellet at any given instance. As expected, the temperature continuously increased with time as long as the reaction proceeds. The largest increase in temperature is obtained for the reduction reaction but this increase is only 6 K. However, this temperature increase is estimated using the mass transfer results from the shrinking core model, which severely over predicted the rate of conversion. Upon using moving interface profile generated by using a modified value of parameter a_1 that matches the experimental data (Figure 4.3b), the estimated temperature increase over time for the actual time of reaction is approximately 33 K.

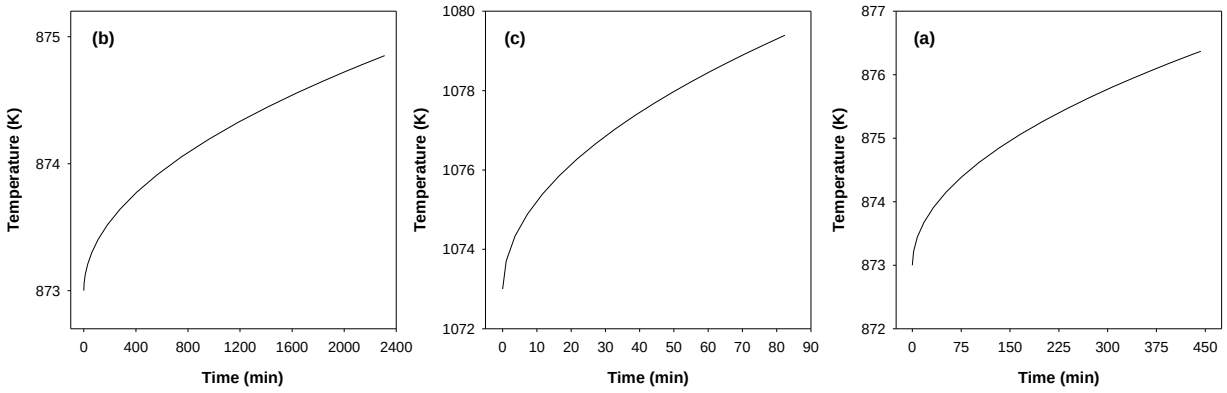

Figure 4.5. Evolution of temperature with time for each stage - (a) Carbonation reaction (b) Reduction reaction (c) Oxidation reaction.

This result would suggest reduction stage may be the most important one for thermal management to reduce sintering related degradation of pellets. Reducing the temperature in this stage could be achieved by slowing down the chemical reaction, which could be accomplished by lowering the operating temperature or using a lower concentration of reducing agent, although that would increase the time of reaction. Nonetheless, sintering could be prevented to some extent and the lifetime of the pellets could be extended.

4.3.2 Temperature difference profiles within the pellet

The temperature difference profiles within the pellet, i.e. difference between the center of the pellet and the external shell, for each stage are illustrated in Figure 4.6. The largest difference, ~3.8 K, is obtained in the reduction stage. For this case, the difference between the non-converted and the converted parts of the core is negligible. It is between the internal part of the shell and the ambient where the 3.8 K difference is observed. For the carbonation and oxidation, the largest differences are smaller than 0.05 K, which means that the entire pellet is at the same temperature. The model indicates that internal thermal resistance is negligible. Further, although the temperature difference is small, it may be recalled that this result is obtained based on the conversion-time response obtained from the shrinking core model. The actual difference may be larger if the process is not transport-limited and the actual reaction rates are faster.

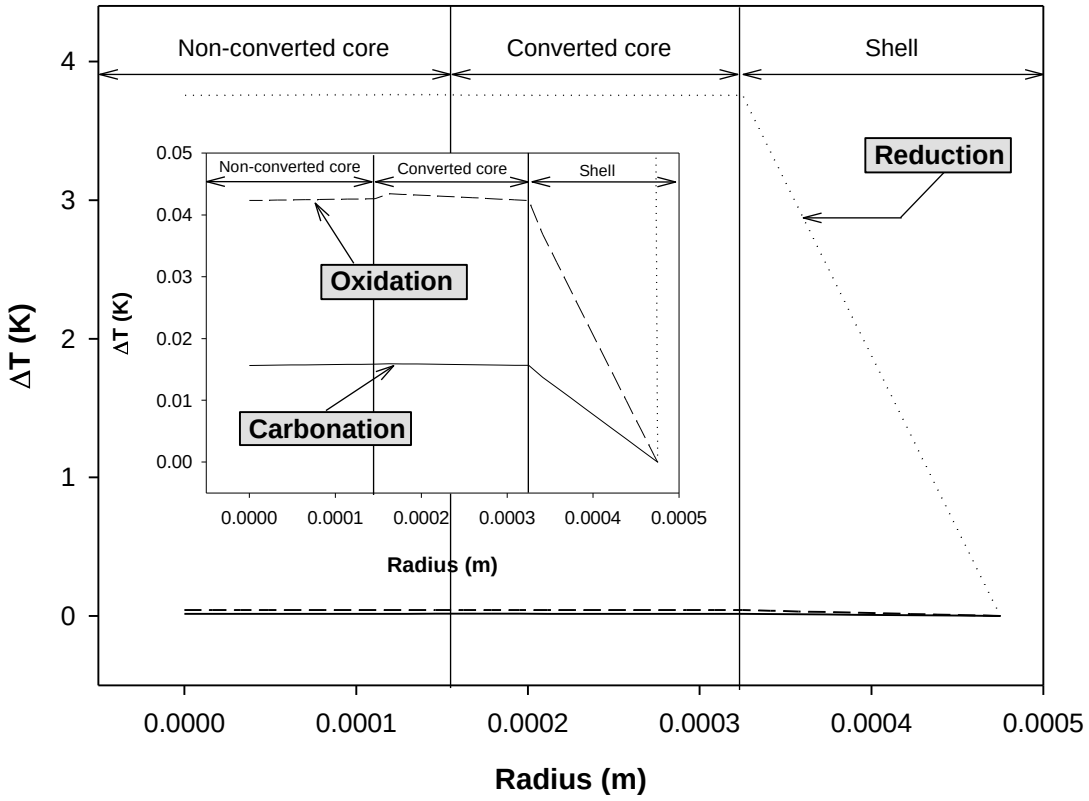

Figure 4.6. Temperature difference profile inside pellet for each stage – Carbonation (750 min), Reduction (44 min), Oxidation (202 min) (LHS ≡ Non-converted core, Centre ≡ Converted core, RHS ≡ Shell).

4.4 Results for different calcination temperatures

The estimated temperature increase for the reduction stage when the actual time of reaction was used was 33 K, which was much larger than any other result. This, along with the observation that the calcination was complete by the time the reduction started (see Figure 4.2), led to the performance of experiments in which the calcination would be carried out at temperatures lower than 1073 K. Hence, 1023 K and 973 K were tested as temperatures for the

calcination stage, and the results are summarized in Table 4.3. After five cycles, the capacity of the pellets to capture CO_2 decreased by 50% when the calcination temperature was 1073 K.

Table 4.3. Results of carbonation percent and capacity loss for different calcination temperatures.

	Cycle					
Temperature (K)	**1st**	**2nd**	**3rd**	**4th**	**5th**	**CCL (%)***
1073	46.9 ± 3.0	35.8 ± 2.2	29.4 ± 2.0	25.7 ± 1.3	23.4 ± 0.9	50.0 ± 1.2
1023	47.1 ± 0.8	36.4 ± 1.2	31.0 ± 1.5	27.5 ± 1.1	25.8 ± 0.9	45.3 ± 1.4
973	42.4 ± 0.7	33.7 ± 2.6	29.8 ± 1.5	25.8 ± 1.0	23.4 ± 0.6	44.7 ± 1.3

*CCL = CO_2 Capacity Loss

On the other hand, at 1023 K, the capacity to capture CO_2 decreased by 45%, although it took 10 min instead of 3 min to reach full conversion. However, it must be noted that at this temperature, unlike the case where calcination was performed at 1073 K, the carbonate was only partially decomposed when CH_4 started to be fed, which means that the heat of combustion could be used to decompose the carbonate. Likewise, at 973 K, the capacity decreased by 45%, which is similar to the loss at 1023 K. However, at this temperature, the time of reaction was 30 min, which is significantly longer than the time needed to reach complete conversion at 1073 K (3 min), and at 1023 K (10 min).

Therefore, as it was commented before, it is observed that the temperature for the calcination stage plays an important role in the process. At 1023 K the capacity to capture CO_2 decreased by 5% less than at 1073 K, with minimal time increase. Similar reduction of the

capacity loss is obtained when the temperature is further decreased to 973 K, but with the drawback of the CH_4 consumption.

4.5 Chapter summary

The theoretical model developed to simulate the temperature profile of the core-in-shell pellets has shown that the temperature profile inside the pellets, under the conditions used in the process, was small enough to assume uniform temperature at all times. On the other hand, the model has also shown that the maximum temperature increases for each stage were 2 K for the carbonation reaction, 6 K for the reduction reaction and 3 K for the oxidation reaction. However, in the actual process the temperature increase for the reduction stage would likely be larger because the time of reaction predicted by the shrinking core model was more than 25 times longer than the actual time of reaction. The estimated temperature increase was 33 K.

Therefore, decreasing the temperature for this stage was suggested in order to diminish the temperature rise and, accordingly, preliminary tests were conducted. After five cycles, the capacity loss is reduced by 5% when the reduction/calcination is performed at 1023 K and 973 K. However, the times of reaction were longer than at 1073 K, especially at 973 K, for which the time was 10 times longer (i.e. 30 min). This fact resulted in a larger consumption of methane.

Chapter Five - Performance of homogeneous pellets over multiple CaL/CLC cycles

After developing the heat transfer model and demonstrating better performance of the pellets at lower calcination temperatures, the conditions for the calcium looping and chemical looping combustion cycles needed to be changed based on the energy balances and partial pressure limitations. The energy balances performed by our collaborators at the University of Ottawa determined that the temperatures for every stage needed to be higher. The temperatures were increased to 923 K, 1148 K and 1173 K for the carbonation, calcination/reduction, and oxidation, respectively. For the calcination/reduction it is important to remark that the temperature was increased because the content of CO_2 in the calciner would be high as part of the CO_2 separated in the process would be recycled for fluidization purposes. Therefore, in order to reach the equilibrium pressure, the temperature needed to be increased. Otherwise, based on the Le Chatelieur's principle, the calcination could not be achieved because the partial pressure of CO_2 in the reactor would prevent the calcination reaction from occurring.

In addition, the configuration of pellets was narrowed to only homogeneous pellets. The attrition tests performed at the École Polytechnique de Montréal demonstrated that the core-in-shell structure behaved similarly to the homogeneous configuration, and the latter one involved a less complicated process of manufacturing. Furthermore, the fluidization tests, which were also performed at École Polytechnique determined that the size of the pellets should be smaller. Consequently, instead of 0.425-1.425 mm, the range was reduced to 0.250-0.600 mm.

Therefore, the performance of homogeneous pellets with different compositions at the conditions mentioned was studied, and the results are provided in this chapter. The flowrates and compositions of the gases did not change, i.e., 300 ml/min for furnace, heating and reaction gases

and 330 ml/min for the purge gas. For the experiments that are about to be discussed, the number of cycles was increased to 20 because the modified setup of the TGA enabled this option.

Depending on the pellet composition, a different maximum number of cycles could be performed: pellets containing CaO and CE (90/10), and CuO and CE (50/50) were subjected to 20 cycles, while composite pellets with CuO, CaO and cement (50/40/10), which required additional oxidation step, were only subjected to 16 cycles. The TGA software could only handle a total of 99 steps - each heating ramp was a step, each time that the temperature was kept constant was another step and each cooling ramp was another step. Therefore, each cycle involved 6 steps, and the breakdown is shown in Table 5.1.

Table 5.1. Steps required per cycle of combined CaL and CLC, and per cycle of only CaL.

Step	Combined Calcium Looping and Chemical Looping Combustion	Calcium Looping
1	Constant temperature for carbonation (923 K)	Constant temperature for carbonation (923 K)
2	Heating ramp from 923 to 1148 K	Heating ramp from 923 to 1148 K
3	Constant temperature for calcination/reduction (1148 K)	Constant temperature for calcination (1148 K)
4	Heating ramp from 1148 K to 1173 K	Cooling ramp from 1148 to 923 K
5	Constant temperature for oxidation (1173 K)	-
6	Cooling ramp from 1173 to 923 K	-

The TGA software only allowed up to 99 steps, which is almost the number of steps for 16 cycles of combined Calcium Looping and Chemical Looping Combustion (96). In contrast, for the pellets with compositions 90/10, and 50/50 fewer steps were required because these compositions were subjected to cycles of only carbonation/calcination, or oxidation/reduction. The same number of steps was required for both compositions. The breakdown of steps for Calcium Looping is also summarized in Table 5.1.

In total, four steps per cycle were required, which enabled to perform more than 20 cycles. However, the scope of this thesis was to enhance the performance of the pellets over cycles rather than only study their performance over cycles. Furthermore, the first target number of cycles was 15, which makes 20 a reasonable number of cycles for this thesis. Also, note that for the composite pellets the limit of 15 cycles was also achieved.

In this chapter, in addition to the study of the performance of each composition of pellets, the analysis of the surface area, pore volume and pore size distribution is provided.

5.1 Results of surface area, pore volume and pore size distribution

The analysis of the surface area, pore volume and pore size distribution was performed three times for each composition of pellets. The results of surface area and pore volume are summarized in Table 5.2. The two compositions of pellets that were developed for the dual configuration of reactors, i.e., 50/50 and 90/10, had surface areas higher than the composite pellets, 50/40/10. If we compare these two compositions, the 50/50 pellets have the highest surface area. According to the literature, CuO usually presents low values of surface area and pore volume[97]. However, it must be noted that this composition of pellets has a high proportion

of cement, which contains alumina, a support that has high surface area. Therefore, the higher surface area for the 50/50 is probably associated with the higher content of alumina.

Table 5.2. Results of surface area and pore volume.

Composition	**S_{BET} (m^2/g)**	**V_p (cm^3/g)**
50% CuO, 40% CaO, 10% Cement (50/40/10)	15.2 ± 1.1	0.078 ± 0.006
90% CaO, 10% Cement (90/10)	19.7 ± 0.6	0.112 ± 0.008
50% CuO, 50% Cement (50/50)	34.2 ± 3.1	0.052 ± 0.004

On the other hand, the pellets with 90/10 had smaller surface area than the 50/50 pellets, but the highest value of pore volume. It must be taken into account that high surface area does not necessarily involve large pore volume. For example, a sample with many micropores can provide a high surface area. However, if all the micropores are combined, in the end a large pore, with lower surface area, would be obtained, and that pore would have exactly the same volume as all the micropores together (see Figure 5.1).

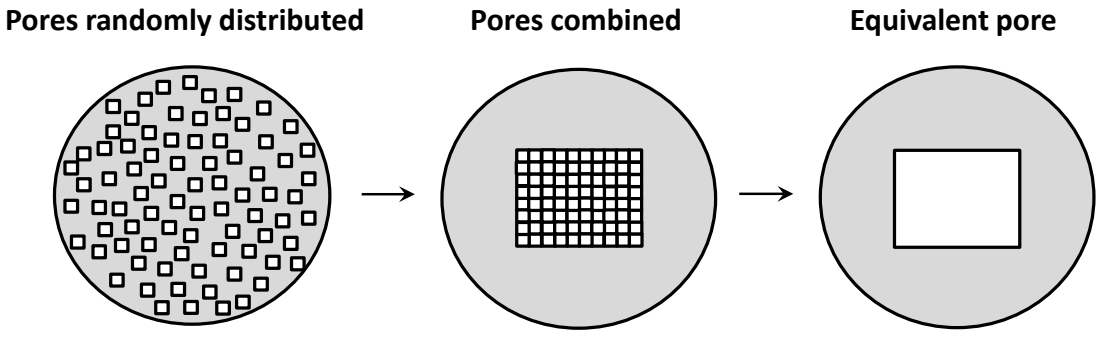

Figure 5.1. Schematic showing that surface area and pore volume are not directly related.

In Figure 5.2 it can be observed that for the pellets with 50% CuO and 50% CE, the majority of the pores were located within the micro and meso-pore ranges (w<20 Å and 20 Å <w<500 Å respectively)[81], while for the pellets with 90% CaO and 10% CE, most of the pores were within the meso and macro-pores (w>500 Å) ranges. Therefore, based on the explanation given, this result is consistent with the pore volume and surface area results; the 50/50 pellets had the highest surface area because most of the pores were located in the micro and meso-pore ranges, but since the surface area was very low, the total pore volume is consequently very small. On the other hand, the 90/10 pellets had less surface area than the 50/50 pellets because most of the pores were within the meso and macro-pore ranges, but, as opposed to the surface area, they had a larger pore volume.

As for the composite pellets (50/40/10), they had an intermediate pore volume; according to Figure 5.2, for this composition there is a combination of the results obtained for the 50/50 and 90/10 pellets, i.e., there are micro, meso and macropores. However, the mesopores seem to be the most common based on the number of points located within that range for both compositions.

In summary, the pellets with composition of 50/40/10 had the smallest surface area and intermediate pore volume with respect with the other two compositions, 90/10 and 50/50. The pore size distribution indicated that the majority of the pores were located within the mesopore range, followed by the micro and macro-pore ranges. The 50/50 composition provided the highest surface area but also the lowest pore volume. In this case, the majority of the pores were located within the micro and meso-pore ranges, without any sign of macropores. Last, the 90/10 pellets provided the second highest surface area, and the largest pore volume. The pore size distribution indicated that the majority of the pores were located within the mesopore range.

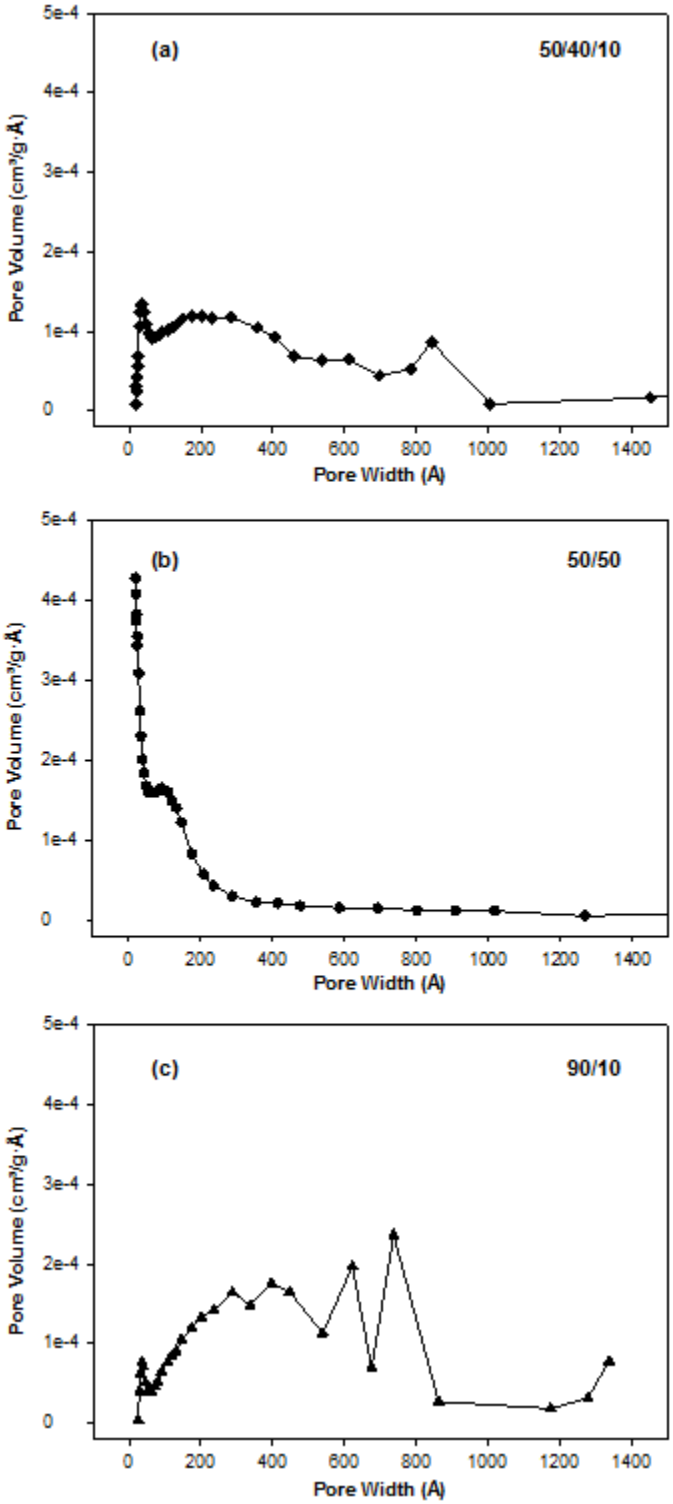

Figure 5.2. Pore size distributions of each composition of pellets – (a) 50% CuO, 40% CaO, 10% CE; (b) 50% CuO, 50% CE; (c) 90% CaO, 10% CE.

Taking into consideration these results, it could be inferred what would be trend of the surface area and pore volume when the composition of the pellets changes. For instance, after carbonation, the 90/10 pellets will have smaller surface area and pore volume because the CO_2 molecules will occupy the void space. Eventually, the diffusion of the CO_2 molecules will be hampered because the void space will have diminished, which is in agreement with the preliminary results provided in Chapter Three. Likewise, the 50/50 pellets will have larger pore volume and surface area after reduction since the Cu atom is smaller than the CuO molecule. Same comments apply for the composite pellets, 50/40/10.

5.2 Results of performance of pellets with 50% CuO, 40% CaO and 10% CE (50/40/10)

This composition of pellets is the same as that of the first batch of pellets (see Table 3.1). The homogeneous configuration of the first batch was not tested because the size of pellets was recommended to be reduced before any experiment with the homogeneous pellets could be performed. Nonetheless, even if any experiment would have been carried out, since the size of pellets is smaller than that of the first batch, studying this composition is necessary in order to compare its performance with that of the other two compositions prepared in the second batch.

The 50/40/10 composition could only be studied for 16 cycles because of the reasons that have been explained at the beginning of this chapter. Each experiment was repeated three times to check the reproducibility, and for the study of errors. An example of the TGA report is illustrated in Figure 5.3. To better understand Figure 5.3, Figure 5.4 shows the first cycle in detail. Also, to guide the reader through Figure 5.3, labels for each cycle have been added.

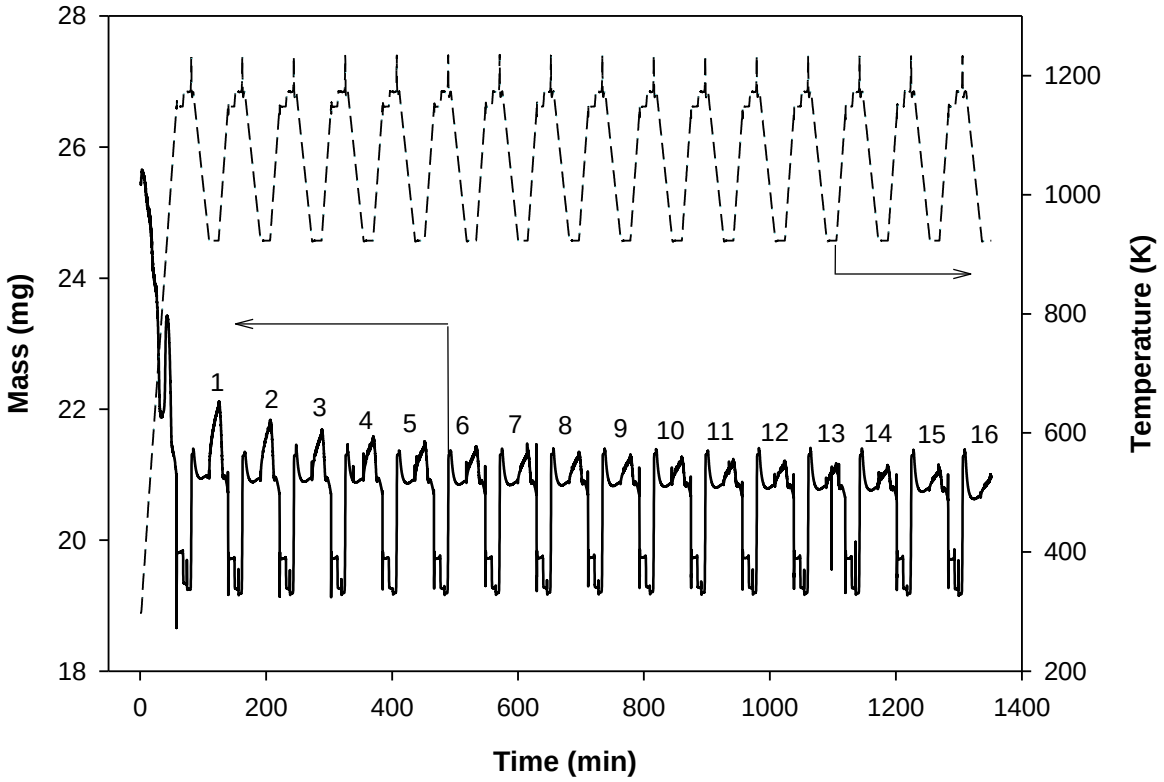

Figure 5.3. TGA report of 16 cycles of calcium looping and chemical looping combustion for 50/40/10 homogeneous pellets.

Figure 5.4 shows the moment after the pellets have been calcined at 1148 K under pure CH_4. The temperature is then increased to 1173 K to perform the oxidation step (A). The gas used for this step is air, and it is fed for 10 min. Afterwards, the sample needs to be cooled to 923 K to perform the carbonation. The cooling takes approximately 25 min and the carrier gas used for this step is N_2. Then, once the cooling is completed, the carbonation (B) is carried out by feeding the mixture of 20% CO_2/N_2 balance into the TGA for 15 min. Next, the sample is heated to 1148 K under N_2 to perform the calcination/reduction step. As the sample is heated, the decomposition of $CaCO_3$ is occurring (C).

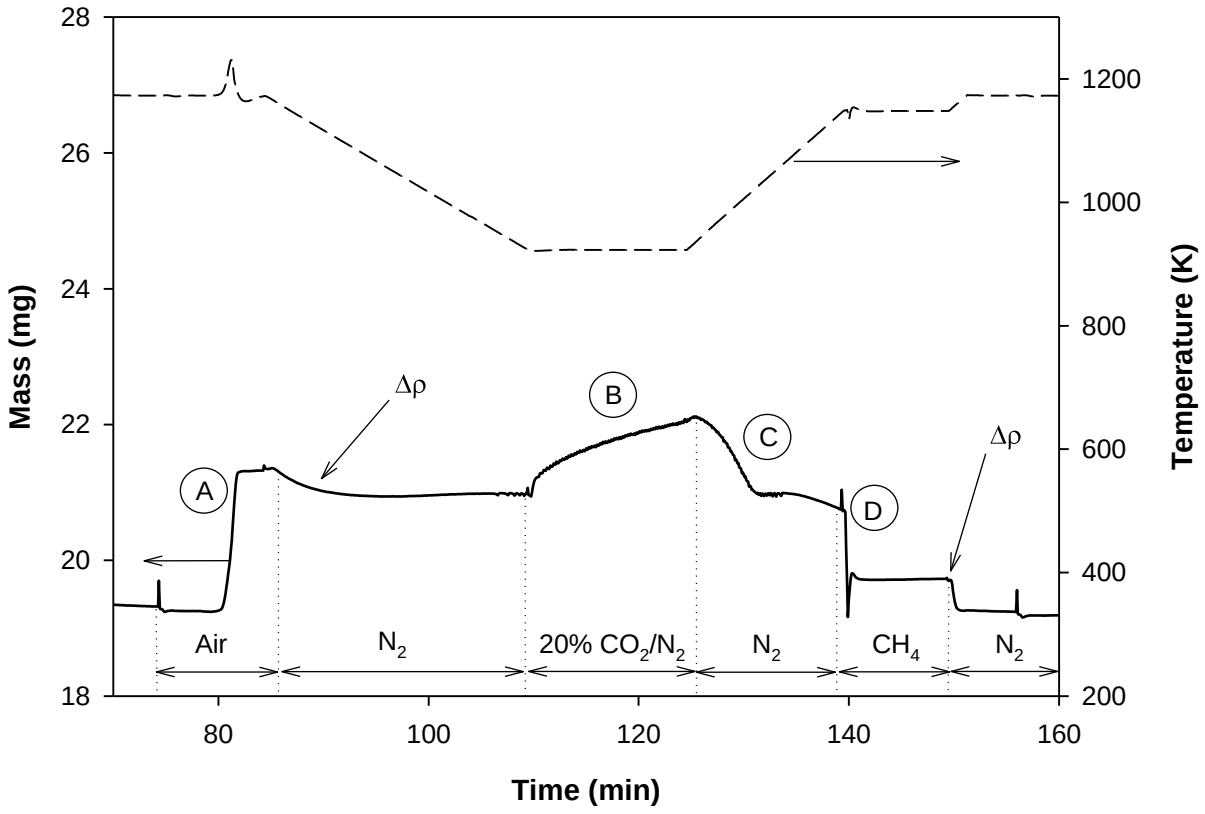

Figure 5.4. Magnification of first cycle of calcium looping and chemical looping combustion with 50/40/10 pellets shown in Figure 5.3. (A) oxidation, (B) carbonation, (C) calcination, (D) reduction. *Δρ* are differences of buoyancies due to either the change of temperature or change of gas.

This phenomenon is unavoidable since it depends on the temperature of decomposition of the carbonate, which according to the literature[98] is within the range of ~910 K to ~1140 K. At 1148 K, CH_4 is fed for 10 min, although the reduction of CuO and decomposition of any remaining $CaCO_3$ takes place in approximately 3 min (D). After this step, the next cycle starts.

Also, in Figure 5.4 there are two significant drops, labelled as Δρ, that are worth mentioning. These drops are due to different densities; in the first case, the gas is switched from air to N_2, and although there is not a significant difference between the densities of these two gases, the temperature is decreased from 1148 K to 923 K, which affects the density of the gas, making it heavier at 923 K than at 1148 K. Therefore, the mass of sample decreases since the buoyancy produced by the gas is stronger. As for the second drop, the difference of density is more noticeable because the gas is switched from CH_4 to N_2. In this case, the density of methane is almost half the density of N_2 (0.65 kg/m^3 of CH_4 versus 1.13 kg/m^3 of N_2 at 298 K)[99]. Thus, when the gas is switched, the mass of sample decreases dramatically because the buoyancy in N_2 is different than the buoyancy in CH_4.

In Figure 5.3, the carbonation becomes less significant as the number of cycles increases. It is within the first five cycles where the decrease is more noticeable, and as per previous discussion, it is believed to be due to sintering. Another hypothesis for the loss of capacity to capture CO_2 is that part of the CaO reacts with the cement, thus reducing the amount of CaO for CO_2 capture. To test this hypothesis, two XRD analyses were performed, 1) with raw 90/10 pellets, and 2) with 90/10 pellets subjected to 50 cycles of carbonation/calcination. The results are summarized in Table 5.3, and the spectra are included in Appendix D.1 (Figure D.1 and D.2). The data provided in this table is approximated and it does not represent the exact composition since the analyses were conducted to obtain an estimate and determine whether the fraction of CaO changed over time. Nevertheless, it can be seen that mayenite is present ($Ca_{12}Al_{14}O_{33}$) in the pellets subjected to 50 cycles. In the literature it has been reported that katoite ($Ca_3Al_2(OH)_{12}$) is the precursor for mayenite[100], as is shown below:

$$7\ Ca_3Al_2(OH)_{12} \rightarrow Ca_{12}Al_{14}O_{33} + 9\ CaO + 42\ H_2O \qquad (5\text{-}1)$$

However, according to Eqn. 5-1, and based on the results provided in Table 5.3, it is not feasible that the mayenite was exclusively formed from the katoite (see Appendix D.2 for calculation). The formation of this compound has also been observed in Ca-Al-based sorbents[101]. Therefore, part of the loss of capacity could be associated to the formation of mayenite.

Table 5.3. Results of XRD analyses of 90/10 pellets prior and after carbonation/calcination cycles.

Pellets	Components	Chemical formula	Mass fraction (%)
90/10 (raw)	Portlandite	$Ca(OH)_2$	74.5
	Katoite	$Ca_3Al_2(OH)_{12}$	6.3
	Calcite	$CaCO_3$	17.9
	Quartz	SiO_2	1.4
90/10 (after 50 cycles)	Lime	CaO	89.9
	Mayenite	$Ca_{12}Al_{14}O_{33}$	10.1

On the other hand, the oxidation remains stable over cycles, which means that the Cu/CuO does not lose capacity to be re-oxidized. This fact also means that the CuO does not suffer from sintering, or if it does, it does not affect its capacity for oxidation. Also in both Figures 5.3 and 5.4, there is a spike in the temperature during the oxidation. This issue was associated with carbon deposition, which was already suggested in Chapter Four. In the literature, other authors have also reported carbon formation while using CH_4 at high temperatures[102,103]. As a matter of fact, at the end of some experiments, a black residue was observed on the hanging wire of the TGA, but no further analysis was performed on this residue.

Although the study of this issue was not included in the scope of this thesis, in order to confirm this hypothesis and explain the temperature spikes, separate experiments were conducted and the results are presented in the next section.

The results corresponding to this composition of pellets are summarized in Table D.1 (Appendix D.3); for this section, in Table 5.4 there is an extract of Table D.1, and it provides the results of the first and last cycle, which are the most significant for the discussion. The methodology to calculate each parameter, as it was already mentioned in Chapter Three, it can be found in Appendix B.6.

Table 5.4. Results of performance of 50/40/10 pellets for first and last cycle.

Cycle	$\chi_{oxidation}$ (%)	$\chi_{carbonation}$ (%)	O_2 Capacity (gO_2/gPellets)	CO_2 Capacity (gCO_2/gPellets)	OCL (%)[a]	CCL (%)[b]
1	85.3 ± 2.6	16.0 ± 1.8	0.107 ± 0.003	0.050 ± 0.005	N/A	N/A
16	88.2 ± 1.7	4.2 ± 1.0	0.111 ± 0.002	0.013 ± 0.003	-3.5 ± 1.2	73.2 ± 8.1

a. O_2 Capacity Loss
b. CO_2 Capacity Loss

For this composition of pellets, the oxidation capacity remained constant over cycles, even showing a slight improvement after 16 cycles, which demonstrates the stability of Cu/CuO, and its good performance as oxygen carrier. After 16 cycles, the oxygen capacity was 0.111 gO_2/gPellets. In contrast, the carbonation capacity decreased dramatically, losing more than 70% of the capacity after 16 cycles. This loss in capacity (CCL) is depicted in Figure 5.5. Within the first 5-6 cycles, already more than 50% of the capacity is lost. Initially, the capacity was 0.050 gCO_2/gPellets, but after 16 cycles, decreased to 0.013 gCO_2/gPellets.

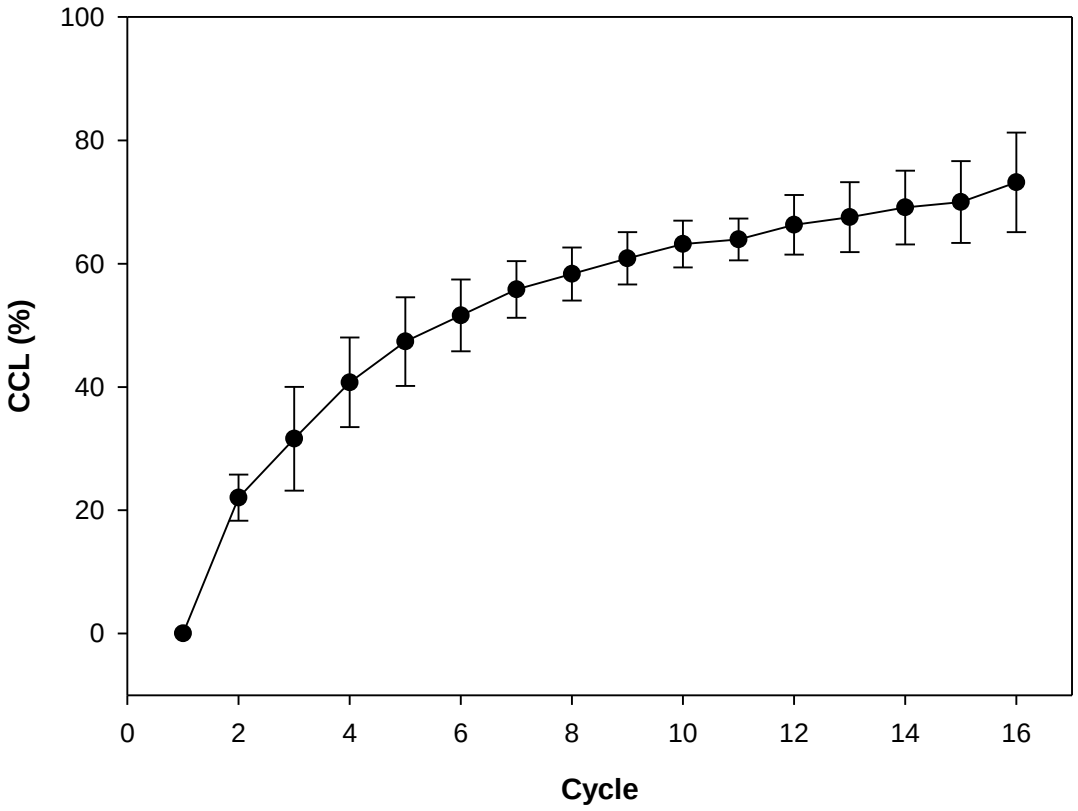

Figure 5.5. CO_2 capacity loss CCL (%) vs cycles for 50/40/10 pellets. Error bars represent the confidence interval.

In summary, the composition of pellets 50/40/10 showed a good performance over cycles in terms of oxidation capacity. However, regarding the capacity to capture CO_2, it diminishes significantly after only 5-6 cycles, and up to 73% after 16 cycles. Also, in these experiments was observed that carbon deposition may be occurring during the reduction, which affected the temperature during the oxidation step.

5.3 Carbon deposition due to use of CH_4 of high purity at high temperature

In Chapter Four it was already suggested that during the reduction stage it was possible that hydrogen could be produced since the effective diffusivity that was obtained to fit the experimental results for this stage was higher than the theoretical diffusivity based on CH_4, CO_2 and water/steam being present. However, the time predicted for this stage was much longer than the actual time of reaction. By changing the value of the diffusivity it was possible to achieve a good fit for this stage, and the final value suggested that other gases with higher diffusivities could be present, with hydrogen being one of possibilities.

According to the results shown in Section 5.2, this hypothesis takes more relevance since it seems reasonable that hydrogen is produced as a result of the carbon deposition. In order to test this hypothesis, a test in which no crucible was placed into the TGA was conducted. The purpose of this test was to check first if the carbon deposition was due to the presence of pellets or not.

For this test, the outlet gases were analyzed by means of the ABB Gas Analyzer. This instrument enables the analysis of CO, CO_2, H_2 and CH_4. The result of the test is illustrated in Figure 5.6. The steps followed for this test were the same as those used for a normal test of the 50/40/10 pellets with the only exception that CH_4 was fed for 30 min instead of 10 min with the purpose of ensuring enough time to observe whether there was formation of H_2 or not. As CH_4 was fed into the TGA, the ABB detected the presence of H_2, as well as small fractions of CO and CO_2. The curve for CH_4 reaches a plateau because the concentration was higher than the upper level of the detector. The brief formation of CO and CO_2 could be due to the presence of remaining oxygen in the line. This result is in agreement with the idea that the black residue observed on the hanging wire was indeed carbon. Once the flow of CH_4 was stopped, and the line purged with N_2, air was fed into the TGA and then the presence of CO and CO_2 was

detected, which suggests the oxidation of the carbon residue. Also, to understand the fact that the carbon deposited onto the hanging wire surface, the nature of this material, platinum, must be taken into account. Deposition of carbon on platinum surface has been reported by other authors who used ethylene at high temperatures (700 – 1400 K)[104].

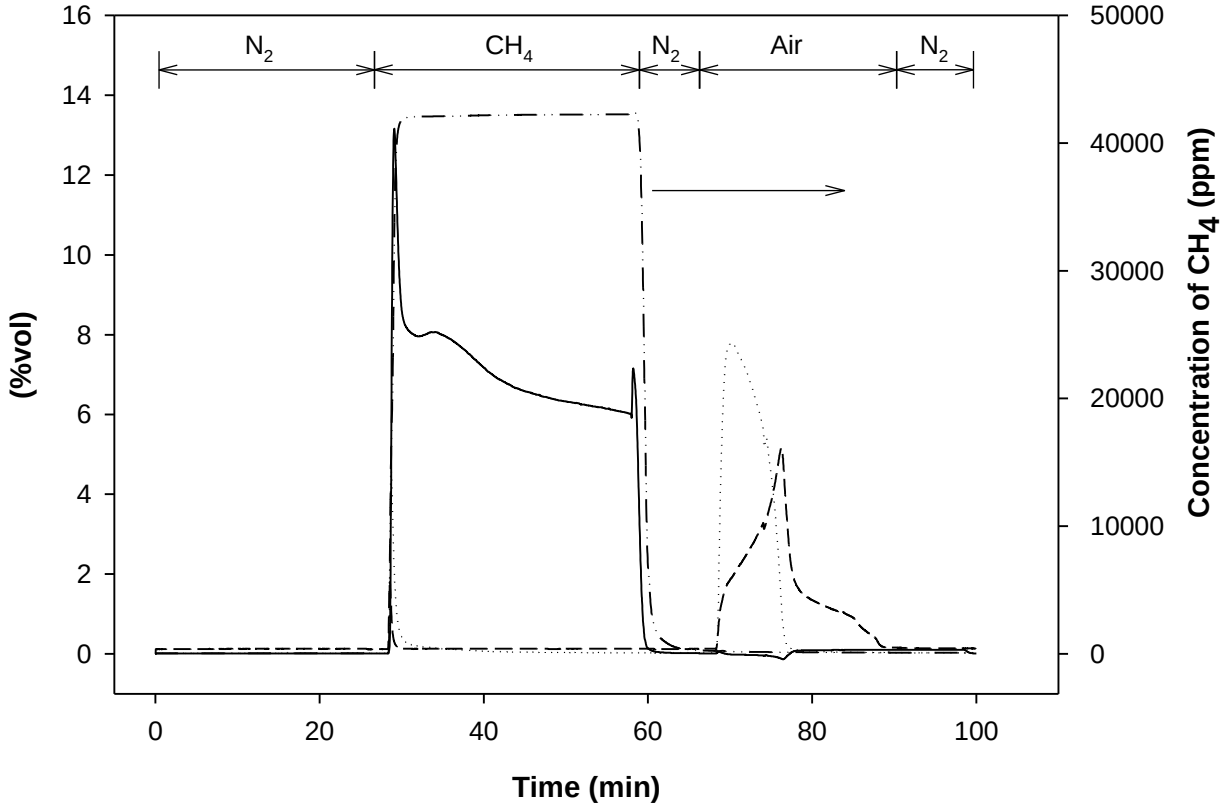

Figure 5.6. Analysis of the outlet gases for test of carbon deposition. —— H_2 (%vol.); ····· CO (%vol.); – – – – CO_2 (%vol.); —·—· CH_4 (ppm).

Further analysis of Figure 5.6 was performed in order to determine if the amount of H_2 detected was consistent with the amounts of CO and CO_2. To that end, the areas under the curves of H_2, CO and CO_2 were calculated, and the values were 217 for H_2, 53 for CO and 48 for CO_2. It is important to note that the moles of H_2 are double the moles of CO and CO_2 respectively,

because from each molecule of CH_4, two molecules of H_2 and one molecule of C are obtained, as is shown in Equation 5-1. Thus, the area of H_2 should be two times the combined area of CO and CO_2. The combined area of CO and CO_2 is 101, which means that the area for H_2 should be 202. Therefore, there is a slight deviation between the amount of H_2 detected and the combined amounts of CO and CO_2. That deviation could be associated to the accuracy of the analyzer. Nonetheless, the results were considered consistent since the deviation was less than 7%.

$$CH_4 \rightarrow C + 2\,H_2 \qquad (5\text{-}2)$$

Note that in addition to the formation of carbon deposits on the hanging wire, it could be possible that the pellets also promoted the formation of carbon deposits[105]. However, for this thesis, no further investigation was performed since the goal was to determine whether the formation of carbon was occurring or not.

In summary, the test performed shows that, even though the presence of the pellets could be affecting the formation of the carbon deposits, its formation took also place separately from the pellets. This information could support the change of the diffusivity that was made to fit the experimental data in Chapter Four since the formation of hydrogen using CH_4 at high temperatures has been detected.

5.4 Results of performance of pellets with 50% CuO and 50% CE (50/50)

This composition of pellets was designed for the dual configuration of reactors that was described in detail in the Introduction. In this dual configuration, instead of composite pellets of CuO, CaO and cement, pellets with only CuO and cement (50/50), and pellets with only CaO and cement (90/10) were considered. The 50/50 pellets would circulate between the calciner and the air reactor, going through reduction and oxidation in each reactor, respectively.

For this configuration of reactors, it is interesting to have a high content of CuO to guarantee that enough energy would be produced to carry out the decomposition of $CaCO_3$. To start, it was considered to test pellets with the same content of CuO as those with the composition of 50/40/10. As per the comments made at the beginning of this chapter, this composition of pellets could be tested for 20 cycles, and the conditions used were the same as those that were used for reduction and oxidation for the 50/40/10 pellets, i.e., 10 min for reduction at 1148 K under pure CH_4, and 10 min for oxidation at 1173 K under air. In Figure 5.7, the first cycle is depicted to illustrate these steps.

On the other hand, in Figure 5.8 the full TGA report that was obtained in one of the experiments is shown. The capacity of the pellets to be re-oxidized multiple times remained stable after 20 cycles, as it happened with the 50/40/10 composition. Also, this composition of pellets showed a better performance after 20 cycles (2-3%), which confirmed the result obtained for the 50/40/10 pellets.

However, this composition presented one drawback, which was agglomeration. This issue might not become relevant in a fluidized bed reactor since the pellets would not be static but in continuous movement. In the TGA experiments, this phenomenon was observed when the pellets were removed from the crucible. The full sample was agglomerated and it was necessary to use the tweezers to remove the pellets. In addition, a pink residue remained on to the surface of the crucible, which was associated to Cu based on the colour and the recently observed agglomeration issue.

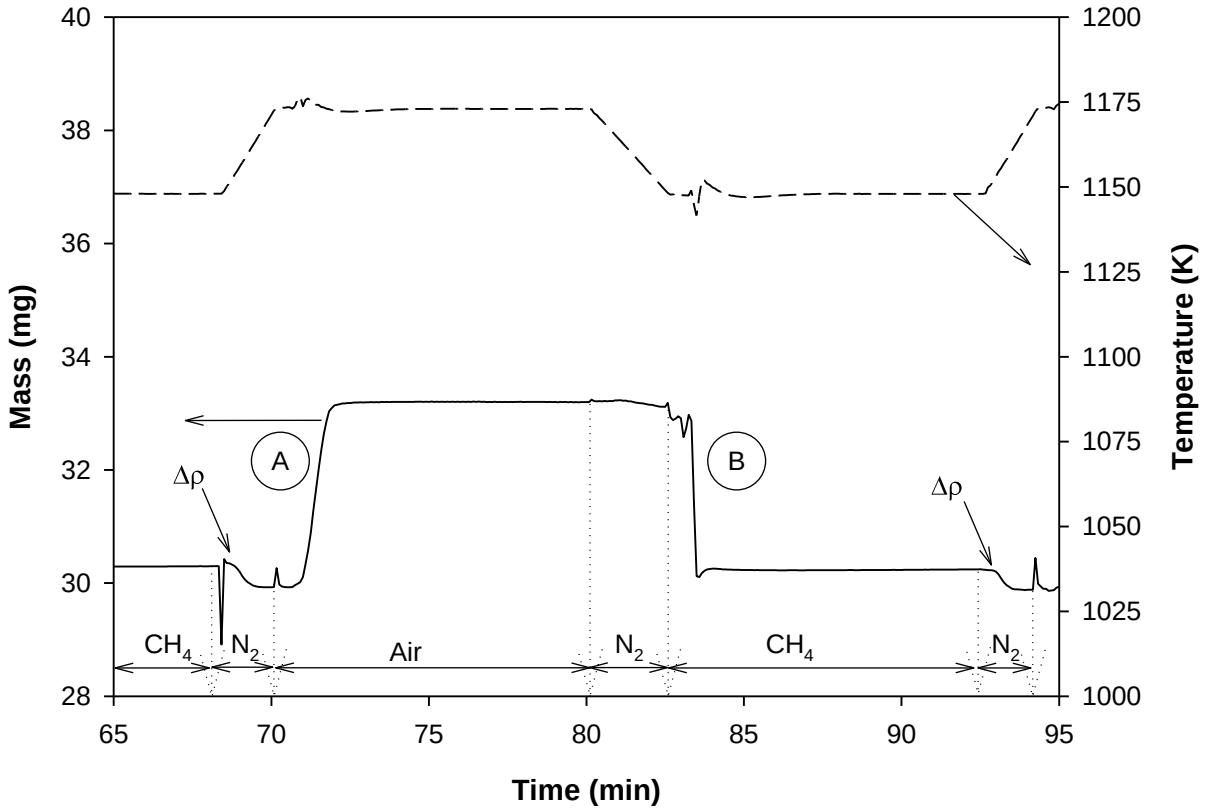

Figure 5.7 Magnification of first cycle of chemical looping combustion with 50/50 pellets. (A) oxidation; (B) reduction. *Δρ* are differences of buoyancies due to change of gas.

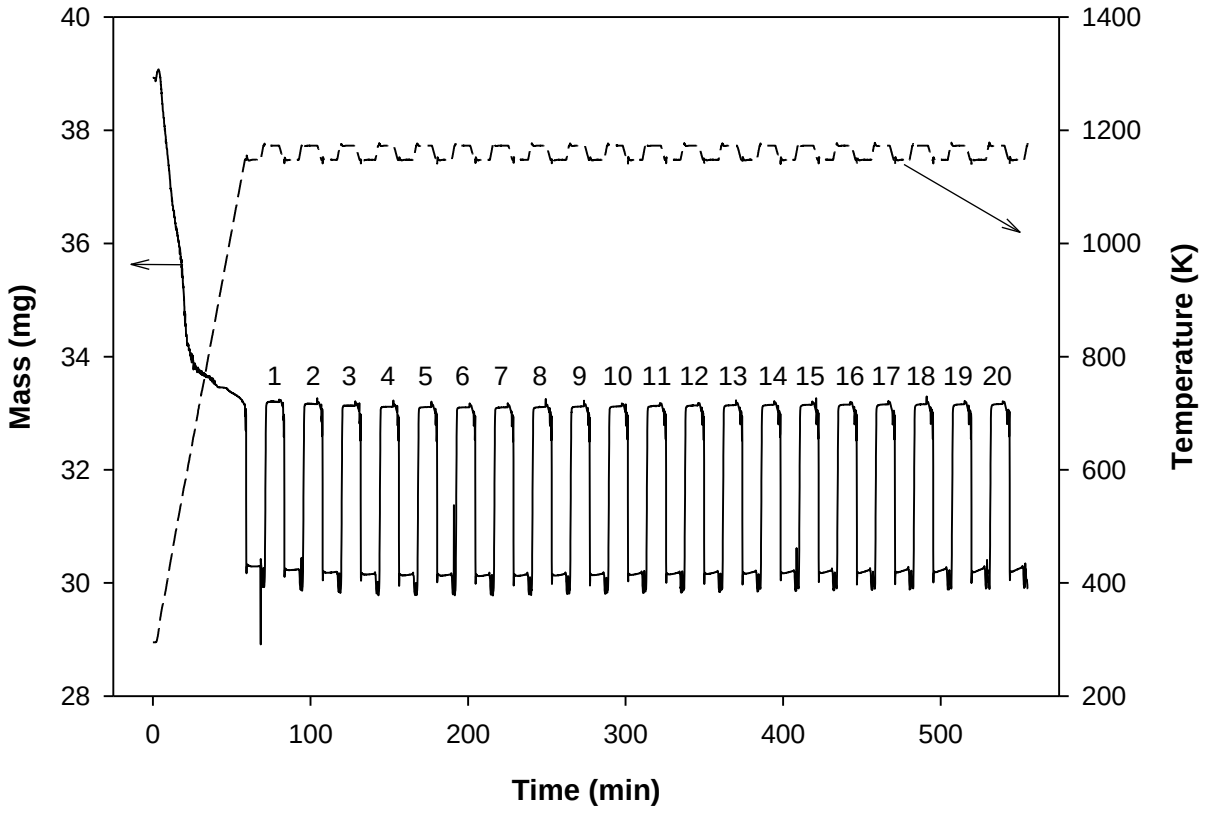

Figure 5.8. TGA report of 20 cycles of chemical looping combustion for 50/50 homogeneous pellets.

The full table of results for this composition can be found in Appendix D.3 (Table D.2), but in this section only the results for the first and last cycle are provided (Table 5.5). The level of conversion remained within the same range (almost 80%) after 20 cycles. Also, comparing the gO_2/gPellets after 20 cycles with those of the 50/40/10 pellets after 16 cycles, the values are similar, which is reasonable since the loading of CuO is the same in both compositions.

Table 5.5. Results of performance of 50/50 pellets for first and last cycle.

Cycle	$\chi_{oxidation}$ (%)	O_2 Capacity (gO_2/gPellets)	OCL (%)*
1	87.8 ± 1.7	0.111 ± 0.002	N/A
20	89.2 ± 3.4	0.112 ± 0.004	-1.6 ± 2.4

*OCL ≡ O_2 Capacity Loss

5.5 Results of performance of pellets with 90% CaO and 10% CE (90/10)

The dual configuration of reactors involves, in addition to the 50/50 pellets, the 90/10 pellets, which would circulate between the carbonator and the calciner. In this case, it is interesting to have a high loading of CaO so that the capture of CO_2 would be high as well. This composition of pellets, as well as the 50/50, could be tested over 20 cycles. The conditions used were 15 min for carbonation, under a mixture of 20% CO_2/N_2 balance, and 3 min under N_2 for the calcination. As opposed to the time for calcination/reduction that was used for the composite pellets (10 min), for these tests the calcination stage was reduced to 3 min because the decomposition of $CaCO_3$ took place while the pellets were heated. Since for this composition of pellets it was not necessary to perform the reduction, there was no reason to extend the time for this stage. In Figure 5.9 the steps followed for each cycle of carbonation and calcination are shown. Then, Figure 5.10 depicts the full report obtained after 20 cycles, in which each cycle has been labelled.

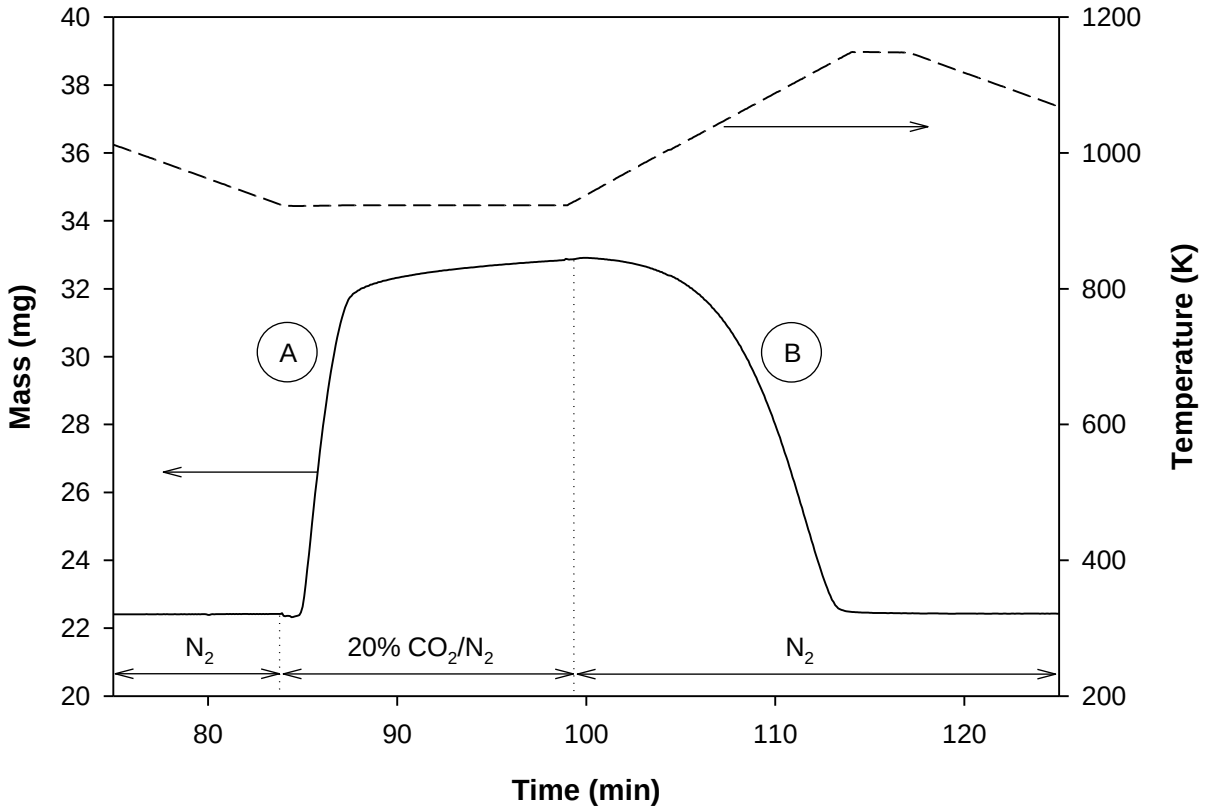

Figure 5.9. Magnification of first cycle of calcium looping. (A) carbonation; (B) calcination.

Recalling what has been commented regarding the time for the calcination, in Figure 5.9 even before the temperature for calcination was reached (1148 K), the mass of sample had returned to the initial point. Therefore, this supports the idea that extending the time for calcination is not necessary.

Figure 5.10 shows the evolution of the carbonation over 20 cycles. As happened with the 50/40/10 pellets, the level of carbonation decreased dramatically after a few cycles, especially the first 5-6 cycles (see Figure 5.11). In this regard, this decrease can also be observed in Figure 5.12, which shows the 20 cycles overlapped. Figure 5.12 shows that the decrease of capacity is

mainly due to the decrease of the kinetically-controlled stage of the carbonation. This result suggests that the number of available active sites was reduced, or that the pores that offer a more accessible path to these sites were blocked, which forced the molecules to diffuse through the particle. As a consequence, the time to reach the active sites increased, and since the time for the carbonation staged was fixed (15 min), the conversion achieved was smaller.

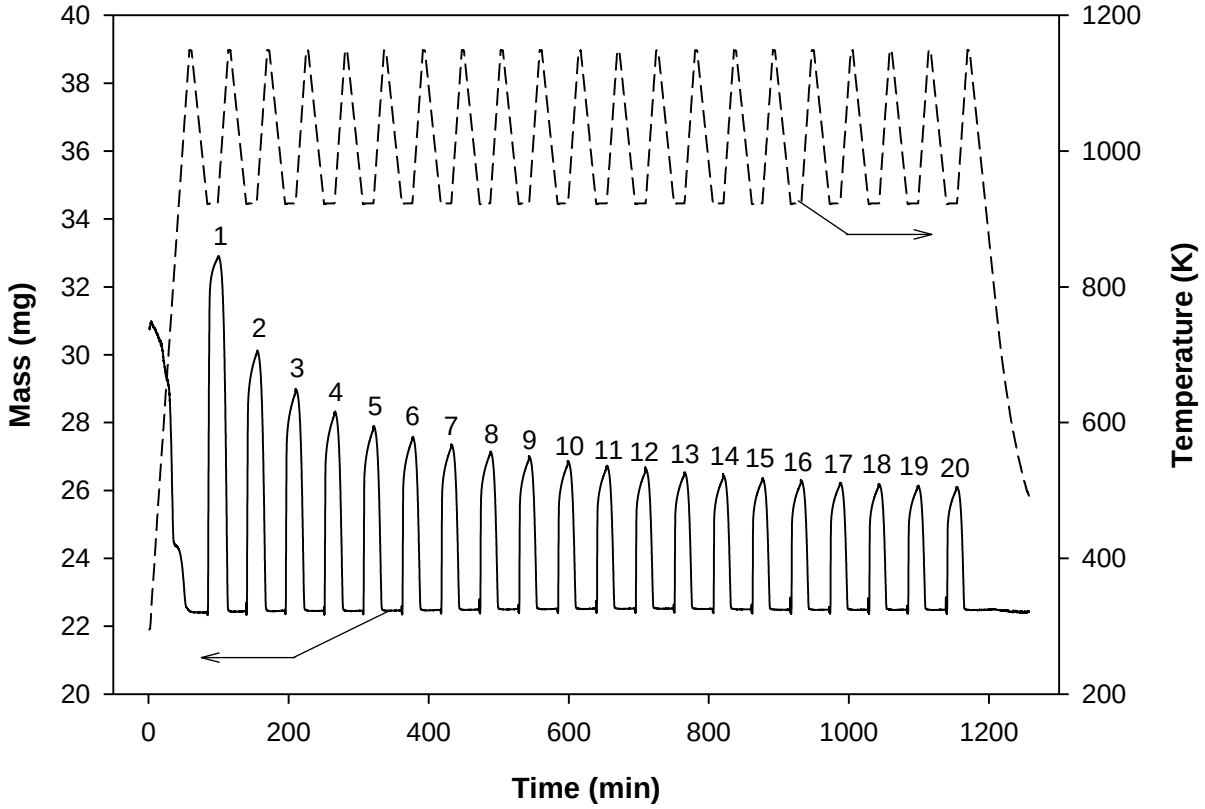

Figure 5.10. TGA report of 20 cycles of calcium looping for 90/10 homogeneous pellets.

Table 5.6 summarizes the results for this composition of pellets for the first and last cycle, but the full table of results can be found in Appendix D.3 (Table D.3). It is noticeable that the CCL (%) decreases by 66.3% after 20 cycles, which is slightly smaller than the CCL (%) obtained for the 50/40/10 pellets (73.2%). Although since the confidence interval for the

50/40/10 pellets is broader, the value of CCL (%) obtained for the 90/10 pellets falls within the confidence interval of the 50/40/10 pellets. Therefore, it is not clear if the performance of the 90/10 pellets was slightly better than the 50/40/10 pellets, or if the change of the time for the calcination stage could have had any influence. This fact becomes more significant if the conversion of CaO is taken into consideration; for the 50/40/10 pellets, the conversion of CaO was approximately 16% in the first cycle, while for the 90/10 it was almost 66%.

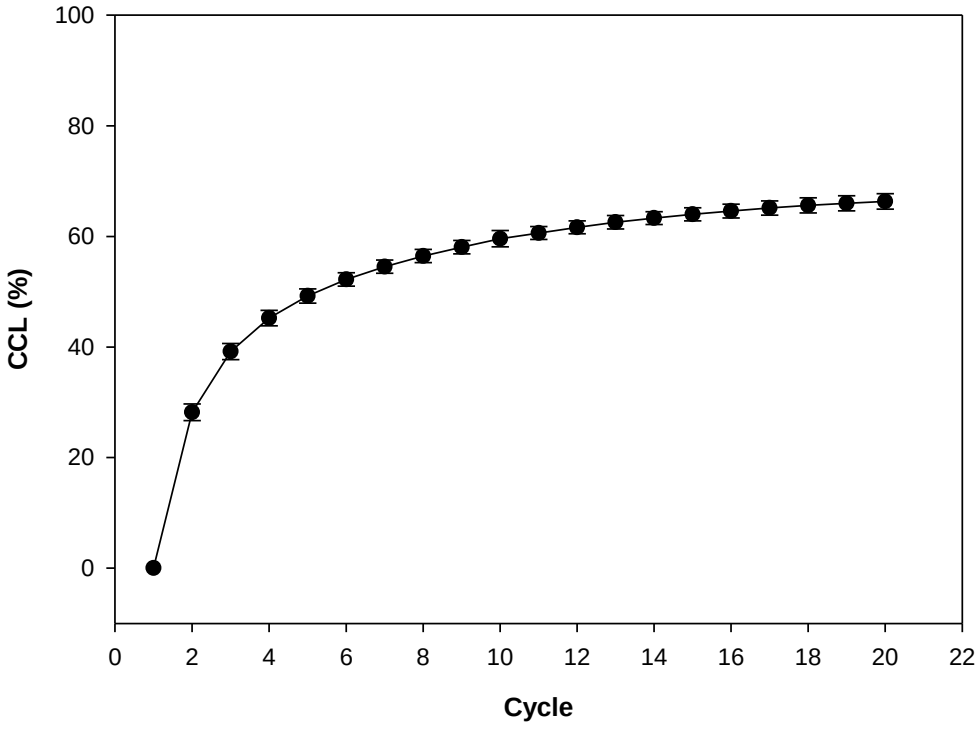

Figure 5.11. CO_2 capture capacity loss vs cycles for 90/10 pellets. Error bars represent the confidence interval.

This result could be explained by the presence of CuO, which reduces the void space as it was shown before in Section 5.1 (discussion of pore volume). It is possible that if, for the 50/40/10 pellets, the carbonation would be performed prior to the oxidation, the conversion of

CaO would be higher. However, it was explained in Chapter Three that the sequence of reactions was established to be first oxidation, next carbonation, and then calcination/reduction. Nevertheless, the CCL (%) is high in both cases, which suggests that regardless of the conversion, the capacity of the pellets decreases over time, and that can be explained by the sintering process.

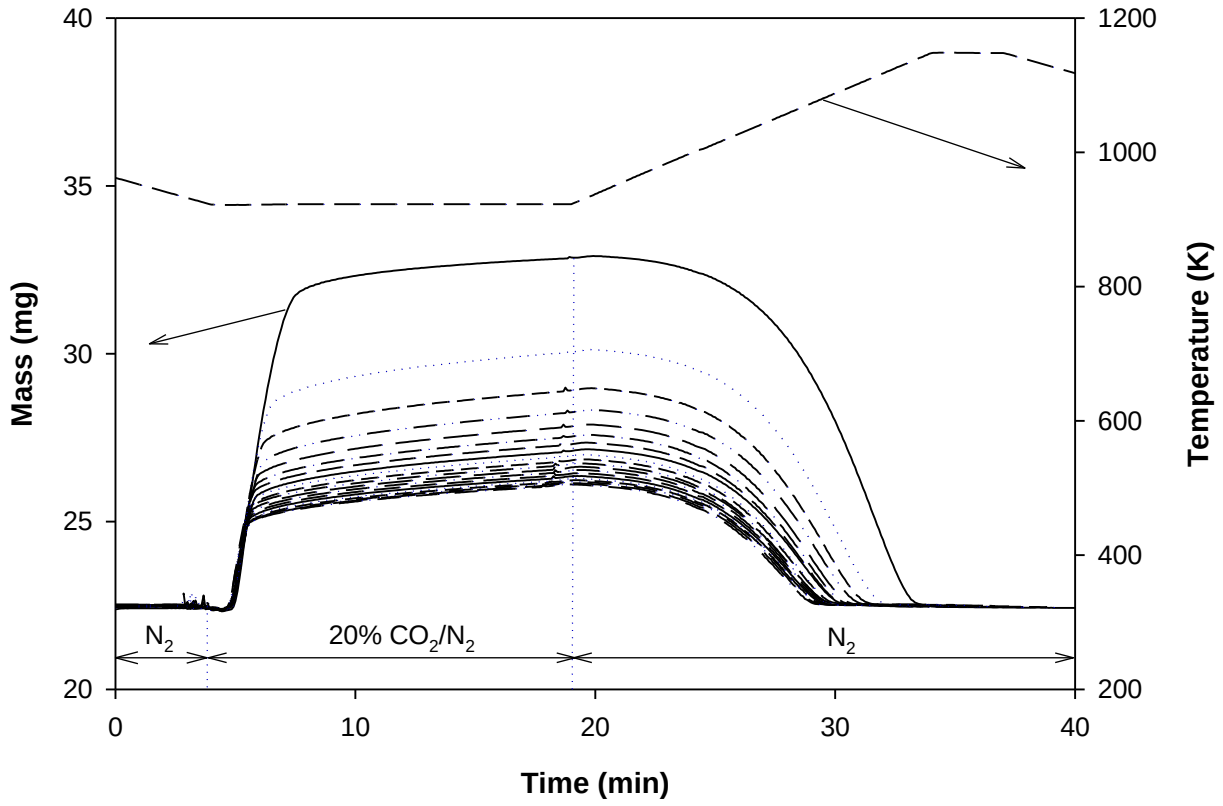

Figure 5.12. Overlapped calcium looping cycles performed with 90/10 pellets.

As for the CO_2 capacity, in this case the capacity cannot be compared to that of the 50/40/10 pellets in terms of $gCO_2/gPellets$ because the loading of CaO in the 90/10 pellets is more than two times the loading in the 50/40/10 pellets. For this composition of pellets (90/10)

the final capacity after 20 cycles was 0.157 gCO_2/gPellets, which is more than 10 times the capacity of the 50/40/10 pellets subjected to 16 cycles, 0.013 gCO_2/gPellets. If the capacity is compared in terms of gCO_2/gCaO, the results show that the 50/40/10 capture 0.033 gCO_2/gCaO, while the 90/10 capture 0.174 gCO_2/gCaO.

Table 5.6. Results of performance of 90/10 pellets for first and last cycle.

Cycle	$\chi_{carbonation}$ (%)	CO_2 Capacity (gCO_2/gPellets)	CCL (%)*
1	65.8 ± 0.5	0.465 ± 0.004	N/A
20	22.2 ± 1.0	0.157 ± 0.007	66.3 ± 1.4

*CCL ≡ CO_2 Capacity Loss

Therefore, the capacity of CaO to capture CO_2 is decreased when used in combination with CuO. Some reasons could be the less void space in the composite pellets, which hampers the access of the CO_2 molecules. Also, because of the low melting point of Cu (~1360 K), it could be that partial melting of this compound occurs during the calcination/ reduction (1148 K) and oxidation (1173 K) stages, which could lead to blockage of pores of CaO by the Cu.

5.6 Comparison of performance with other sorbents

The results obtained for each composition of pellets have already been compared between them. It seems that the dual configuration, in which the 50/50 and 90/10 pellets are involved, is more suitable to achieve higher levels of CO_2 capture. The oxidation capacity of the oxygen carrier was similar with both the 50/40/10 and 50/50, which suggests that the pair CuO/Cu can operate in either configuration. However, to put the results obtained for each composition of

pellets in context, the performance of these compositions are compared with the performance of other sorbents and oxygen carriers reported in the literature. The 90/10 will be considered as the composition of pellets to be compared with other sorbents because of its better CO_2-uptake. As for the oxygen carrier, the compositions 50/40/10 and 50/50 showed similar performances, but to avoid redundancy, the 50/50 pellets will be taken as the case to be compared.

Starting with the CO_2 capacity, multiple types of sorbents are currently under development, including solid amine-based, carbon-based, graphite/graphene-based or zeolite-based[49,106]. Although some sorbents may have higher capacity to capture CO_2, not every sorbent is designed to work at the same conditions as the pellets developed for this thesis. For instance, one type of graphite/graphene-based sorbent showed a capacity of 2.480 gCO_2/g, but the conditions were 298 K and 30 bar[106], which are completely different to the conditions used in this work. Therefore, in order to make a reasonable comparison, it will be taken into consideration only those sorbents that are designed to work at similar conditions as the pellets described in this thesis.

The highest CO_2-uptake of the 90/10 pellets was 0.465 $gCO_2/gPellets$, which was achieved on the first cycle. However, after 20 cycles of carbonation/calcination, this capacity decreased to 0.157 $gCO_2/gPellets$. In Table 5.7 a number of sorbents, their capacities and the number of cycles performed with them are summarized. The capacity of the 90/10 pellets puts it in the low range of capacities in that table, being only higher than 3 out of 17. However, it must be remarked that the CaO used for the 90/10 pellets did not go through any treatment, modification or synthesis procedure[14], while all of the sorbents mentioned in Table 5.7 did. Therefore, there is still margin to improve the performance of the 90/10 pellets, which will be covered in Chapter Six.

Table 5.7. CO_2-uptake of some calcium-based sorbents[106]. (Reproduced with permission from the Royal Society of Chemistry. A copy of the copyright permission is provided in Appendix D.4).

Sorbent	Cycles	Capacity (gCO_2/gSorbent) after last cycle
CaO by coprecipitation	17	0.700
CaO by sol-gel	70	0.242
CaO by sol-gel	35	0.590
CaO by sol-gel	20	0.510
Synthetic CaO	25	0.651
CaO-$Ga_{12}Al_{14}O_{33}$ hollow spheres	30	0.620
Organic acid modified CaO powder	20	0.251
Organic acid modified CaO pellets	20	0.101
Mineral acid modified CaO powders	13	0.299
Formic acid modified	20	0.308
CaO-$Ga_9Al_6O_{18}$	30	0.590
CaO/meso-SiC	30	0.132
CaO-$Ca_{12}Al_{14}O_{33}$	30	0.321
CaO-$Ca_{12}Al_{14}O_{33}$ nanospheres	30	0.612
CaO-MgO	50	0.700
CaO-SiO_2	50	0.088
$CaCO_3$(a)mesoporous silica	50	0.378

Other sorbents designed for similar conditions are the alkali silica-based sorbents, and their performance is closer to that of the 90/10 pellets, ranging from 0.154 to 0.299 gCO_2/g, although in this case none of them surpassed the number of cycles performed with the 90/10 pellets. The alkali zirconate-based sorbents are in the same range of the 90/10 pellets[106]. The examples given do not summarize the state-of-the-art for sorbents designed to work at the same conditions than the 90/10 pellets, but they provide enough information to put in context the results obtained for the 90/10, which is the purpose of this section.

As for the performance of the 50/50 pellets, they showed stable capacity for oxidation over multiple cycles, providing an oxygen capacity of 0.112 gO_2/gPellets after 20 cycles of oxidation and reduction, which was similar to the capacity in the first cycle. In terms of conversion, almost 90% of conversion was achieved after 20 cycles, and for both the 50/40/10 and 50/50 compositions, there was a slight increase of the conversion over cycles (2-3%).

In the literature, many of the approaches taken by other authors involve the use of CuO as oxygen carrier, either as the sole compound or mixed with other metals, such as Fe_2O_3, and/or supports, such as ZrO_2, $MgAl_2O_4$, sepiolite, TiO_2, or SiO_2[13,107,108]. For instance, Siriwardane et al.[108] reported that the combination of CuO with Fe_2O_3 had a synergetic effect in improving the oxygen release capacity. In addition, the agglomeration issues, which have also been reported in this thesis, were diminished because of the presence of Fe_2O_3. Therefore, the capacity of the pellets to provide more oxygen for the combustion of CH_4 could be enhanced by adding Fe_2O_3 to the mixture, as well as preventing in some extent the agglomeration issue.

5.7 Chapter summary

Three different compositions of pellets have been evaluated. One of them contained CuO, CaO and cement. These pellets showed low surface area (15.2 m^2/g) and low pore volume (0.078 cm^3/g). This composition of pellets showed good performance over cycles in terms of oxygen capacity stability, but poor performance in terms of CO_2 capture stability. After 16 cycles, the capacity to capture CO_2 decreased from 0.050 to 0.013 $gCO_2/gPellets$ (decreased by 73.2%).

The other two compositions were designed to operate in a dual configuration of reactors. The pellets that contained 50% CuO and 50% cement had a surface area of 34.2 m^2/g, which was the highest among the three compositions, and suspected to be a result of the high cement (alumina) content rather than the CuO. In contrast, these pellets had the lowest pore volume (0.052 cm^3/g). This composition showed high stability over cycles, even improving around 2-3% after 20 cycles. On the other hand, they suffered from agglomeration, which can be a limiting factor if the content of CuO is required to be very high. The last composition of pellets contained 90% CaO and 10% cement. These pellets had low surface area (19.7 m^2/g), but the highest value of pore volume (0.112 cm^3/g). The capacity of these pellets to capture CO_2 decreased substantially after 20 cycles (65.8%), going from 0.465 to 0.157 $gCO_2/gPellets$.

To end, deposition of carbon during the reduction stage was inferred based on temperature spikes during the oxidation stage, and the presence of a black residue at the end of several experiments. Separate tests confirmed the hypothesis that the black residue was carbon, and also that hydrogen was produced during this process. This issue was associated with the decomposition of CH_4 due to the high temperatures.

Chapter Six – Effect of thermal treatment, impregnation with potassium and steam

The results that have been discussed in the previous chapter have showed that the main issue with the pellets is the decay of the capacity to capture CO_2 over cycles. The capacity for oxidation remained stable and even showed a slight increase over cycles. Therefore, the next steps were oriented to enhance the capacity of the pellets to capture CO_2. As it was explained in Chapter Three, two different approaches were taken, namely a thermal treatment and impregnation with potassium. In addition to these two approaches, experiments at CanmetENERGY – Ottawa were performed using steam as part of the mixture of gases during the carbonation stage. According to the literature[109–113], steam could have a positive effect on the capacity to capture CO_2. In Section 6.3 the setup, compositions of pellets, conditions, and results are presented.

6.1 Effect of thermal treatment on pellets with 90% CaO and 10% cement (90/10)

The pellets that were chosen for this treatment contained 90% CaO and 10% cement (90/10), and the nomenclature given to each batch of pellets was 1) TT1.5N-90/10 for pellets thermally treated (TT) under N_2 using the 1.5 K/min ramp, 2) TT1.5A-90/10 for those treated under air with a heating rate of 1.5 K/min, and 3) TT7.5N-90/10 for those treated under N_2 and using 7.5 K/min as the heating rate. The goal of this study was to determine if the heating rate had any influence on the performance of the pellets.

The calcium looping method applied to these compositions of pellets was the same as that used for the non-treated pellets, i.e., 20 cycles of carbonation at 923 K under a mixture of 20% CO_2/N_2 balance, and calcination in N_2 atmosphere. Each batch of pellets was tested three times.

In order to evaluate the results obtained, the performance of the 90/10 pellets without treatment will be taken as the base case. Table 6.1 provides a summary of the results; the full results can be found in Appendix E.1, Tables E.1, E.2 and E.3.

Table 6.1. Summary of results of thermally treated pellets; results of raw pellets included for comparison.

Sample	Cycle	$\chi_{carbonation}$ (%)	CO_2 Capacity (gCO_2/gPellets)	CO_2 Capacity Loss, CCL (%)
90/10 (raw)	1	65.8 ± 0.5	0.465 ± 0.004	N/A
90/10 (raw)	20	22.2 ± 1.0	0.157 ± 0.007	66.3 ± 1.4
TT1.5N-90/10	1	57.2 ± 0.7	0.404 ± 0.005	N/A
TT1.5N-90/10	20	28.3 ± 1.9	0.200 ± 0.014	50.5 ± 3.8
TT1.5A-90/10	1	58.6 ± 0.5	0.414 ± 0.004	N/A
TT1.5A-90/10	20	27.7 ± 2.0	0.196 ± 0.014	52.7 ± 3.8
TT7.5N-90/10	1	55.4 ± 0.8	0.391 ± 0.006	N/A
TT7.5N-90/10	20	29.6 ± 0.6	0.209 ± 0.004	46.6 ± 0.6

The capacity is higher in the first cycle for the raw pellets than for those that were thermally treated. As depicted in Figure 6.1, after three cycles the thermally treated pellets had higher capacities, demonstrating that the thermal treatment stabilizes the pellets. The capacity is increased from 0.157 to 0.196 gCO_2/gPellets (24.8%) with the TT1.5A-90/10 pellets, to 0.200 gCO_2/gPellets (27.4%) with the TT1.5N-90/10 pellets, and to 0.209 gCO_2/gPellets (33.1%) with the TT7.5N-90/10 pellets.

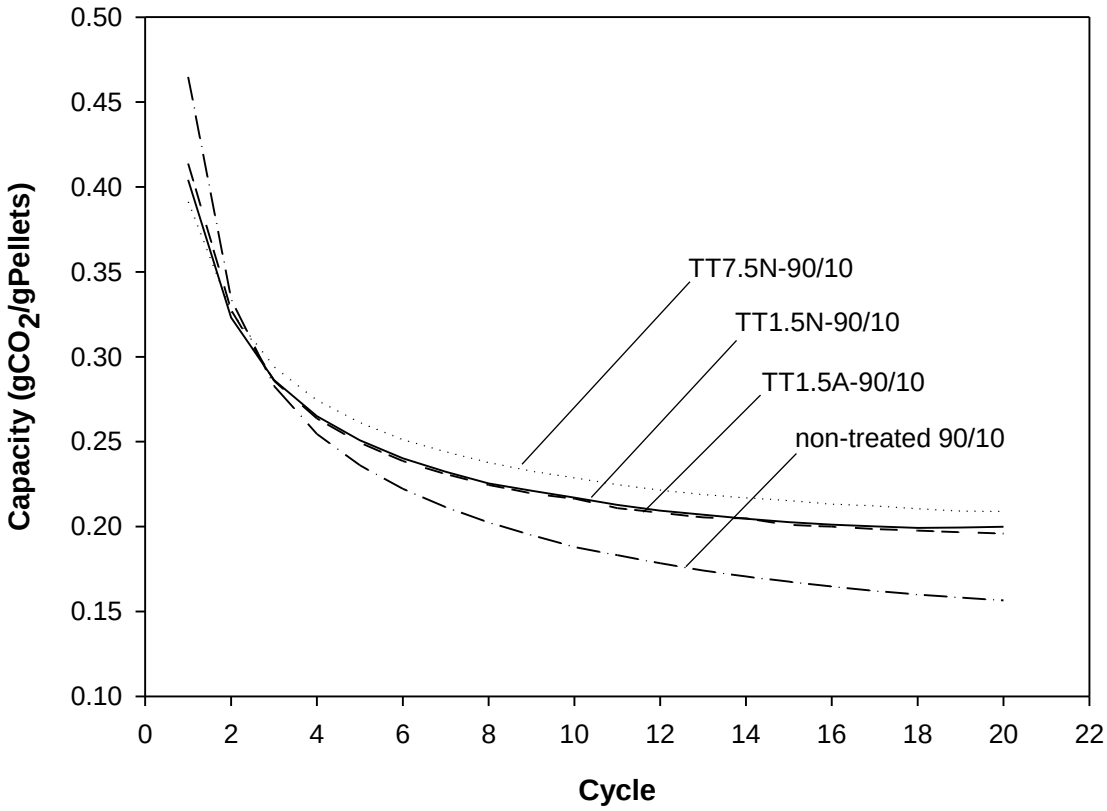

Figure 6.1. Evolution of CO_2 capacity over cycles for raw 90/10 pellets, TT1.5N-90/10, TT.7.5N-90/10, and TT1.5A-90/10. Each curve is the average of three runs.

The better capacities are explained by the higher conversion of CaO, which is increased by 6.1%, 5.5%, and 7.4% respectively. Also, the CCL (%) is smaller for the thermally treated pellets, but it must be taken into account that the capacity of these samples was already smaller in the first cycle than it was for the raw 90/10 pellets. Therefore, the initially smaller capacity, along with the better performance after 20 cycles, results in a smaller CCL (%).

Comparing the thermally treated pellets, the results for TT1.5N-90/10 and TT1.5A-90/10 show that the pellets treated under N_2 and under air, using the same heating rate, provide the

same capacity, which indicates that the presence of O_2 does not affect the capacity of the pellets. Therefore, since air is cheaper and more accessible, it would be recommended as the carrier gas.

On the other hand, between the TT1.5N-90/10 and TT7.5N-90/10 there is a slight difference. The pellets treated using a faster heating (7.5 K/min) rate performed better than those treated with a slower heating rate (1.5 K/min). The TT7.5N-90/10 provides 4.5% more capacity than the TT1.5N-90/10. According to the confidence intervals, both results are within the same range. Therefore, it is unclear if the faster heating rate slightly enhances the performance of the pellets over cycles, or if the heating rate does not really affect the performance. Thus, it is possible that the better performance of the pre-treated pellets could be due to the temperature at which the pellets are heated up, and the time at which they are kept at such temperature. For the three cases studied, the temperature was 1173 K and the holding time was 2 h. Other authors reported similar treatments on CaO compounds, although with different temperatures and holding times[67,82], and the results of the performance were also better after the thermal treatment.

In summary, the thermal treatment enhanced the stability of the pellets. The smallest increase was that of the TT1.5A-90/10 (24.8%), and the largest increase was obtained with the TT7.5N-90/10 pellets (33.1%). Treating the pellets under N_2 and air provided the same results, which indicates that the presence of O_2 is not detrimental. Finally, it is not clear if the heating rate has any influence on the performance of the pellets because the difference in the results between TT7.5N-90/10 and TT1.5N-90/10 was within the confidence interval. It is possible that the key variable would be the temperature at which the samples are treated, and/or the holding time.

6.2 Effect of impregnation with KOH on pellets with 90% CaO and 10% cement

The second approach that was taken parallel to the thermal treatment was the addition of potassium. Potassium has been reported to have a high mobility[69], and the purpose of impregnating the pellets with this element was to check if the high mobility could prevent sintering. Additionally, by adding potassium hydroxide, there was the possibility of increasing the capacity to capture CO_2 since different potassium-based compounds have been applied for CO_2 capture process[70–72]. Also, other types of sorbents, such as carbon-based sorbents, have been treated with KOH to enhance their capacity[73].

Two different loadings of potassium hydroxide were tested, 5% and 20% (%wt.). These loadings refer to the ratio of elemental potassium and CaO. See Appendix B.1 for an example of the calculations made to determine the amount of KOH required to achieve the loading of potassium sought. The nomenclature used for the batches of pellets prepared for these tests is 20K-90/10 for pellets with 20% loading, and 5K-90/10 for pellets with 5% loading.

The TGA results obtained for each composition of pellets are shown in Figure 6.2. The mass increases for the 20K-90/10 pellets were significantly smaller than the mass increases for the 5K-90/10. In Figure 6.3, the first cycle is depicted in more detail, and for that figure, the first cycle of the raw 90/10 pellets was included for comparison.

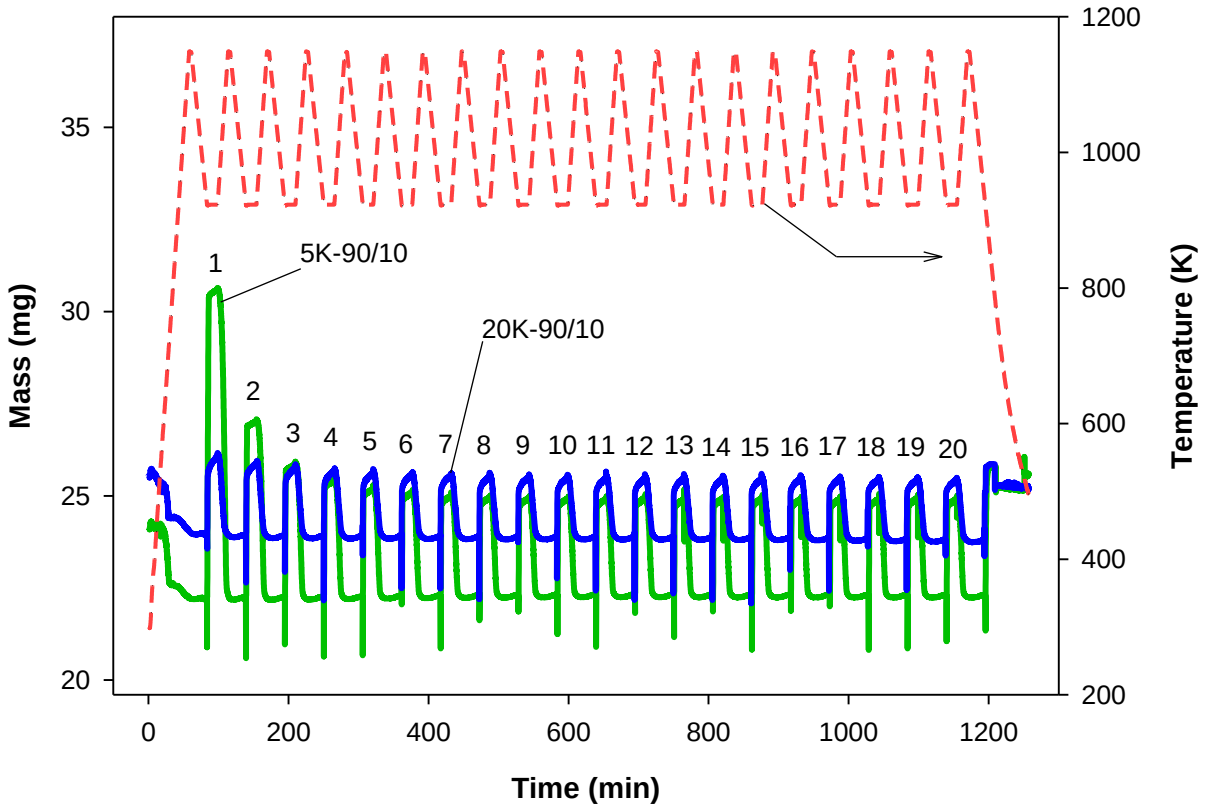

Figure 6.2. TGA results for 5K-90/10 and 20K-90/10 pellets.

Figure 6.3 is aimed to show, first, the capacity to capture CO_2 of the impregnated pellets, which compared to that of the raw pellets decreased since the first cycle. For the 20K-90/10 the capacity decreased from 0.089 to 0.068 $gCO_2/gPellets$ after 20 cycles. The capacity was considerably smaller than that of the raw 90/10 pellets (0.157$gCO_2/gPellets$ after 20 cycles). For this case, only two tests were performed to confirm the results, but given the low performance, it was considered unnecessary to perform the third replicate and the study of errors. For the 5K-90/10, the capacity diminishes from 0.387 to 0.123 $gCO_2/gPellets$ after 20 cycles, which is also worse than the results obtained for the raw 90/10 pellets. Therefore, these results indicate that the

addition of potassium hydroxide did not have the expected effect and did not enhance the performance of the pellets. Second, there is a significant difference between the results of the 5K-90/10 and the 20K-90/10 pellets. In both cases the capacity to capture CO_2 is diminished, but more so for the 20K-90/10 pellets.

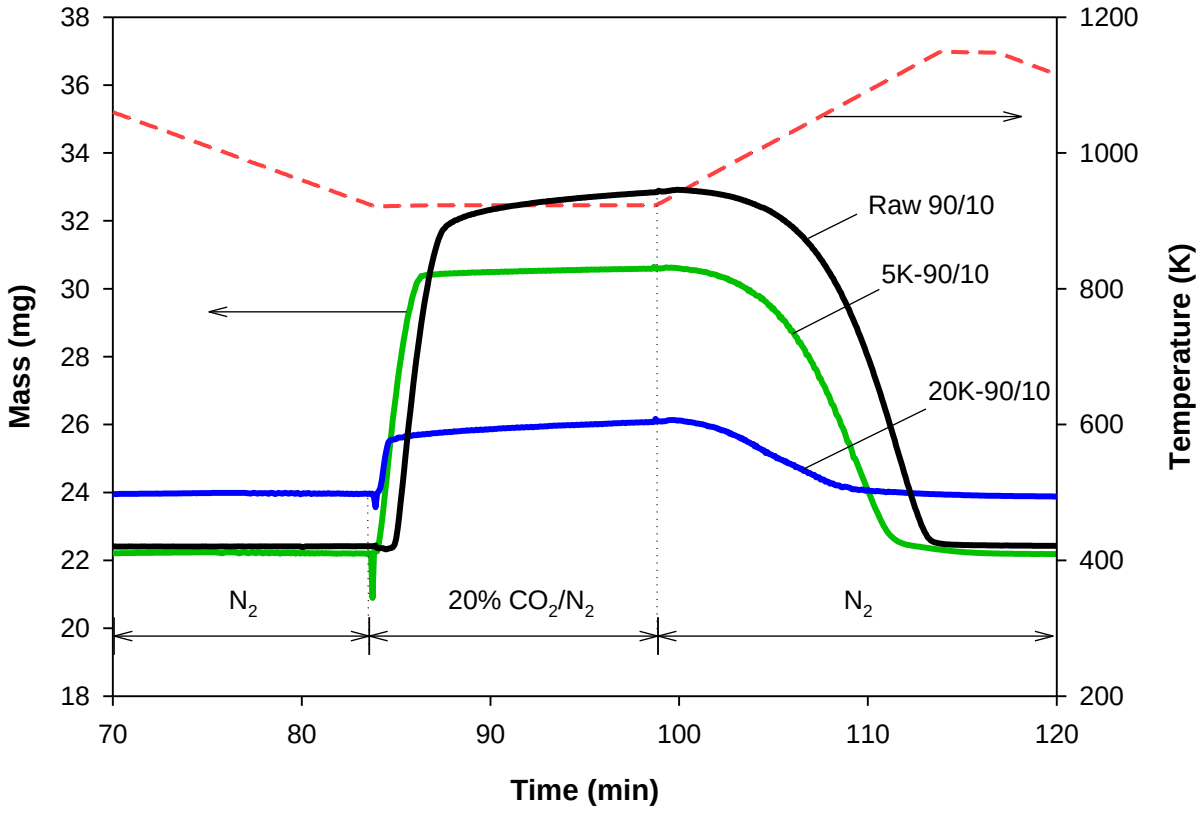

Figure 6.3. TGA report - first cycle for raw 90/10, 5K-90/10, and 20K-90/10 pellets.

A reasonable explanation would be that the potassium hydroxide blocked the pores of the pellets, thus hampering the capture of CO_2. That would explain why for the 20K-90/10 the decrease was substantially larger than for the 5K-90/10. It is also possible that the impregnation

treatment had affected the pellets, that is, some of the CaO may have dissolved in the water used for the KOH impregnation.

In addition, the transition from kinetic to diffusional control becomes more abrupt for the impregnated pellets, especially for the 5K-90/10. To determine if this was indeed happening, the reaction rate of the carbonation reaction in the first cycle for each case is shown in Figure 6.4. The calculations made to determine the reaction rate are described in Appendix E.2. Also, to plot the reaction rate, the data from the TGA was smoothed in order to eliminate noise and reduce data points (see Appendix E.3).

Initially, all 90/10 pellets begin with the same reaction rate, but the analysis of the low conversion zone shows that the raw 90/10 pellets had the fastest reaction rate at all times. Hence, the observation regarding the transition from the kinetic to diffusional control seems to be confirmed. The reaction rate for the 5K-90/10 pellets decreased faster than for the raw 90/10 pellets. In the case of the 20K-90/10 pellets the reaction rate rapidly reached a maximum at 1% conversion, decreased slightly to ~10% and then sharply to zero.

The conversions obtained for the impregnated pellets are smaller than that of the raw pellets. In the first cycle, for the 20K-90/10 pellets the conversion achieved was 13%, and for the 5K-90/10 it was 55%, both below the 66% obtained for the raw pellets in the first cycle. After 20 cycles, these conversions decreased to 10%, 17% and 22% for the 20K-90/10, 5K-90/10 and raw pellets, respectively.

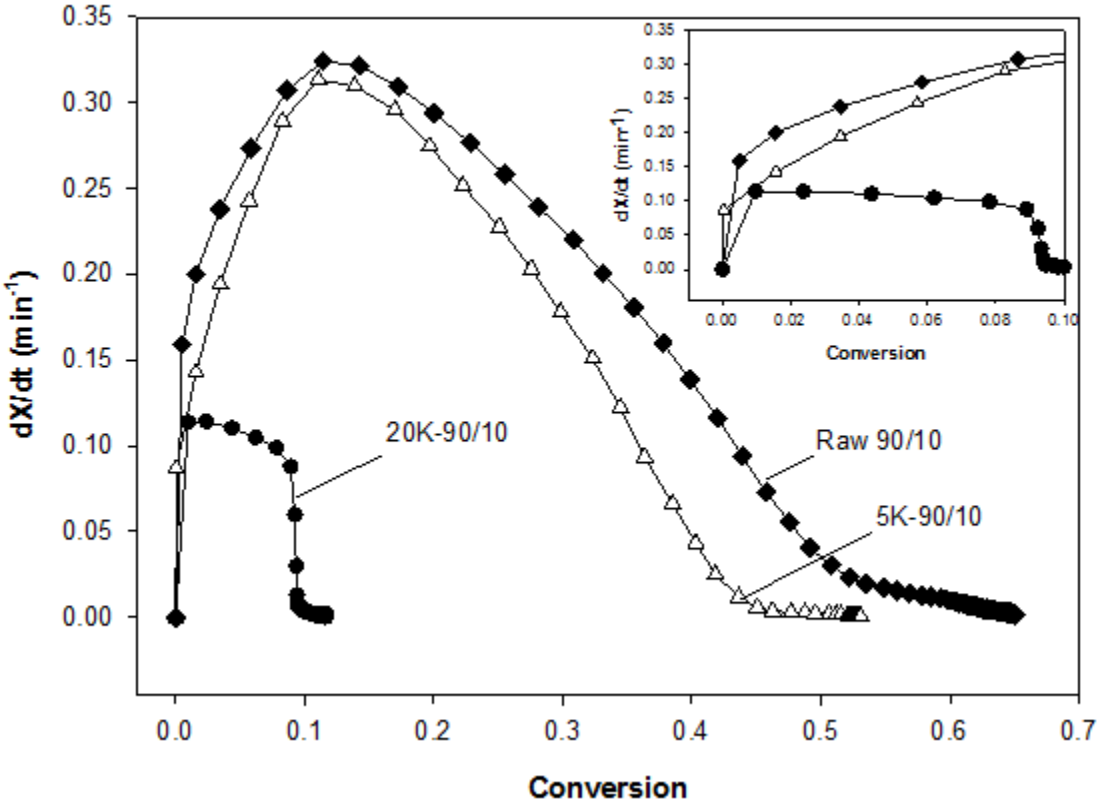

Figure 6.4. Kinetics of the carbonation reaction in the first cycle for the raw 90/10, and KOH-impregnated 90/10 pellets.

In summary, the addition of KOH was not beneficial in terms of enhancing the capacity of the pellets to capture CO_2. The presence of KOH slowed down the kinetics of the reaction and made the diffusional limitations more significant than in the case of the raw 90/10 pellets. As mentioned, it is probable that the KOH blocked the pores of the pellets, thus hindering the access of the CO_2 molecules. The difference of the results between the 5K-90/10 and 20K-90/10 could be explained by this effect.

6.3 Effect of steam on pellets with 90% CaO and 10% cement (90/10)

The last approach that was taken to improve the capacity of the pellets was the addition of steam as part of the inlet gases for the carbonation stage. In an actual coal-fired plant, in addition to other gases, such as sulfur oxides, nitrogen oxides, or particulate matter, steam will be present since it is a product in the combustion reaction. According to some authors, the presence of steam can enhance the performance of the pellets to capture CO_2 over multiple cycles[109–113]. The mechanism that leads to the improvement of the performance is unclear. Dou et al. suggested the formation of $Ca(OH)_2$, which reacts with the CO_2 molecule[114]. In contrast, Yang and Xiao[111] reported that the performance of CaO was improved even if $Ca(OH)_2$ was not formed. In general, it is accepted that the presence of steam leads to larger pores, which facilitates the diffusion. In fact, Arias et al.[115] showed that the kinetic-controlled part of the carbonation was not affected by the presence of steam, but the diffusion-controlled part was enhanced, which is in agreement with the formation of larger pores. Therefore, performing cycles of carbonation including steam as part of the mixture of gases has significant interest.

Due to incompatibilities between some materials of the TGA apparatus and steam, the experiments with steam were performed at the facilities of CanmetENERGY – Ottawa. In this section the setup of the TGA at CanmetENERGY, composition of pellets used, testing conditions, methodology of the experiments, and the results are explained.

6.3.1 Experimental conditions

The composition of pellets that was selected for the experiments with steam was the same as that used for the other two approaches taken, i.e., the pellets that contained 90% CaO and 10% cement (90/10). Two different carbonation conditions were used, 1) mixture of 20% CO_2 (Linde,

Grade 4, 99.99%), 10% steam, and 70% N_2 (Linde, Grade 5.0, 99.999%), and 2) 20% CO_2, 30% steam and 50% N_2. The temperatures and holding times were almost exactly the same as before; the only difference was that the time for carbonation was extended from 15 min to 21 min because the length of the line that went from the CO_2 cylinder to the reactor was longer and that caused a delay of 5-6 min in the start of the reaction. This issue was found after the first experiment, which was run without steam to test the differences between the setup at Canmet and the setup at Calgary. In this first run an unexpected shape at the end of the carbonation was observed, as illustrated in Figure 6.5. The increase in the reaction rate is due to the increase of the temperature.

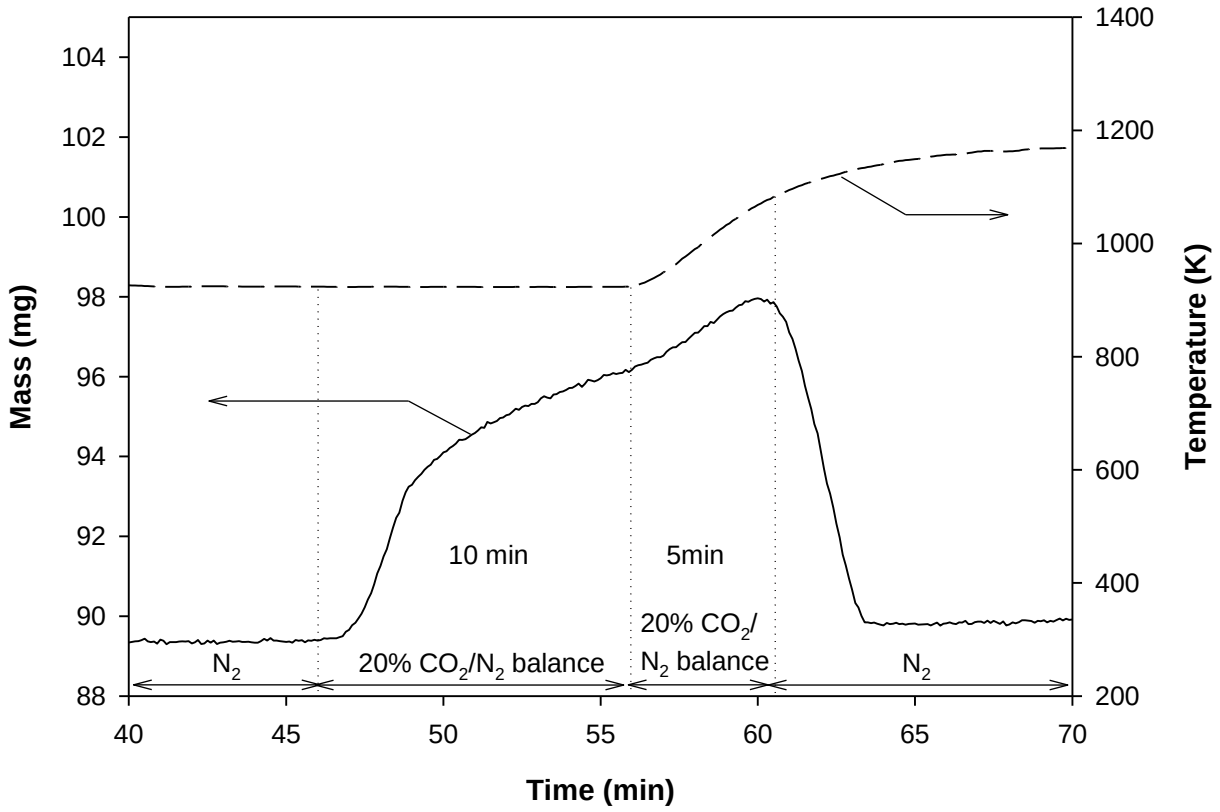

Figure 6.5. Carbonation/calcination cycle of the first experiment performed at Canmet with 90/10 pellets and without steam.

Therefore, in order to compare the results at Canmet with those obtained at Calgary, it was necessary to ensure 15 min of carbonation at 923 K, and for that, the time for this stage was extended to 21 min. Thus, the carbonation was performed under the conditions already mentioned, and the calcination at 1148 K under N_2, with 3 min of holding time. As for the number of cycles, due to limited availability of the TGA at Canmet, it was not possible to perform the same number of cycles as in the TGA of the LECA group. At Canmet, the total number of cycles needed to be reduced to 15.

Two different experiments were planned with the 90/10 pellets, and they are summarized in Table 6.2. Each experiment was carried out three times to check the reproducibility and conduct the study of errors.

Table 6.2. Summary of the experiments performed at CanmetENERGY-Ottawa.

Pellets	Carbonation	Calcination	Cycles
	923 K	1148 K	
90% CaO, 10% cement	20% CO_2, 70% N_2, 10% $H_2O_{(v)}$	N_2	15
	15 min	3 min	
	923 K	1148 K	
90% CaO, 10% Cement	20% CO_2, 50% N_2, 30% $H_2O_{(v)}$	N_2	15
	15 min	3 min	

6.3.2 TGA setup

The configuration of the TGA at Canmet is depicted in Figure 6.6. Compared to the TGA at the Laboratory for Environmental Catalytic Applications (LECA), the main differences were that the reactor was made of steel instead of quartz, and the furnace was not attached to the reactor as in the TGA in LECA, but it was a separate piece. Once the sample was placed and reactor mounted, the furnace was placed around the reactor so that it remained in the center of the furnace. The fact that the furnace was a separate piece of the equipment involved the absence of furnace gas. Instead, the air between the furnace and the reactor acted as the furnace gas. Also, the sensitivity of this TGA was 1 μg, which is one order less than that of the TGA at Calgary (0.1 μg). Additionally, the hanging wire was not surrounded by a baffle (see Figure 6.7), which increases the chances of the wire to sway and makes the reading of the weight less accurate. Regarding the sample holder, it was not a quartz crucible, but a platinum pan.

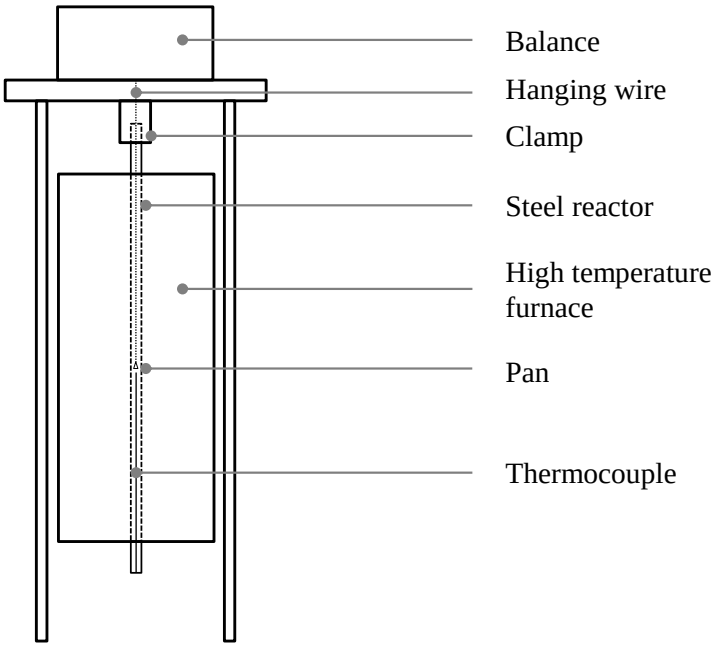

Figure 6.6. Schematic of the TGA apparatus at CanmetENERGY.

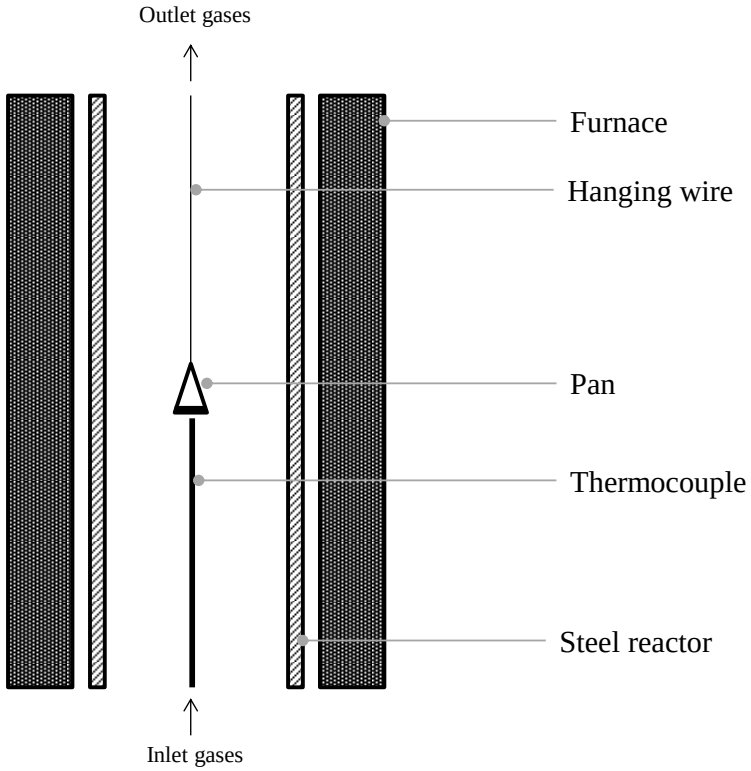

Figure 6.7. Cross section of the configuration of the TGA at Canmet.

Figure 6.8 illustrates the general setup for the TGA at Canmet. The most significant differences with respect to the TGA at LECA are related to the addition of steam. To add steam, a syringe was filled with deionized water and placed onto a syringe pump. The syringe pump infused the amount of water needed to produce the steam flowrate required. Next, the water went through the steam generator, which heated the water up to ~405 K. Then, the steam was further heated to ~435 K by means of a heating trace. The main purpose of this heating trace was to keep the steam hot enough so that it did not condense along the line. Last, prior to entering the reactor, the line containing the steam, already mixed with the other gases (N_2 and CO_2), was covered with heating tape to increase the temperature to 518 K.

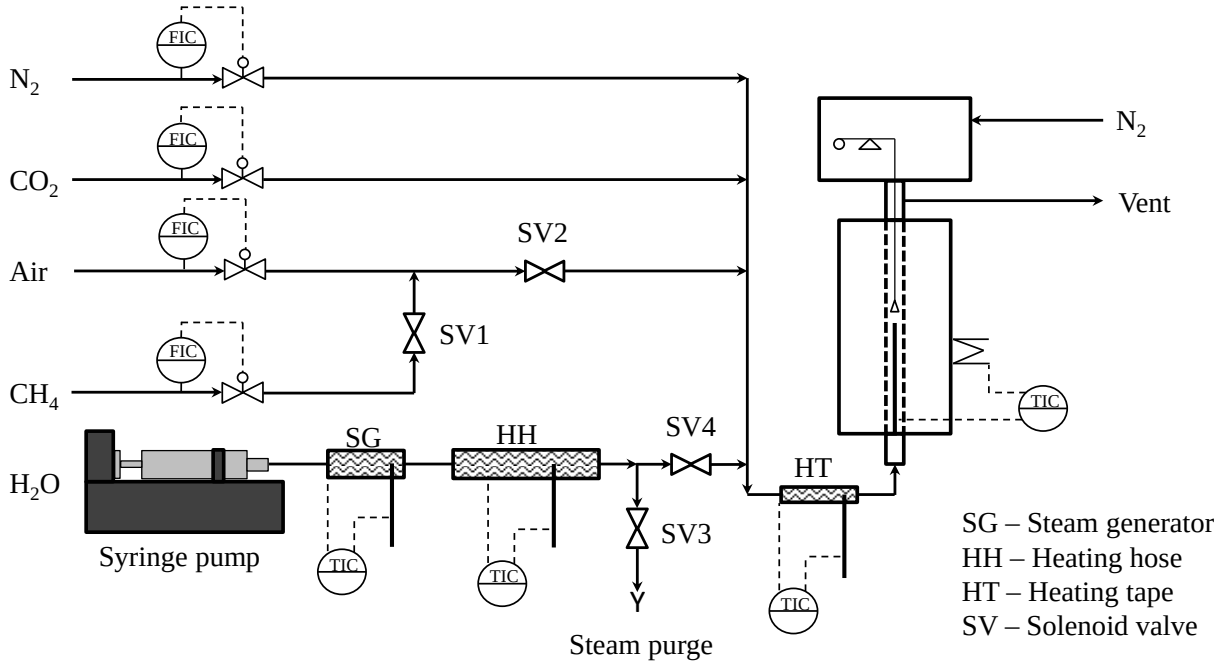

Figure 6.8. General schematic of the setup of TGA at CanmetENERGY-Ottawa.

The control of the rest of gases was performed by mass flow controllers. Although for the experiments with these pellets CH_4 and air were not necessary, these gases could be used when working with pellets containing CuO, which require CH_4 and air for reduction and oxidation respectively. For these gases, in addition to the mass flow controllers, there were two solenoid valves, namely SV1 and SV2, which enabled switching between the gases. The SV3 was used to purge steam, and SV4 enabled the flow of steam into the TGA. The entire setup was monitored and controlled through two LabVIEW interfaces, which in this case cannot be shown in this thesis because they were developed by CanmetENERGY – Ottawa.

6.3.3 Results of pellets with 90% CaO and 10% cement (90/10)

In addition to the study of the effect of steam, tests without steam were run for two reasons, 1) quantify the performance of the pellets in the setup at Canmet, so that there was a base case to compare the effect of steam, 2) determine if the results at Canmet could be directly compared with the results at Calgary. It must be taken into consideration that each setup behaves differently, which affects the performance of the samples studied. In such case, the comparison of the results should be made based on the trends and not the absolute values.

For the 90/10 pellets, the addition of steam seems to enhance the performance of the pellets over cycles. According to the results shown in Table 6.3, the conversion of the pellets after 15 cycles was 18.2% for the case without steam, and 24.3% with 10% steam. The case for 30% steam is explained separately next. The evolution of the capacity to capture CO_2 (gCO_2/gPellets) is depicted in Figure 6.9.

Table 6.3. Summary of the results of the 90/10 pellets obtained at Canmet.

Experiment	Cycle	$\chi_{carbonation}$ (%)	CO_2 Capacity (gCO_2/gPellets)	CCL (%)
90/10 pellets without steam	1	65.1 ± 14.9	0.46 ± 0.11	N/A
	15	18.2 ± 0.4	0.13 ± 0.01	71.3 ± 6.7
90/10 pellets with 10% steam	1	69.2 ± 6.2	0.49 ± 0.04	N/A
	15	24.3 ± 9.6	0.17 ± 0.07	64.6 ± 14.3
90/10 pellets with 30% steam*	1	65.9 ± 8.8	0.47 ± 0.06	N/A
	15	38.0 ± 4.4	0.27 ± 0.04	39.8 ± 7.1

*Results of 5 experiments

Although it seems that adding 10% steam slightly increased the capacity, the analysis of these results by means of t-test indicated that the mean obtained in each cycle, for both cases, could not be considered different. In other words, the results are not significantly different to consider that the steam had any effect on the capacity to capture CO_2 (full tables of experimental results are provided in Appendix E.4, and results of the t-test are summarized in Appendix E.5).

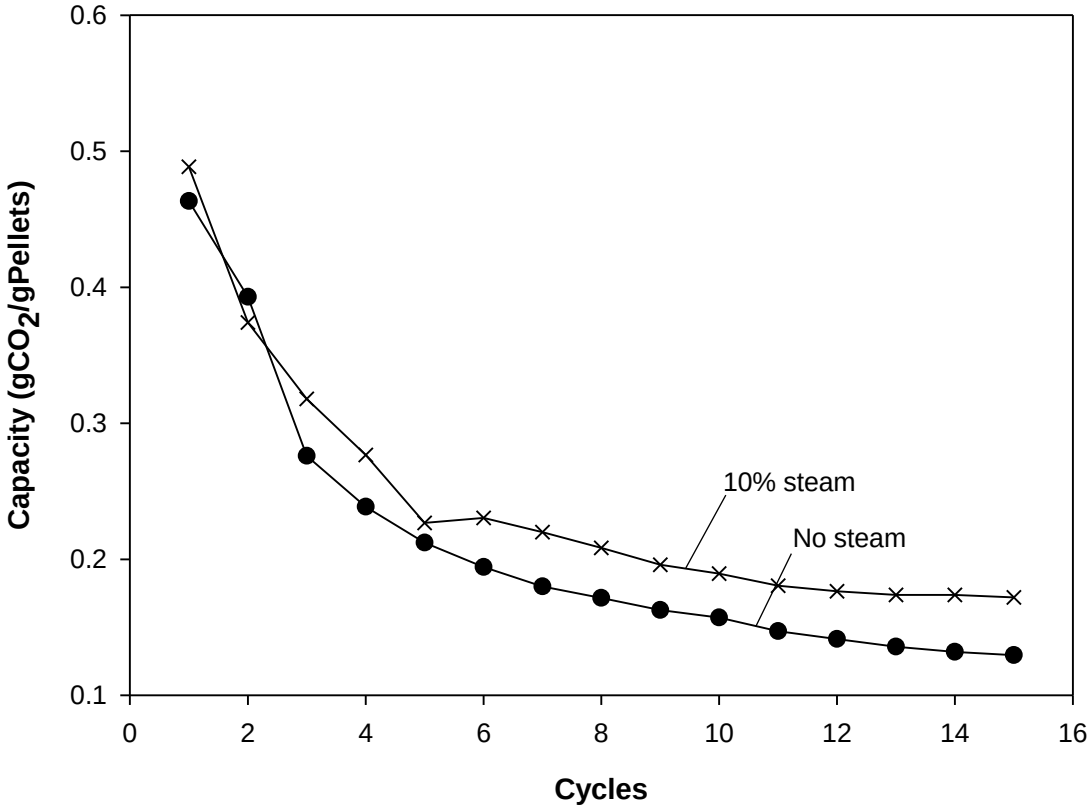

Figure 6.9. Evolution of capacity to capture CO_2 over cycles of 90/10 pellets for two carbonation conditions.

This result could be inferred by the confidence intervals provided in Table 6.3. In this regard, comparing these results with those obtained at Calgary (for instance see Table 6.1), it is

noticeable that the confidence intervals are broader for the results at Canmet. This indicates that the reproducibility of the experiments at Canmet is lower. The sensitivity of the TGA at Canmet was one order smaller than that of the TGA at Calgary (1 μg versus 0.1 μg). In addition, the hanging wire of the TGA at Canmet, as opposed to the TGA at Calgary, was not protected by a baffle. This part of the equipment surrounds the hanging wire and prevents it from swaying, which creates disruption in the reading of the weight (noise), thus, decreasing the accuracy.

The capacities of the pellets to capture CO_2 decreased from 0.46 to 0.13 $gCO_2/gPellets$ for the case in which steam was not added, which means 71.3% of capacity loss. For the case in which 10% was added, the capacity diminished from 0.49 to 0.17 $gCO_2/gPellets$, i.e., 68.6%. Therefore, it seems that a low fraction of steam may have influence in the capacity to capture CO_2, but based on the results and the errors, it would be small or even negligible, which is still positive as industrially the gases will contain steam.

With 30% steam, the experiments were more complicated than expected, and several issues limited the performance of the tests. The main issue that could not be completely addressed was the partial condensation of the steam throughout the line that connected the steam generator with the reactor of the TGA. This line was thoroughly insulated and heated by a heating trace, and heating tapes that kept the temperature always higher than 430 K. However, the results obtained suggest that condensation of steam was occurring. Figure 6.10 illustrates the result obtained for one of the experiments, which represents perfectly the results for the other experiments conducted (five in total) under the same conditions, i.e., 923 K for 21 min under 20% CO_2, 30% steam and balance N_2 for carbonation, and 1148 K for 3 min under N_2 for calcination. For this case, the total number of experiments conducted was higher than usual (five versus three) because of the condensation issue.

In Figure 6.10, the carbonation does not follow a normal trend, but it shows alternating increases and decreases, as opposed to the ordinary decrease that could be expected. This phenomenon can only be explained by the presence of steam, which should enhance the capacity to capture CO_2 when it reached the reactor. In those cycles in which a low capacity was observed, it is believed that steam was present in a fraction smaller than expected, or not present at all. Although Figure 6.10 only illustrates one experiment, the other four tests showed similar results, with the only difference that the maximums and minimums did not necessarily occur in the same cycles as those of the experiment shown in Figure 6.10.

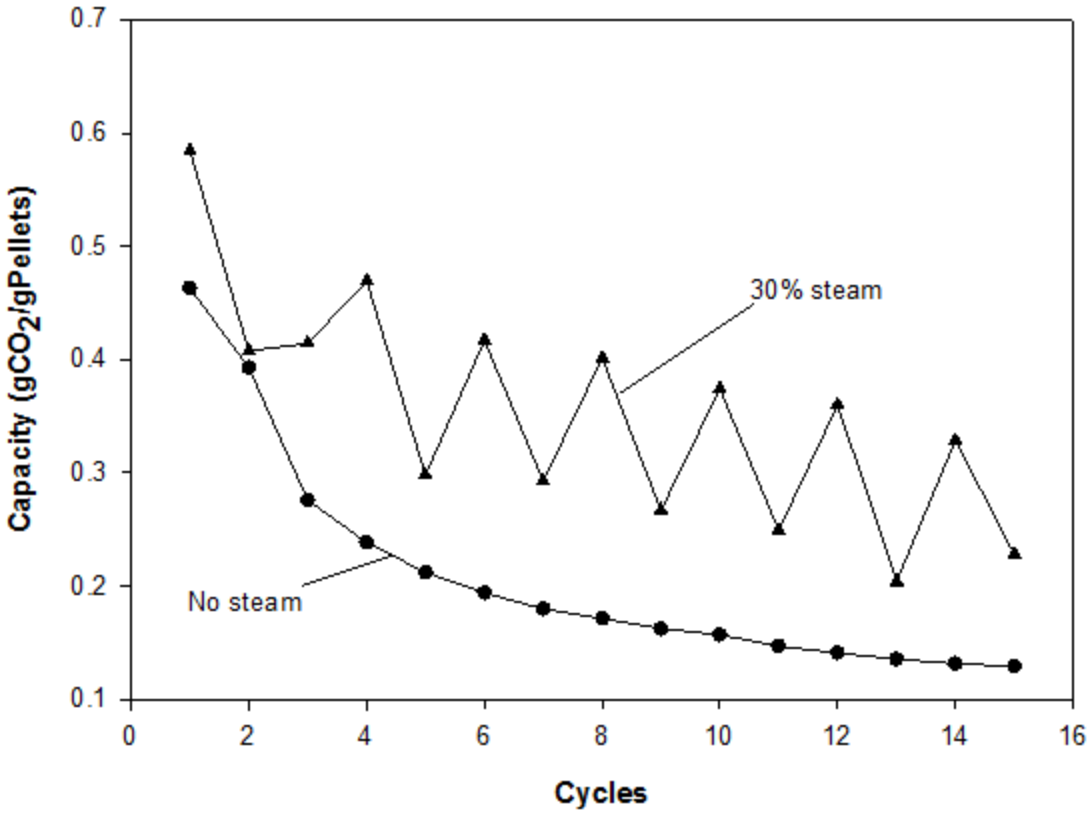

Figure 6.10. Evolution of the capacity to capture CO_2 over cycles of 90/10 pellets under two carbonation conditions.

To offer a clearer view of the impact of the steam on the 90/10 pellets, in Figure 6.11 there are five curves depicted: 1) the results obtained for pellets treated in the absence of steam, 2) pellets treated with 10% steam during carbonation, 3) average of all the experiments performed with 30% steam, ignoring if the steam was present in the expected amount or not, 4) highest value obtained for each cycle among the experiments performed with 30% steam, and 5) lowest value obtained for each cycle among the experiments performed with 30% steam.

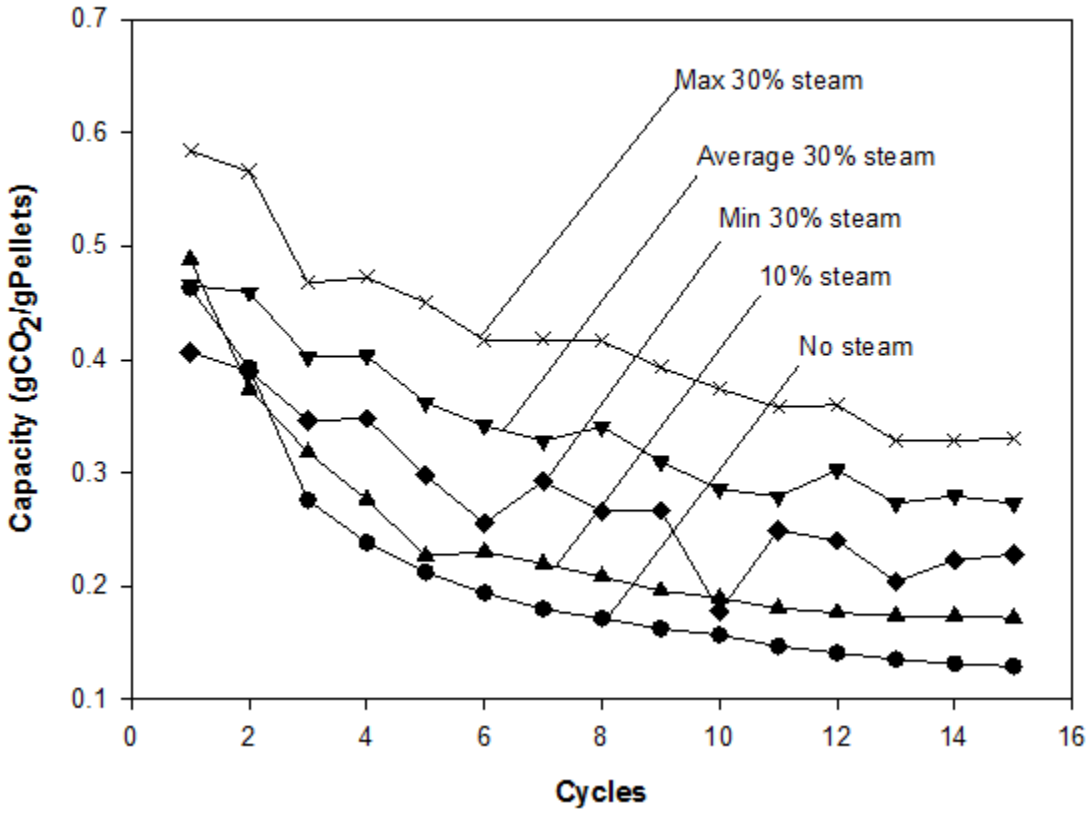

Figure 6.11. Summary of results obtained with 90/10 pellets under different carbonation conditions.

The purpose of this figure is exclusively qualitative, not quantitative (except for the experiments without steam and with 10% steam). For the curve of maximum values of the experiments with 30% steam is assumed that steam was present in the correct amount, and that no condensation took place whatsoever. On the other hand, as mentioned before, for the minimum values of the experiments with 30% steam, the fraction of steam is assumed to be smaller than 30%, or null because of the condensation issue.

According to these results, for the experiments in which the target was 30% steam, even the lowest values of CO_2 capture capacity are higher than the average values of the experiments with 10% steam. On average, the capacity to capture CO_2 in each cycle of the 30% steam minimums is 1.2 times larger than each value of the 10% steam. Regarding the maximums of the 30% steam experiments, on average the capacity in each cycle is 1.8 times larger when compared to that of the 10% steam experiments. Therefore, it seems that a higher fraction of steam has a more significant and noticeable impact on the capacity of the pellets to capture CO_2.

In summary, the results indicate that the presence of steam may enhance the capacity of the pellets to capture CO_2. Also, while for the 10% fraction of steam the experiments could be conducted without issues, for the 30% fraction it was not possible to obtain consistent results. Nonetheless, the results obtained seemed to indicate that a higher fraction of steam could involve a significant enhancement of the capacity to capture CO_2. In addition, it must be noted that in any of the cases studied in this thesis it has been observed the opposite effect, i.e., decrease of the capacity due to the presence of steam, which towards the industrial scale would have been an important drawback.

6.4 Chapter summary

In this chapter, three different approaches to address the loss of capacity to capture CO_2 have been presented. The thermal treatment of pellets resulted in a significant enhancement of the capacity to capture CO_2 after multiple cycles. The best result was obtained for pellets subjected to a heating rate of 7.5 K/min up to 1173 K, held for 2 h, under air, whose capacity after 20 cycles was 33% than that of the non-pre-treated pellets. Also, no difference between pellets treated under pure nitrogen and air was found. The heating rate seemed to have little influence in the performance of the pellets. It is believed that the actual key parameters are the temperature and the holding time.

On the other hand, the impregnation with potassium hydroxide did not improve the capacity of the pellets to capture CO_2. Pellets impregnated with 5% loading had better performance than pellets impregnated with 20%. Although the reason for the lower capacities of the impregnated pellets is unclear, it has been suggested that the KOH molecules may block the pores of the pellets, thus hindering the diffusion of molecules through them.

Last, the presence of steam had a positive effect on the capacity of the pellets to capture CO_2. Experiments in which 10% steam was injected as part of the mixture of gases during the carbonation seemed to have higher conversion (6%) after 15 cycles than pellets for which steam was not used. The experiments with 30% steam involved condensation issues and, consequently, the quantitative analysis was complicated. Nevertheless, the results showed better capacity than for the experiments in which 10% steam was used, although it was not possible to determine the exact fraction of steam injected.

Chapter Seven – Conclusions and Recommendations

7.1 Conclusions

In this thesis, pellets developed to integrate calcium looping and chemical looping combustion have been studied. The goals of this thesis were to study the performance of the pellets over multiple cycles, and improve their capacity to capture CO_2. Two different configurations of pellets were tested, namely core-in-shell and homogeneous. The core-in-shell pellets contained 50% CuO, 40% CaO and 10% calcium aluminate cement (CS-50/40/10), while for the homogeneous configuration, in addition to the 50/40/10 composition, two more compositions were tested, 90% CaO and 10% cement (90/10), and 50% CuO and 50% cement (50/50).

Both configurations of composite pellets, with 50/40/10 composition, showed excellent performance in terms of capacity to be oxidized and reduced multiple times. However, the capacity to capture CO_2 decreased substantially after a few cycles, 50% after five cycles for the core-in-shell, and 47% after five cycles for the homogeneous (73% after 20 cycles). This issue was their main limitation.

The homogeneous pellets containing 50% CuO and 50% cement (50/50), and 90% CaO and 10% cement (90/10), were designed to work in the dual configuration of reactors. The 50/50 pellets showed excellent performance during 20 cycles, but agglomeration issues occurred. Therefore, the content of CuO may need to be reduced in order to avoid this problem. The 90/10 pellets lost 66% of the capacity to capture CO_2 after 20 cycles. However, even though the content of CaO for the 90/10 is barely two times that of the 50/40/10, the capacity was more than 10 times that of the composite 50/40/10. The comparison of the capacity in terms of $gCO_2/gCaO$

showed that the 90/10 had better performance, which indicated that the combination of CaO with CuO leads to a lower capacity to capture CO_2.

Pure methane as a fuel for the chemical looping combustion can lead to carbon deposits. Thus, this issue should be addressed because, if the carbon deposits onto the surface of the pellet, in the air reactor CO_2 would be produced, which would reduce the efficiency of the process.

Finally, the capacity of the pellets to capture CO_2 can be enhanced by subjecting the pellets to a thermal pre-treatment. Also, the presence of steam during the carbonation can lead to significantly higher capacity to capture CO_2. In contrast, the addition of KOH does not improve the capacity whatsoever.

7.2 Recommendations for future research

The major limitation of the pellets studied in this thesis was the loss of capacity to capture CO_2 after multiple cycles. Different approaches were taken in order to address this problem, but each approach was taken separately. Since pellets thermally pre-treated, and pellets subjected to carbonation in the presence of steam, showed better performances, the combination of these two approaches may lead to even better results.

Also, regarding the thermal treatment, different temperatures, holding times and atmospheres should be tested. For instance, Mastin et al. pre-treated CaO samples at 1053 K under a mixture of CO_2 and steam for 20 h, and obtained remarkable results[116].

The addition of KOH did not improve performance, but other potassium-based compounds, such as potassium carbonate may produce different results. Also, adding such compounds during the preparation of pellets could be an option to take into consideration.

Therefore, further work on the addition of compounds to enhance the capacity to capture CO_2 should be performed.

Another option to avoid the decrease of the capacity to capture CO_2 is to use a different preparation method and/or support. For instance, Broda et al. reported high CO_2 uptakes when using a co-precipitation method to synthesize the CaO-based sorbent[101]. Also, supports that could enable good dispersion of the CaO molecules may help to prevent sintering issues, ultimately leading to the enhancement of the capacity to capture CO_2 over multiple cycles.

Also, characterization of the pellets prior and after being subjected to multiple cycles can provide insights into the changes that may be occurring in the structure and/or composition of the pellets. BET and BJH analyses can help to find whether changes on the surface area, pore volume and pore size distribution take place or not. Also, elemental mapping across the pellet can provide information about the internal composition of the pellet.

The oxygen carrier used in this thesis presented agglomeration issues. Other authors overcame this problem by preparing a mixture of iron and copper oxides. Thus, either smaller fractions of oxygen carrier, or mixtures with other oxygen carriers are recommended.

In addition, two different ranges of pellets size were studied, but the configurations were different, core-in-shell with sizes between 0.425 – 1.425 mm, and homogeneous with sizes between 0.250 – 0.600 mm. Therefore, the pellet size may have an effect on their performance, in either chemical looping combustion and/or calcium looping. Therefore, it is recommended to study the effect of this variable.

In this thesis, it has not been studied the effect of other gases present in a coal-fired power plant, such as NOx and SOx. Therefore, it is vital to determine how the pellets would perform under those circumstances. Depending on the configuration of reactors, not every

composition of pellets should be subjected to such gases. For instance, in the dual configuration, the 50/50 pellets would not need to be tested in the presence of NOx or SOx because in an actual process they would not be in contact with those gases.

Last, some studies on the kinetics of the carbonation reaction have been done[52]. However, there is little information on the oxidation, calcination and reduction. Such information would have been of great use for the mass transfer model. Therefore, the kinetics of those reactions could be of major interest in other studies, such as modeling of reactors.

References

1. IPCC. *IPCC AR4 SYR Appendix Glossary*. 75–104 (2007).

2. Global Emissions _ Climate Change _ US EPA. at <http://www.epa.gov/climatechange/ghgemissions/global.html>. Date accessed: March 8th, 2015

3. IEA - May - Global carbon-dioxide emissions increase by 1. at <http://www.iea.org/newsroomandevents/news/2012/may/global-carbon-dioxide-emissions-increase-by-10-gt-in-2011-to-record-high.html>. Date accessed: March 8th, 2015

4. *Canada's Emissions Trends*. (2013).

5. *Alberta Environment and Sustainable Resource Development : Report on 2011 Greenhouse Gas Emissions*. (2013).

6. Reduction of Carbon Dioxide Emissions from Coal-Fired Generation of Electricity Regulations - Current Regulation - Regulations and Other Instruments - CEPA Environmental Registry. at <http://www.ec.gc.ca/lcpe-cepa/eng/regulations/detailReg.cfm?intReg=209>. Date accessed: March 8th, 2015

7. Innovations - Canada's Plan to reduce Greenhouse Gases. at <http://actionplancanada.weebly.com/innovations.html>. Date accessed: March 8th, 2015

8. CCS technologies show long, safe history - Canada. at <http://www.shell.ca/en/aboutshell/our-business-tpkg/upstream/oil-sands/quest/technology.html>. Date accessed: March 8th, 2015

9. Herzog, H. The Economics of CO2 Separation and Capture. *Second Dixy Lee Ray Meml. Symp.* 2–19 (1999).

10. SaskPower. Boundary Dam Integrated Carbon Capture and Storage Demonstration Project. (2012). at <http://www.saskpower.com/wp-content/uploads/clean_coal_information_sheet.pdf>

11. Carbon Capture and Storage key to addressing climate change - Canada. at <http://www.shell.ca/en/aboutshell/our-business-tpkg/upstream/oil-sands/quest/ccs.html>. Date accessed: March 8th, 2015

12. Dean, C. C., Blamey, J., Florin, N. H., Al-Jeboori, M. J. & Fennell, P. S. The calcium looping cycle for CO2 capture from power generation, cement manufacture and hydrogen production. *Chem. Eng. Res. Des.* **89,** 836–855 (2011).

13. Adanez, J., Abad, A., Garcia-Labiano, F., Gayan, P. & de Diego, L. F. Progress in Chemical-Looping Combustion and Reforming technologies. *Prog. Energy Combust. Sci.* **38,** 215–282 (2012).

14. Manovic, V., Wu, Y., He, I. & Anthony, E. J. Core-in-Shell CaO / CuO-Based Composite for CO2 Capture. *Ind. Eng. Chem. Res.* **50,** 12384–12391 (2011).

15. Li, L., Zhao, N., Wei, W. & Sun, Y. A review of research progress on CO2 capture, storage, and utilization in Chinese Academy of Sciences. *Fuel* **108,** 112–130 (2013).

16. Manovic, V. & Anthony, E. J. CaO-Based Pellets with Oxygen Carriers and Catalysts. *Energy & Fuels* **25,** 4846–4853 (2011).

17. Lyon, R. K. & Cole, J. A. Unmixed Combustion: An Alternative to Fire. *Combust. Flame* **121,** 249–261 (2000).

18. Abanades, J. C., Murillo, R., Fernandez, J. R., Grasa, G. & Martinez, I. New CO2 Capture Process for Hydrogen Production Combining Ca and Cu Chemical Loops. *Environ. Sci. Technol.* **44,** 6901–6904 (2010).

19. Murillo, R. & Abanades, J. C. Method of capturing CO2 by means of CaO and the exothermal reduction of a solid. (2006).

20. Manovic, V. & Anthony, E. J. Integration of calcium and chemical looping combustion using composite CaO/CuO-based materials. *Environ. Sci. Technol.* **45,** 10750–6 (2011).

21. CanmetENERGY. *Combined Calcium looping and Chemical looping combustion process applied to CO2 capture*. (2014).

22. What is CCS? – The Carbon Capture & Storage Association (CCSA). at <http://www.ccsassociation.org/what-is-ccs/>. Date accessed: March 10th, 2015

23. *Accelerating the Uptake of CCS : Industrial Use of Captured Carbon Dioxide*. (2011).

24. Applications of CO2 - Applications of Carbon Dioxide, CO2 Gas Applications. at <http://www.co2gasplants.com/applications-co2.html>. Date accessed: March 10th, 2015

25. *Developments and innovation in carbon dioxide (CO2) capture and storage technology*. **1,** (Woodhead Publishing Limited, 2010).

26. Toftegaard, M. B., Brix, J., Jensen, P. A., Glarborg, P. & Jensen, A. D. Oxy-fuel combustion of solid fuels. *Prog. Energy Combust. Sci.* **36,** 581–625 (2010).

27. Wall, T., Stanger, R. & Liu, Y. Gas cleaning challenges for coal-fired oxy-fuel technology with carbon capture and storage. *Fuel* **108,** 85–90 (2013).

28. Uses and Applications of Oxygen Gas and Liquid Oxygen by Industry | Praxair, Inc. at <http://www.praxair.com/gases/buy-liquid-oxygen-or-compressed-oxygen-gas#!tab=applications>. Date accessed: March 10th, 2015

29. Universal Industrial Gases, Inc. at <http://www.uigi.com/hydrogen.html>. Date accessed: March 10th, 2015

30. CCS Global Institute. *CO2 Capture Technologies Pre Combustion Capture*. (2012).

31. Mondal, M. K., Balsora, H. K. & Varshney, P. Progress and trends in CO2 capture/separation technologies: A review. *Energy* **46,** 431–441 (2012).

32. MacDowell, N., Florin, N., Buchard, A., Hallett, J., Galindo, A., Jackson, G., Adjiman, C. S., Williams, C. K., Shah, N. & Fennell, P. An overview of CO2 capture technologies. *Energy Environ. Sci.* **3,** (2010).

33. B.M., A., J.G., A., E.P., L. & A.P.S., T. Coal-oxygen process provides CO2 for enhanced recovery. *Oil Gas J.* **80,** 68–70 (1982).

34. L. Horn, F. & Steinberg, M. Control of carbon dioxide emissions from a power plant (and use in enhanced oil recovery). *Fuel* **61,** 415–422 (1982).

35. Chakroun, N. W. & Ghoniem, A. F. Techno-economic assessment of sour gas oxy-combustion water cycles for CO2 capture. *Int. J. Greenh. Gas Control* **36,** 1–12 (2015).

36. Li, S., Li, W., Xu, M., Wang, X., Li, H. & Lu, Q. The experimental study on nitrogen oxides and SO2 emission for oxy-fuel circulation fluidized bed combustion with high oxygen concentration. *Fuel* **146,** 81–87 (2015).

37. Wang, H., Zheng, Z.-M., Yang, L., Liu, X.-L., Guo, S. & Wu, S.-H. Experimental investigation on ash deposition of a bituminous coal during oxy-fuel combustion in a bench-scale fluidized bed. *Fuel Process. Technol.* **132,** 24–30 (2015).

38. Wang, W., Ramkumar, S. & Fan, L. S. Energy penalty of CO2 capture for the Carbonation–Calcination Reaction (CCR) Process: Parametric effects and comparisons with alternative processes. *Fuel* **104,** 561–574 (2013).

39. Abanades, J. C., Anthony, E. J., Wang, J. & Oakey, J. E. Fluidized Bed Combustion Systems Integrating CO2 Capture with CaO. *Environ. Sci. Technol.* **39,** 2861–2866 (2005).

40. Shimizu, T., Hirama, T., Hosoda, H., Kitano, K., Inagaki, M. & Tejima, K. A Twin-Bed Reactor for Removal of CO2 from Combustion Processes. *Chem. Eng. Res. Des.* **77,** 62–68 (1999).

41. Wang, M., Lawal, A., Stephenson, P., Sidders, J. & Ramshaw, C. Post-combustion CO2 capture with chemical absorption: A state-of-the-art review. *Chem. Eng. Res. Des.* **89,** 1609–1624 (2011).

42. Post-combustion capture - The Carbon Capture & Storage Association (CCSA). at <http://www.ccsassociation.org/what-is-ccs/capture/post-combustion-capture/>. Date accessed: March 10th, 2015

43. Boundary Dam Integrated Carbon Capture and Sequestration Demonstration Project - Global Carbon Capture and Storage Institute.

44. Shi, H., Naami, A., Idem, R. & Tontiwachwuthikul, P. Catalytic and non catalytic solvent regeneration during absorption-based CO2 capture with single and blended reactive amine solvents. *Int. J. Greenh. Gas Control* **26,** 39–50 (2014).

45. Mazari, S. A., Si Ali, B., Jan, B. M., Saeed, I. M. & Nizamuddin, S. An overview of solvent management and emissions of amine-based CO2 capture technology. *Int. J. Greenh. Gas Control* **34,** 129–140 (2015).

46. Van Garderen, N., Clemens, F. J. & Graule, T. Development of copper impregnated porous granulates for chemical-looping combustion. *Fuel* **119,** 323–327 (2014).

47. Blamey, J., Anthony, E. J., Wang, J. & Fennell, P. S. The calcium looping cycle for large-scale CO2 capture. *Prog. Energy Combust. Sci.* **36,** 260–279 (2010).

48. Rashidian, M. Thermal degradation study by continuous thermal stability rig. (Norwegian University of Science and Technology, 2013).

49. Samanta, A., Zhao, A., Shimizu, G. K. H., Sarkar, P. & Gupta, R. Post-combustion CO2 capture using solid sorbents: A review. *Ind. Eng. Chem. Res.* **51,** 1438–1463 (2011).

50. Abbasi, E., Hassanzadeh, A. & Abbasian, J. Regenerable MgO-based sorbent for high temperature CO2 removal from syngas: 2. Two-zone variable diffusivity shrinking core model with expanding product layer. *Fuel* **105,** 128–134 (2012).

51. Butler, J. W., Jim Lim, C. & Grace, J. R. Kinetics of CO2 absorption by CaO through pressure swing cycling. *Fuel* **127,** 78–87 (2014).

52. Rout, K. R., Fermoso, J., Chen, D. & Jakobsen, H. A. Kinetic rate of uptake of a synthetic Ca-based sorbent: Experimental data and numerical simulations. *Fuel* **120,** 53–65 (2014).

53. Donat, F., Florin, N. H., Anthony, E. J. & Fennell, P. S. Influence of high-temperature steam on the reactivity of CaO sorbent for CO_2 capture. *Environ. Sci. Technol.* **46,** 1262–9 (2012).

54. Ridha, F. N., Manovic, V., Wu, Y., Macchi, A. & Anthony, E. J. Post-combustion CO2 capture by formic acid-modified CaO-based sorbents. *Int. J. Greenh. Gas Control* **16,** 21–28 (2013).

55. Li, Y., Zhao, C., Chen, H., Liang, C., Duan, L. & Zhou, W. Modified CaO-based sorbent looping cycle for CO2 mitigation. *Fuel* **88,** 697–704 (2009).

56. Chen, H., Zhao, C. & Yu, W. Calcium-based sorbent doped with attapulgite for CO2 capture. *Appl. Energy* **112,** 67–74

57. Chen, H. & Zhao, C. Development of a CaO-based sorbent with improved cyclic stability for CO2 capture in pressurized carbonation. *Chem. Eng. J.* **171,** 197–205 (2011).

58. Mattisson, T. & Ja, A. Reactivity of Some Metal Oxides Supported on Alumina with Alternating Methane and Oxygens-Application for Chemical Looping Combustion. *Energy & Fuels* 643–651 (2003).

59. García-Labiano, F., de Diego, L. F., Adánez, J., Abad, A. & Gayán, P. Temperature variations in the oxygen carrier particles during their reduction and oxidation in a chemical-looping combustion system. *Chem. Eng. Sci.* **60,** 851–862 (2005).

60. Leion, H., Lyngfelt, A. & Mattisson, T. Solid fuels in chemical-looping combustion using a NiO-based oxygen carrier. *Chem. Eng. Res. Des.* **87,** 1543–1550 (2009).

61. Yang, H., Xu, Z., Fan, M., Slimane, R. B., Bland, A. E. & Wright, I. Progress in carbon dioxide seperation and capture: A review. *J. Environ. Sci.* **20,** 14–27 (2008).

62. Adánez-Rubio, I., Abad, A., Gayán, P., de Diego, L. F., García-Labiano, F. & Adánez, J. Performance of CLOU process in the combustion of different types of coal with CO2 capture. *Int. J. Greenh. Gas Control* **12,** 430–440 (2013).

63. Fan, L. S., Zeng, L., Wang, W. & Luo, S. Chemical looping processes for CO2 capture and carbonaceous fuel conversion – prospect and opportunity. *Energy Environ. Sci.* **5,** 7254 (2012).

64. Kim, H. R., Wang, D., Zeng, L., Bayham, S., Tong, A., Chung, E., Kathe, M. V., Luo, S., McGiveron, O., Wang, A., Sun, Z., Chen, D. & Fan, L. S. Coal direct chemical looping combustion process: Design and operation of a 25-kWth sub-pilot unit. *Fuel* **108,** 370–384 (2013).

65. Markström, P., Linderholm, C. & Lyngfelt, A. Analytical model of gas conversion in a 100kW chemical-looping combustor for solid fuels—Comparison with operational results. *Chem. Eng. Sci.* **96,** 131–141 (2013).

66. Thunman, H., Lind, F., Breitholtz, C., Berguerand, N. & Seemann, M. Using an oxygen-carrier as bed material for combustion of biomass in a 12-MWth circulating fluidized-bed boiler. *Fuel* **113,** 300–309 (2013).

67. Manovic, V. & Anthony, E. J. Lime-based sorbents for high-temperature CO2 capture-a review of sorbent modification methods. *Int. J. Environ. Res. Public Health* **7,** 3129–3140 (2010).

68. Hann, J. Annealing of glass containers and hollowware. *Glas. Int.* 22–28 (2013).

69. Kopyscinski, J., Lam, J., Mims, C. A. & Hill, J. M. K2CO3 catalyzed steam gasification of ash-free coal. Studying the effect of temperature on carbon conversion and gas production rate using a drop-down reactor. *Fuel* **128,** 210–219 (2014).

70. Carbon Engineering, L. Our Technology. at <http://www.steinberg.net/en/company/technologies.html>. Date accessed: March 10th, 2015

71. Wu, Y., Chen, X., Radosz, M., Fan, M., Dong, W., Zhang, Z. & Yang, Z. Inexpensive calcium-modified potassium carbonate sorbent for CO2 capture from flue gas: Improved SO2 resistance, enhanced capacity and stability. *Fuel* **125,** 50–56 (2014).

72. Cho, J. S., Kim, S. M., Chun, H. D., Han, G. W. & Lee, C. H. Carbon Dioxide Capture with Accelerated Carbonation of Industrial Combustion Waste. *Int. J. Chem. Eng. Appl.* **2,** 60–65 (2011).

73. Ello, A. S., de Souza, L. K. C., Trokourey, A. & Jaroniec, M. Development of microporous carbons for CO2 capture by KOH activation of African palm shells. *J. CO2 Util.* **2,** 35–38 (2013).

74. Watkins, R. S., Lee, A. F. & Wilson, K. Li-CaO catalysed tri-glyceride transesterification for biodiesel applications. *Green Chem.* **6,** 335–340 (2004).

75. Kumar, D. & Ali, A. Potassium Ion Impregnated Calcium Oxide as a Nanocrystalline Solid Catalyst for Biodiesel Production from Waste Cotton Seed Oil. *Energy Sources Part A Recover. Util. Environ. Eff.* **36,** 1093–1102 (2014).

76. Qin, C., Yin, J., Liu, W., An, H. & Feng, B. Behavior of CaO/CuO based composite in a combined calcium and copper chemical looping process. *Ind. Eng. Chem. Res.* **51,** 12274–12281 (2012).

77. Liew, S. C. Impacts of Vanadium and Coke Deposition on CO2 Gasification of Nickel Catalysts Supported on Activated Carbon from Petroleum Coke. (University of Calgary, 2014).

78. Micromeritics TriStar 3000 Manual. (2007).

79. Waseda, Y., Matsubara, E. & Shinoda, K. *X-Ray Diffraction Crystallography - Introduction, Examples and Solved Problems*. (Springer, 2011).

80. Cahn Thermax 500 Thermogravimetric Analyzer Manual. (2006).

81. International Union of Pure and Applied Chemistry (IUPAC). Manual on catalyst characterization. *Pure Appl. Chem.* **63,** 1227–1246 (1991).

82. Valverde, J. M., Sanchez-Jimenez, P. E. & Perez-Maqueda, L. A. High and stable capture capacity of natural limestone at Ca-looping conditions by heat pretreatment and recarbonation synergy. *Fuel* **123,** 79–85 (2014).

83. Rahaman N., M. *Ceramic processing and sintering*. 875 (CRC Press, 2003).

84. Farid, M. A unified approach to the heat and mass transfer in melting, solidification, frying and different drying processes. *Chem. Eng. Sci.* **56,** 5419–5427 (2001).

85. Farid, M. The moving boundary problems from melting and freezing to drying and frying of food. *Chem. Eng. Process.* **41,** 1–10 (2002).

86. Shi, J., Donskoi, E., McElwain, D. L. S. & Wibberley, L. J. Modelling the reduction of an iron ore-coal composite pellet with conduction and convection in an axisymmetric temperature field. *Math. Comput. Model.* **42,** 45–60 (2005).

87. Chatterjee, A. & Chaturvedi, S. Heat transfer in a reaction–diffusion system with a moving heat source. *Int. J. Heat Mass Transf.* **54,** 326–337 (2011).

88. Enibe, S. O. & Iloeje, O. C. Heat and mass transfer in porous spherical pellets of CaCl2 for solar refrigeration. *Renew. Energy* **20,** 305–324 (2000).

89. Lim, J. Y. & Dennis, J. S. Modeling Reaction and Di ff usion in a Spherical Catalyst Pellet Using Multicomponent Flux Models. *Ind. Eng. Chem. Res.* **51,** 15901–15911 (2012).

90. Byron Bird, R., E. Stewart, W. & N. Lightfoot. *Transport Phenomena*. 897 (John Wiley & Sons, 2002).

91. Scott Fogler, H. *Elements of Chemical Reaction Engineering*. (Prentice Hall, 1992).

92. Kiel, J. H. A., Prins, W. & Van Swaaij, W. P. M. Modelling of non-catalytic reactions in a gas-solid trickle flow reactor: regenerative flue gas desulphurisation using a silica-supported oxide. *Chem. Eng. Sci.* **47,** 4271–4286 (1992).

93. Froment, G. F., Bischoff, K. B. & De Wilde, J. *Chemical Reactor Analysis and Design*. (John Wiley & Sons, 2011).

94. Navarre-Sitchler, A., Steefel, C. I., Yang, L., Tomutsa, L. & Brantley, S. L. Evolution of porosity and diffusivity associated with chemical weathering of a basalt clast. *J. Geophys. Res.* **114,** F02016 (2009).

95. National Institute of Standards and Technology (NIST). at <www. nist.gov>. Date accessed: March 1st, 2015

96. Kwak, K. & Kim, C. Viscosity and thermal conductivity of copper oxide nanofluid dispersed in ethylene glycol. *Korea-Australia Rheol. J.* **17,** 35–40 (2005).

97. Xu, L., Sithambaram, S., Zhang, Y., Chen, C. H., Jin, L., Joesten, R. & Suib, S. L. Novel urchin-like CuO synthesized by a facile reflux method with efficient olefin epoxidation catalytic performance. *Chem. Mater.* **21,** 1253–1259 (2009).

98. Halikia, I., Zoumpoulakis, L., Christodoulou, E. & Prattis, D. Kinetic study of the thermal decomposition of calcium carbonate by isothermal methods of analysis. *Eur. J. Process. Enviromental Prot.* **1,** 89–102 (2001).

99. National Insitute of Standards and Technology (NIST). NIST Chemistry WebBook. at <http://webbook.nist.gov/chemistry/>. Date accessed: March 1st, 2015

100. Kazi, S. S., Aranda, A., Meyer, J. & Mastin, J. High performance CaO-based sorbents for pre- and post- combustion CO2 capture at high temperature. *Energy Procedia* **63,** 2207–2215 (2014).

101. Broda, M. & Kierzkowska, A. M. *Development of synthetic Ca-based sorbents for CO2 capture using the co-precipitation technique*. (2011).

102. Claridge, J. B., Green, M. L. H., Tsang, S. C., York, A. P. E., Ashcroft, A. T. & Battle, P. D. A study of carbon deposition on catalyst during the partial oxidation of methane to synthesis gas. *Catal. Letters* **22,** 299–305 (1993).

103. Jin, H., Okamoto, T. & Ishida, M. Development of a Novel Chemical-Looping Combustion: Synthesis of a Solid Looping Material of NiO/NiAl2O4. *Ind. Eng. Chem. Res.* **38,** 126–132 (1999).

104. Kvon, R. I., Boronin, A. I., Shaikhutdinov, S. K. & Buyanov, R. A. XPS and STM study of carbon deposits at the surface of platinum (110). *Appl. Surf. Sci.* **120,** 239–242 (1997).

105. Cho, P. Development and characterisation of oxygen-carrier materials for chemical-looping combustion. (Chalmers University of Technology, 2005).

106. Wang, J., Huang, L., Yang, R., Zhang, Z., Wu, J., Gao, Y., Wang, Q., O'Hare, D. & Zhong, Z. Recent advances in solid sorbents for CO2 capture and new development trends. *Energy Environ. Sci.* **7,** 3478–3518 (2014).

107. Hamers, H. P., Gallucci, F., Cobden, P. D., Kimball, E. & van Sint Annaland, M. A novel reactor configuration for packed bed chemical-looping combustion of syngas. *Int. J. Greenh. Gas Control* **16,** 1–12 (2013).

108. Siriwardane, R., Tian, H., Simonyi, T. & Poston, J. Synergetic effects of mixed copper–iron oxides oxygen carriers in chemical looping combustion. *Fuel* **108,** 319–333 (2013).

109. Manovic, V., Fennell, P. S., Al-jeboori, M. J. & Anthony, E. J. Steam-Enhanced Calcium Looping Cycles with Calcium Aluminate Pellets Doped with Bromides. (2013).

110. Dobner, S., Sterns, L., Graff, R. A. & Squires, A. M. Cyclic Calcination and Recarbonation of Calcined Dolomite. *Ind. Eng. Chem. Process Des. Dev.* **16,** 479–486 (1977).

111. Yang, S. & Xiao, Y. Steam Catalysis in CaO Carbonation under Low Steam Partial Pressure. *Ind. Eng. Chem. Res.* **47,** 4043–4048 (2008).

112. Manovic, V. & Anthony, E. J. Carbonation of CaO-Based Sorbents Enhanced by Steam Addition. *Ind. Eng. Chem. Res.* **49,** 9105–9110 (2010).

113. Symonds, R. T., Lu, D. Y., Macchi, A., Hughes, R. W. & Anthony, E. J. CO2 capture from syngas via cyclic carbonation/calcination for a naturally occurring limestone: Modelling and bench-scale testing. *Chem. Eng. Sci.* **64,** 3536–3543 (2009).

114. Dou, B., Song, Y., Liu, Y. & Feng, C. High temperature CO2 capture using calcium oxide sorbent in a fixed-bed reactor. *J. Hazard. Mater.* **183,** 759–65 (2010).

115. Arias, B., Grasa, G., Abanades, J. C., Manovic, V. & Anthony, E. J. The Effect of Steam on the Fast Carbonation Reaction Rates of CaO. *Ind. Eng. Chem. Res.* **51,** 2478–2482 (2012).

116. Mastin, J., Aranda, A. & Meyer, J. New synthesis method for CaO-based synthetic sorbents with enhanced properties for high-temperature CO2-capture. *Energy Procedia* **4,** 1184–1191 (2011).

117. Standard Normal Distribution. at <https://www.stat.tamu.edu/~lzhou/stat302/standardnormaltable.pdf>. Date accessed: February 8th, 2015

APPENDIX A – COPYRIGHT PERMISSIONS

A.1 - Copyright permission for Figure 1.1

ELSEVIER LICENSE
TERMS AND CONDITIONS

Mar 13, 2015

This is a License Agreement between Alvaro Recio ("You") and Elsevier ("Elsevier") provided by Copyright Clearance Center ("CCC"). The license consists of your order details, the terms and conditions provided by Elsevier, and the payment terms and conditions.

All payments must be made in full to CCC. For payment instructions, please see information listed at the bottom of this form.

Supplier	Elsevier Limited The Boulevard,Langford Lane Kidlington,Oxford,OX5 1GB,UK
Registered Company Number	1982084
Customer name	Alvaro Recio
Customer address	2104 Uxbridge Dr NW Calgary, AB T2N 3Z4
License number	3582260562523
License date	Mar 04, 2015
Licensed content publisher	Elsevier
Licensed content publication	Progress in Energy and Combustion Science
Licensed content title	Progress in Chemical-Looping Combustion and Reforming technologies
Licensed content author	Juan Adanez,Alberto Abad,Francisco Garcia-Labiano,Pilar Gayan,Luis F. de Diego
Licensed content date	April 2012
Licensed content volume number	38
Licensed content issue number	2
Number of pages	68
Start Page	215
End Page	282
Type of Use	reuse in a thesis/dissertation
Portion	figures/tables/illustrations
Number of figures/tables /illustrations	1
Format	both print and electronic
Are you the author of this Elsevier article?	No

Will you be translating?	No
Original figure numbers	Figure 1.
Title of your thesis/dissertation	Study of Composite Sorbent Pellets for Integration of Calcium Looping and Chemical Looping Combustion
Expected completion date	Apr 2015
Estimated size (number of pages)	140
Elsevier VAT number	GB 494 6272 12
Price	0.00 CAD
VAT/Local Sales Tax	0.00 CAD / 0.00 GBP
Total	**0.00 CAD**

Terms and Conditions

INTRODUCTION

1. The publisher for this copyrighted material is Elsevier. By clicking "accept" in connection with completing this licensing transaction, you agree that the following terms and conditions apply to this transaction (along with the Billing and Payment terms and conditions established by Copyright Clearance Center, Inc. ("CCC"), at the time that you opened your Rightslink account and that are available at any time at http://myaccount.copyright.com).

GENERAL TERMS

2. Elsevier hereby grants you permission to reproduce the aforementioned material subject to the terms and conditions indicated.
3. Acknowledgement: If any part of the material to be used (for example, figures) has appeared in our publication with credit or acknowledgement to another source, permission must also be sought from that source. If such permission is not obtained then that material may not be included in your publication/copies. Suitable acknowledgement to the source must be made, either as a footnote or in a reference list at the end of your publication, as follows: "Reprinted from Publication title, Vol /edition number, Author(s), Title of article / title of chapter, Pages No., Copyright (Year), with permission from Elsevier [OR APPLICABLE SOCIETY COPYRIGHT OWNER]." Also Lancet special credit - "Reprinted from The Lancet, Vol. number, Author(s), Title of article, Pages No., Copyright (Year), with permission from Elsevier."
4. Reproduction of this material is confined to the purpose and/or media for which permission is hereby given.
5. Altering/Modifying Material: Not Permitted. However figures and illustrations may be altered/adapted minimally to serve your work. Any other abbreviations, additions, deletions and/or any other alterations shall be made only with prior written authorization of Elsevier Ltd. (Please contact Elsevier at permissions@elsevier.com)
6. If the permission fee for the requested use of our material is waived in this instance, please be advised that your future requests for Elsevier materials may attract a fee.
7. Reservation of Rights: Publisher reserves all rights not specifically granted in the combination of (i) the license details provided by you and accepted in the course of this licensing transaction, (ii) these terms and conditions and (iii) CCC's Billing and Payment terms and conditions.
8. License Contingent Upon Payment: While you may exercise the rights licensed immediately upon issuance of the license at the end of the licensing process for the transaction, provided that you have disclosed complete and accurate details of your proposed use, no license is finally effective unless and until full payment is received from you (either by publisher or by CCC) as provided in CCC's Billing and Payment terms and conditions. If full payment is not received on a timely basis, then any license preliminarily granted shall be deemed automatically revoked and shall be void as if never granted. Further, in the event that you breach any of these terms and conditions or any of CCC's Billing and Payment terms and conditions, the license is automatically revoked and shall be void as if never granted. Use of materials as described in a revoked license, as well as any use of the materials beyond the scope of an unrevoked license, may constitute copyright infringement and publisher reserves the right to take any and all action to protect its copyright in the materials.
9. Warranties: Publisher makes no representations or warranties with respect to the licensed material.
10. Indemnity: You hereby indemnify and agree to hold harmless publisher and CCC, and their respective officers, directors, employees and agents, from and against any and all claims arising out of your use of the licensed material other than as specifically authorized pursuant to this license.

11. No Transfer of License: This license is personal to you and may not be sublicensed, assigned, or transferred by you to any other person without publisher's written permission.
12. No Amendment Except in Writing: This license may not be amended except in a writing signed by both parties (or, in the case of publisher, by CCC on publisher's behalf).
13. Objection to Contrary Terms: Publisher hereby objects to any terms contained in any purchase order, acknowledgment, check endorsement or other writing prepared by you, which terms are inconsistent with these terms and conditions or CCC's Billing and Payment terms and conditions. These terms and conditions, together with CCC's Billing and Payment terms and conditions (which are incorporated herein), comprise the entire agreement between you and publisher (and CCC) concerning this licensing transaction. In the event of any conflict between your obligations established by these terms and conditions and those established by CCC's Billing and Payment terms and conditions, these terms and conditions shall control.
14. Revocation: Elsevier or Copyright Clearance Center may deny the permissions described in this License at their sole discretion, for any reason or no reason, with a full refund payable to you. Notice of such denial will be made using the contact information provided by you. Failure to receive such notice will not alter or invalidate the denial. In no event will Elsevier or Copyright Clearance Center be responsible or liable for any costs, expenses or damage incurred by you as a result of a denial of your permission request, other than a refund of the amount(s) paid by you to Elsevier and/or Copyright Clearance Center for denied permissions.

LIMITED LICENSE

The following terms and conditions apply only to specific license types:
15. **Translation**: This permission is granted for non-exclusive world **English** rights only unless your license was granted for translation rights. If you licensed translation rights you may only translate this content into the languages you requested. A professional translator must perform all translations and reproduce the content word for word preserving the integrity of the article. If this license is to re-use 1 or 2 figures then permission is granted for non-exclusive world rights in all languages.
16. **Posting licensed content on any Website**: The following terms and conditions apply as follows: Licensing material from an Elsevier journal: All content posted to the web site must maintain the copyright information line on the bottom of each image; A hyper-text must be included to the Homepage of the journal from which you are licensing at http://www.sciencedirect.com/science/journal/xxxxx or the Elsevier homepage for books at http://www.elsevier.com; Central Storage: This license does not include permission for a scanned version of the material to be stored in a central repository such as that provided by Heron/XanEdu.
Licensing material from an Elsevier book: A hyper-text link must be included to the Elsevier homepage at http://www.elsevier.com . All content posted to the web site must maintain the copyright information line on the bottom of each image.

Posting licensed content on Electronic reserve: In addition to the above the following clauses are applicable: The web site must be password-protected and made available only to bona fide students registered on a relevant course. This permission is granted for 1 year only. You may obtain a new license for future website posting.
17. **For journal authors:** the following clauses are applicable in addition to the above:

Preprints:

A preprint is an author's own write-up of research results and analysis, it has not been peer-reviewed, nor has it had any other value added to it by a publisher (such as formatting, copyright, technical enhancement etc.).
Authors can share their preprints anywhere at any time. Preprints should not be added to or enhanced in any way in order to appear more like, or to substitute for, the final versions of articles however authors can update their preprints on arXiv or RePEc with their Accepted Author Manuscript (see below).
If accepted for publication, we encourage authors to link from the preprint to their formal publication via its DOI. Millions of researchers have access to the formal publications on ScienceDirect, and so links will help users to find, access, cite and use the best available version. Please note that Cell Press, The Lancet and some society-owned have different preprint policies. Information on these policies is available on the journal homepage.
Accepted Author Manuscripts: An accepted author manuscript is the manuscript of an article that has been accepted for publication and which typically includes author-incorporated changes suggested during submission, peer review and editor-author communications.
Authors can share their accepted author manuscript:

- immediately
  - via their non-commercial person homepage or blog
  - by updating a preprint in arXiv or RePEc with the accepted manuscript
  - via their research institute or institutional repository for internal institutional uses or as part of an invitation-only research collaboration work-group
  - directly by providing copies to their students or to research collaborators for their personal use
  - for private scholarly sharing as part of an invitation-only work group on commercial sites with which Elsevier has an agreement
- after the embargo period
  - via non-commercial hosting platforms such as their institutional repository
  - via commercial sites with which Elsevier has an agreement

In all cases accepted manuscripts should:

- link to the formal publication via its DOI
- bear a CC-BY-NC-ND license - this is easy to do
- if aggregated with other manuscripts, for example in a repository or other site, be shared in alignment with our hosting policy not be added to or enhanced in any way to appear more like, or to substitute for, the published journal article.

Published journal article (JPA): A published journal article (PJA) is the definitive final record of published research that appears or will appear in the journal and embodies all value-adding publishing activities including peer review co-ordination, copy-editing, formatting, (if relevant) pagination and online enrichment.
Policies for sharing publishing journal articles differ for subscription and gold open access articles:
Subscription Articles: If you are an author, please share a link to your article rather than the full-text. Millions of researchers have access to the formal publications on ScienceDirect, and so links will help your users to find, access, cite, and use the best available version.
Theses and dissertations which contain embedded PJAs as part of the formal submission can be posted publicly by the awarding institution with DOI links back to the formal publications on ScienceDirect.
If you are affiliated with a library that subscribes to ScienceDirect you have additional private sharing rights for others' research accessed under that agreement. This includes use for classroom teaching and internal training at the institution (including use in course packs and courseware programs), and inclusion of the article for grant funding purposes.
Gold Open Access Articles: May be shared according to the author-selected end-user license and should contain a CrossMark logo, the end user license, and a DOI link to the formal publication on ScienceDirect.
Please refer to Elsevier's posting policy for further information.
18. **For book authors** the following clauses are applicable in addition to the above: Authors are permitted to place a brief summary of their work online only. You are not allowed to download and post the published electronic version of your chapter, nor may you scan the printed edition to create an electronic version. **Posting to a repository:** Authors are permitted to post a summary of their chapter only in their institution's repository.
19. **Thesis/Dissertation**: If your license is for use in a thesis/dissertation your thesis may be submitted to your institution in either print or electronic form. Should your thesis be published commercially, please reapply for permission. These requirements include permission for the Library and Archives of Canada to supply single copies, on demand, of the complete thesis and include permission for Proquest/UMI to supply single copies, on demand, of the complete thesis. Should your thesis be published commercially, please reapply for permission. Theses and dissertations which contain embedded PJAs as part of the formal submission can be posted publicly by the awarding institution with DOI links back to the formal publications on ScienceDirect.

Elsevier Open Access Terms and Conditions
You can publish open access with Elsevier in hundreds of open access journals or in nearly 2000 established subscription journals that support open access publishing. Permitted third party re-use of these open access articles is defined by the author's choice of Creative Commons user license. See our open access license policy for more information.
Terms & Conditions applicable to all Open Access articles published with Elsevier:
Any reuse of the article must not represent the author as endorsing the adaptation of the article nor should the article

A.2 - Copyright permission for Figure 2.3

ELSEVIER LICENSE
TERMS AND CONDITIONS

Mar 13, 2015

This is a License Agreement between Alvaro Recio ("You") and Elsevier ("Elsevier") provided by Copyright Clearance Center ("CCC"). The license consists of your order details, the terms and conditions provided by Elsevier, and the payment terms and conditions.

All payments must be made in full to CCC. For payment instructions, please see information listed at the bottom of this form.

Supplier	Elsevier Limited The Boulevard,Langford Lane Kidlington,Oxford,OX5 1GB,UK
Registered Company Number	1982084
Customer name	Alvaro Recio
Customer address	2104 Uxbridge Dr NW Calgary, AB T2N 3Z4
License number	3583830348589
License date	Mar 07, 2015
Licensed content publisher	Elsevier
Licensed content publication	Progress in Energy and Combustion Science
Licensed content title	Oxy-fuel combustion of solid fuels
Licensed content author	Maja B. Toftegaard,Jacob Brix,Peter A. Jensen,Peter Glarborg,Anker D. Jensen
Licensed content date	October 2010
Licensed content volume number	36
Licensed content volume number	5
Licensed content issue number	5
Number of pages	45
Start Page	581
End Page	625
Type of Use	reuse in a thesis/dissertation
Intended publisher of new work	other
Portion	figures/tables/illustrations
Number of figures/tables /illustrations	1
Format	both print and electronic

Format	both print and electronic
Are you the author of this Elsevier article?	No
Will you be translating?	No
Original figure numbers	figure 3
Title of your thesis/dissertation	Study of Composite Sorbent Pellets for Integration of Calcium Looping and Chemical Looping Combustion
Expected completion date	Apr 2015
Estimated size (number of pages)	140
Elsevier VAT number	GB 494 6272 12
Price	0.00 CAD
VAT/Local Sales Tax	0.00 CAD / 0.00 GBP
Total	**0.00 CAD**
Terms and Conditions	

For terms and conditions, refer to Appendix A.1.

A.3 - Copyright permission for Figure 2.4

ELSEVIER LICENSE
TERMS AND CONDITIONS

Mar 13, 2015

This is a License Agreement between Alvaro Recio ("You") and Elsevier ("Elsevier") provided by Copyright Clearance Center ("CCC"). The license consists of your order details, the terms and conditions provided by Elsevier, and the payment terms and conditions.

All payments must be made in full to CCC. For payment instructions, please see information listed at the bottom of this form.

Supplier	Elsevier Limited The Boulevard,Langford Lane Kidlington,Oxford,OX5 1GB,UK
Registered Company Number	1982084
Customer name	Alvaro Recio
Customer address	2104 Uxbridge Dr NW Calgary, AB T2N 3Z4
License number	3584520451327
License date	Mar 08, 2015
Licensed content publisher	Elsevier
Licensed content publication	Chemical Engineering Research and Design
Licensed content title	Post-combustion CO2 capture with chemical absorption: A state-of-the-art review
Licensed content author	M. Wang,A. Lawal,P. Stephenson,J. Sidders,C. Ramshaw
Licensed content date	September 2011
Licensed content volume number	89
Licensed content issue number	9
Number of pages	16
Start Page	1609
End Page	1624
Type of Use	reuse in a thesis/dissertation
Intended publisher of new work	other
Portion	figures/tables/illustrations
Number of figures/tables /illustrations	1
Format	both print and electronic

Are you the author of this Elsevier article?	No
Will you be translating?	No
Original figure numbers	figure 2
Title of your thesis/dissertation	Study of Composite Sorbent Pellets for Integration of Calcium Looping and Chemical Looping Combustion
Expected completion date	Apr 2015
Estimated size (number of pages)	140
Elsevier VAT number	GB 494 6272 12
Price	0.00 CAD
VAT/Local Sales Tax	0.00 CAD / 0.00 GBP
Total	**0.00 CAD**
Terms and Conditions	

For terms and conditions, refer to Appendix A.1.

A.4 - Copyright permission for Figure 2.5

ELSEVIER LICENSE
TERMS AND CONDITIONS

Mar 13, 2015

This is a License Agreement between Alvaro Recio ("You") and Elsevier ("Elsevier") provided by Copyright Clearance Center ("CCC"). The license consists of your order details, the terms and conditions provided by Elsevier, and the payment terms and conditions.

All payments must be made in full to CCC. For payment instructions, please see information listed at the bottom of this form.

Supplier	Elsevier Limited The Boulevard,Langford Lane Kidlington,Oxford,OX5 1GB,UK
Registered Company Number	1982084
Customer name	Alvaro Recio
Customer address	2104 Uxbridge Dr NW Calgary, AB T2N 3Z4
License number	3584610269763
License date	Mar 09, 2015
Licensed content publisher	Elsevier
Licensed content publication	Progress in Energy and Combustion Science
Licensed content title	The calcium looping cycle for large-scale CO2 capture
Licensed content author	J. Blamey,E.J. Anthony,J. Wang,P.S. Fennell
Licensed content date	April 2010
Licensed content volume number	36
Licensed content issue number	2
Number of pages	20
Start Page	260
End Page	279
Type of Use	reuse in a thesis/dissertation
Intended publisher of new work	other
Portion	figures/tables/illustrations
Number of figures/tables /illustrations	1
Format	both print and electronic

Are you the author of this Elsevier article?	No
Will you be translating?	No
Original figure numbers	figure 1
Title of your thesis/dissertation	Study of Composite Sorbent Pellets for Integration of Calcium Looping and Chemical Looping Combustion
Expected completion date	Apr 2015
Estimated size (number of pages)	140
Elsevier VAT number	GB 494 6272 12
Price	0.00 CAD
VAT/Local Sales Tax	0.00 CAD / 0.00 GBP
Total	**0.00 CAD**
Terms and Conditions	

For terms and conditions, refer to Appendix A.1.

APPENDIX B – ADDITIONAL INFORMATION FOR CHAPTER THREE

B.1 – Calculations for KOH impregnation

Calculation of amount of KOH for impregnation of pellets

Composition of pellets: 90% CaO and 10% CE (wt%)

wt% of K desired: 20%

Precursor of K: KOH flakes – 85% purity

Molecular weight of K = 39.10 g/mol

Molecular weight of KOH = 56.11 mg/mol

Calculation steps:

mass of pellets = 500 mg

mass of CaO = (500)·(0.90) = 450 mg

mass of K = (450)·(0.20) = 90 mg

$$\text{mass of pure KOH} = 90 \text{ mg of K} \frac{56.11 \text{ mg KOH/mmol}}{39.10 \text{ mg K/mmol}} = 129.1 \text{ mg of KOH}$$

$$\text{mass of KOH flakes} = \frac{129.1\ mg\ of\ KOH}{0.85 \frac{mg\ of\ KOH}{mg\ of\ flakes}} = 151.9 \text{ mg}$$

B.2 – Table of Z values for analysis of errors

Table B.1. Standard Normal Distribution: table values represent area to the left of the Z score[117].

Z	.00	.01	.02	.03	.04	.05	.06	.07	.08	.09
-3.9	.00005	.00005	.00004	.00004	.00004	.00004	.00004	.00004	.00003	.00003
-3.8	.00007	.00007	.00007	.00006	.00006	.00006	.00006	.00005	.00005	.00005
-3.7	.00011	.00010	.00010	.00010	.00009	.00009	.00008	.00008	.00008	.00008
-3.6	.00016	.00015	.00015	.00014	.00014	.00013	.00013	.00012	.00012	.00011
-3.5	.00023	.00022	.00022	.00021	.00020	.00019	.00019	.00018	.00017	.00017
-3.4	.00034	.00032	.00031	.00030	.00029	.00028	.00027	.00026	.00025	.00024
-3.3	.00048	.00047	.00045	.00043	.00042	.00040	.00039	.00038	.00036	.00035
-3.2	.00069	.00066	.00064	.00062	.00060	.00058	.00056	.00054	.00052	.00050
-3.1	.00097	.00094	.00090	.00087	.00084	.00082	.00079	.00076	.00074	.00071
-3.0	.00135	.00131	.00126	.00122	.00118	.00114	.00111	.00107	.00104	.00100
-2.9	.00187	.00181	.00175	.00169	.00164	.00159	.00154	.00149	.00144	.00139
-2.8	.00256	.00248	.00240	.00233	.00226	.00219	.00212	.00205	.00199	.00193
-2.7	.00347	.00336	.00326	.00317	.00307	.00298	.00289	.00280	.00272	.00264
-2.6	.00466	.00453	.00440	.00427	.00415	.00402	.00391	.00379	.00368	.00357
-2.5	.00621	.00604	.00587	.00570	.00554	.00539	.00523	.00508	.00494	.00480
-2.4	.00820	.00798	.00776	.00755	.00734	.00714	.00695	.00676	.00657	.00639
-2.3	.01072	.01044	.01017	.00990	.00964	.00939	.00914	.00889	.00866	.00842
-2.2	.01390	.01355	.01321	.01287	.01255	.01222	.01191	.01160	.01130	.01101
-2.1	.01786	.01743	.01700	.01659	.01618	.01578	.01539	.01500	.01463	.01426
-2.0	.02275	.02222	.02169	.02118	.02068	.02018	.01970	.01923	.01876	.01831
-1.9	.02872	.02807	.02743	.02680	.02619	.02559	.02500	.02442	.02385	.02330
-1.8	.03593	.03515	.03438	.03362	.03288	.03216	.03144	.03074	.03005	.02938
-1.7	.04457	.04363	.04272	.04182	.04093	.04006	.03920	.03836	.03754	.03673
-1.6	.05480	.05370	.05262	.05155	.05050	.04947	.04846	.04746	.04648	.04551
-1.5	.06681	.06552	.06426	.06301	.06178	.06057	.05938	.05821	.05705	.05592
-1.4	.08076	.07927	.07780	.07636	.07493	.07353	.07215	.07078	.06944	.06811
-1.3	.09680	.09510	.09342	.09176	.09012	.08851	.08691	.08534	.08379	.08226
-1.2	.11507	.11314	.11123	.10935	.10749	.10565	.10383	.10204	.10027	.09853
-1.1	.13567	.13350	.13136	.12924	.12714	.12507	.12302	.12100	.11900	.11702
-1.0	.15866	.15625	.15386	.15151	.14917	.14686	.14457	.14231	.14007	.13786
-0.9	.18406	.18141	.17879	.17619	.17361	.17106	.16853	.16602	.16354	.16109
-0.8	.21186	.20897	.20611	.20327	.20045	.19766	.19489	.19215	.18943	.18673
-0.7	.24196	.23885	.23576	.23270	.22965	.22663	.22363	.22065	.21770	.21476
-0.6	.27425	.27093	.26763	.26435	.26109	.25785	.25463	.25143	.24825	.24510
-0.5	.30854	.30503	.30153	.29806	.29460	.29116	.28774	.28434	.28096	.27760
-0.4	.34458	.34090	.33724	.33360	.32997	.32636	.32276	.31918	.31561	.31207
-0.3	.38209	.37828	.37448	.37070	.36693	.36317	.35942	.35569	.35197	.34827
-0.2	.42074	.41683	.41294	.40905	.40517	.40129	.39743	.39358	.38974	.38591
-0.1	.46017	.45620	.45224	.44828	.44433	.44038	.43644	.43251	.42858	.42465
-0.0	.50000	.49601	.49202	.48803	.48405	.48006	.47608	.47210	.46812	.46414

B.3 – Development of Equation 3.2

Mass of sample before analysis [S] = [CS] – [C]

Mass of moisture and volatiles removed after analysis [A] = [CSW] – [CSWA]

Mass of dry mass [D] = [S] – [A] = [CS] – [C] – [CSW] – (– [CSWA]) =

= [CSWA] – [CSW] + [CS] – [C]

B.4 – Calculation of CO_2 partial pressure at two temperatures

Equation below describes the evolution of the partial pressure of CO_2 as a function of temperature[47]:

$$\log_{10}\left(P_{CO_2.eq}\right) = 7.079 - \frac{8308}{T\ (K)} \qquad \text{B-1}$$

At 1073 K, the partial pressure of CO_2 is:

$$P_{CO_2.eq} = 10^{7.079-\frac{8308}{1073}} = 0.22\ \text{atm}$$

At 1148 K, the partial pressure of CO_2 increases significantly:

$$P_{CO_2.eq} = 10^{7.079-\frac{8308}{1148}} = 0.70\ \text{atm}$$

B.5 – Labview interfaces

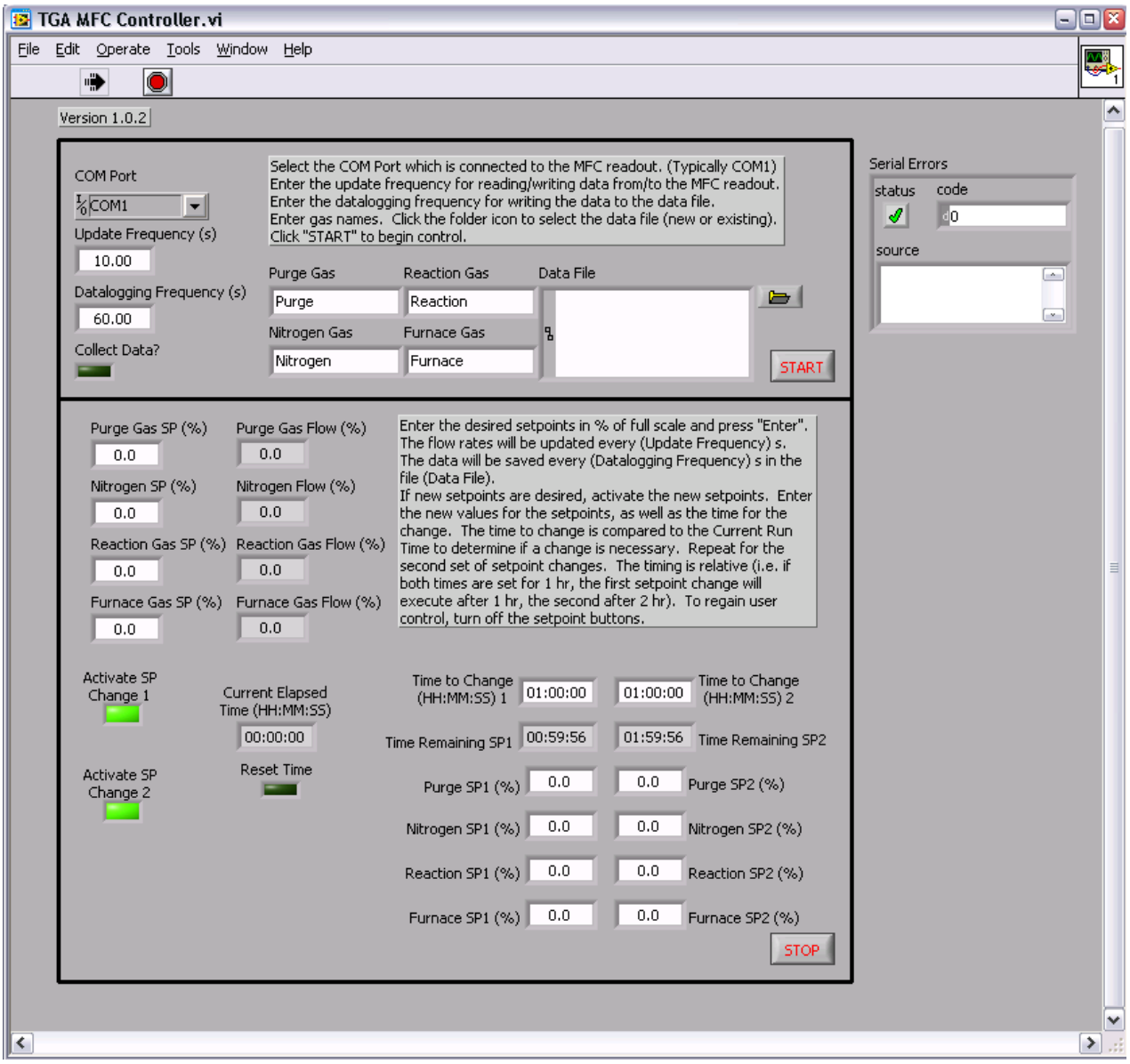

Figure B.1. Initial version of the LabVIEW interface for the TGA.

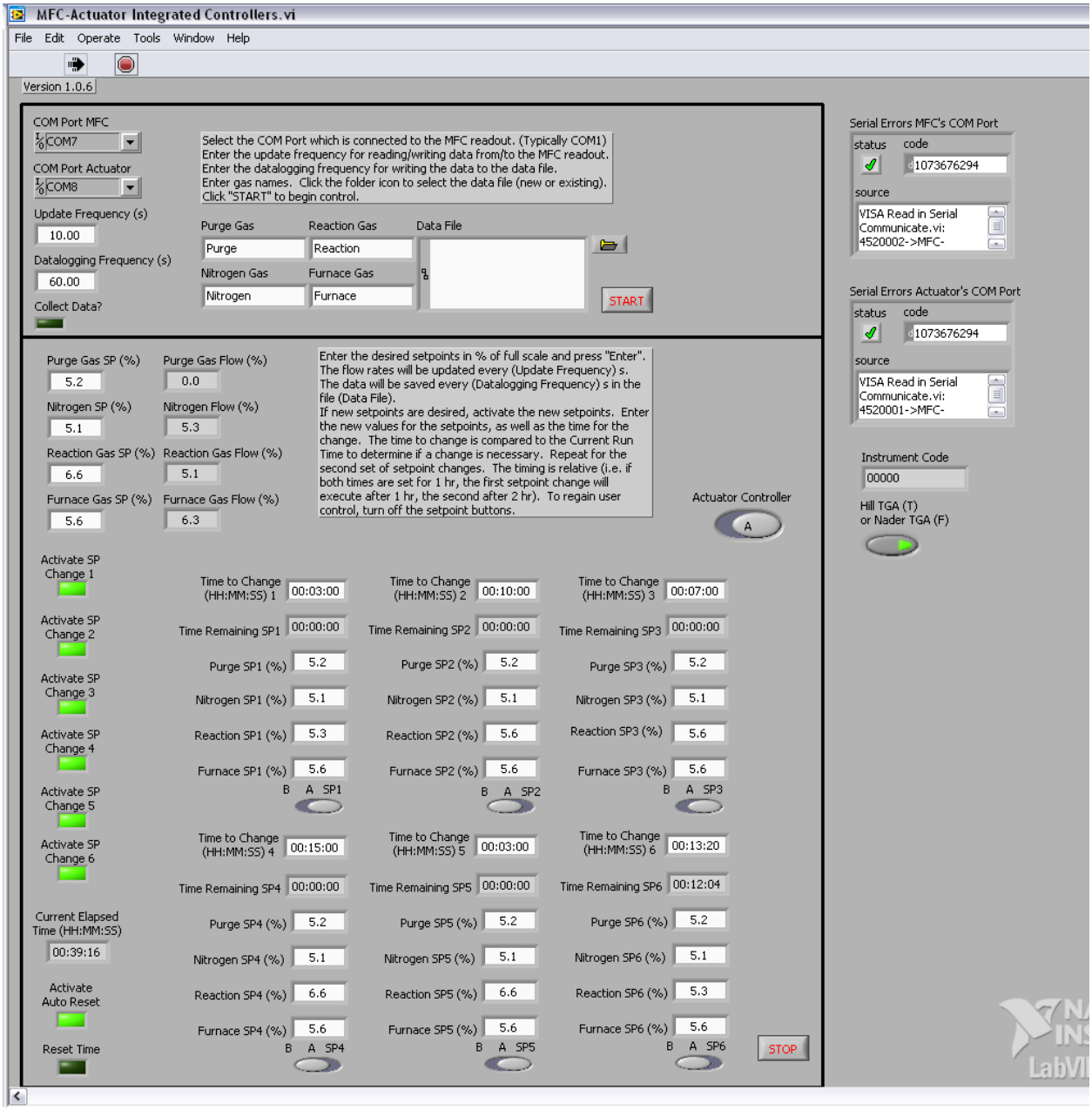

Figure B.2. Last version of the LabVIEW interface for the TGA.

B.6 – Results – calculation methodology

Calculation methodology to determine:

- Conversion for carbonation (%)
- Conversion for oxidation (%)
- CO_2 Capacity (gCO_2/gPellets)
- O_2 Capacity (gO_2/gPellets)
- CO_2 Capacity loss, CCL (%)
- O_2 Capacity Loss, OCL (%)

First, from the TGA report we extract the values of mass of calcined pellets (m_{calc}), mass of oxidized pellets (m_{oxid}), and mass of carbonated pellets (m_{carb}). For each of these parameters, it was made sure that the reading taken was always under N_2 atmosphere, so that the values of mass were normalized. Figure F.1 shows one of the cycles of Figure 3.10 (Section 3.5.2), and for this case, labels to mark the parameters m_{calc}, m_{oxid} and m_{carb} have been added.

Then, the parameters mentioned at the beginning can be calculated with only knowing the molecular weights of CaO, $CaCO_3$, Cu and CuO.

- Conversion for carbonation (%)

$$\chi_{carbonation}(\%) = \frac{m_{carb} - m_{oxid}}{m_{oxid} y_{CaO} \left(\frac{MW_{CaCO_3}}{MW_{CaO}} - 1\right)} \cdot 100 \qquad \text{(B-2)}$$

- Conversion for oxidation (%)

$$\chi_{oxidation}(\%) = \frac{m_{oxid} - m_{calc}}{m_{calc} y_{Cu} \left(\frac{MW_{CuO}}{MW_{Cu}} - 1\right)} \cdot 100 \qquad \text{(B-3)}$$

- CO_2 Capacity, CC (gCO_2/gPellets)

$$CO_2\ Capacity\ \left(\frac{gCO_2}{gPellets}\right) = \frac{m_{carb} - m_{oxid}}{m_{oxid}} \quad \text{(B-4)}$$

- O_2 Capacity, OC (gO_2/gPellets)

$$O_2\ Capacity\ \left(\frac{gO_2}{gPellets}\right) = \frac{m_{oxid} - m_{calc}}{m_{calc}} \quad \text{(B-5)}$$

- CO_2 Capacity Loss, CCL (%)

$$CCL\ (\%) = \frac{(gCO_2/gPellets)_{cycle\ 1} - (gCO_2/gPellets)_{cycle\ n}}{(gCO_2/gPellets)_{cycle\ 1}} \cdot 100 \quad \text{(B-6)}$$

- O_2 Capacity Loss, OCL (%)

$$OCL\ (\%) = \frac{(gO_2/gPellets)_{cycle\ 1} - (gO_2/gPellets)_{cycle\ n}}{(gO_2/gPellets)_{cycle\ 1}} \cdot 100 \quad \text{(B-7)}$$

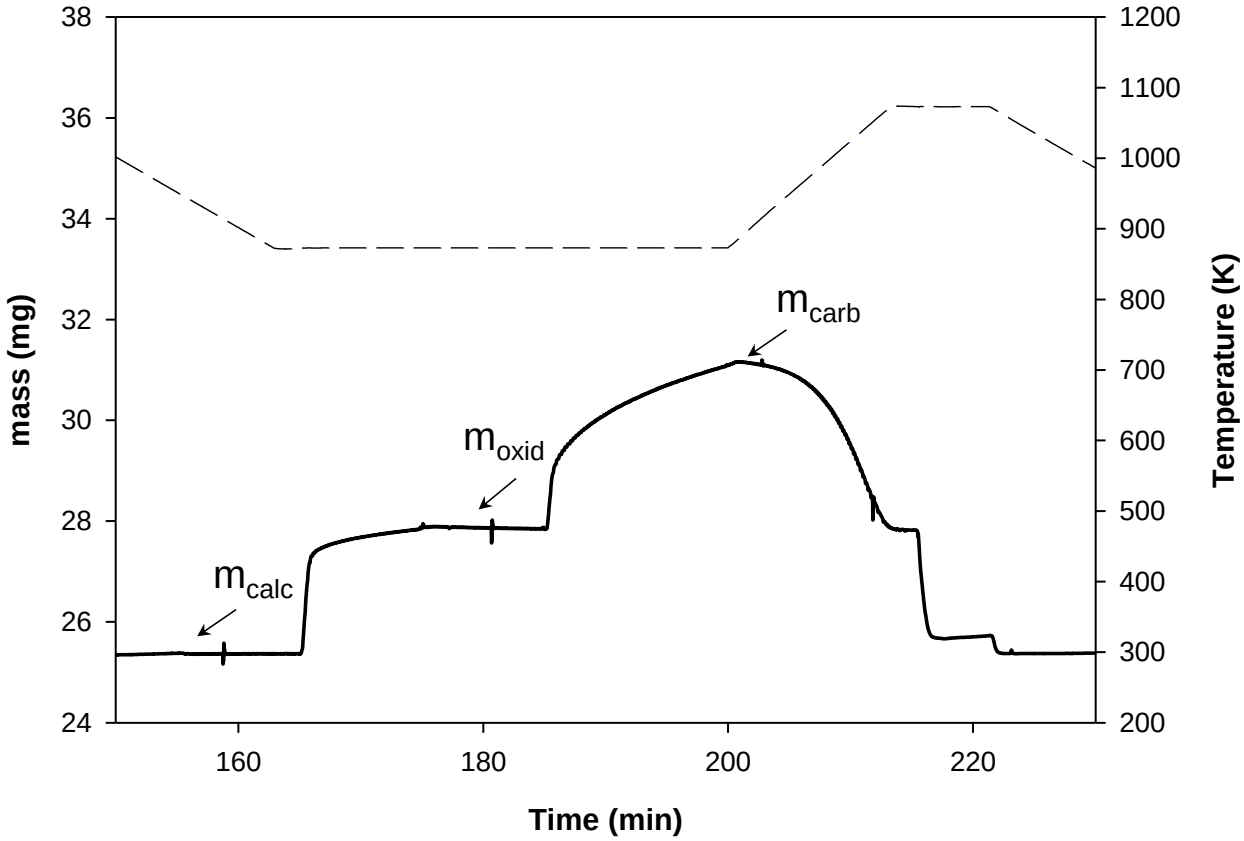

Figure B.3. Illustration of the mass values used for calculations.

B.7 – SEM images of homogeneous pellets

Figure B.4. External part of a non-calcined homogeneous pellet (500X).

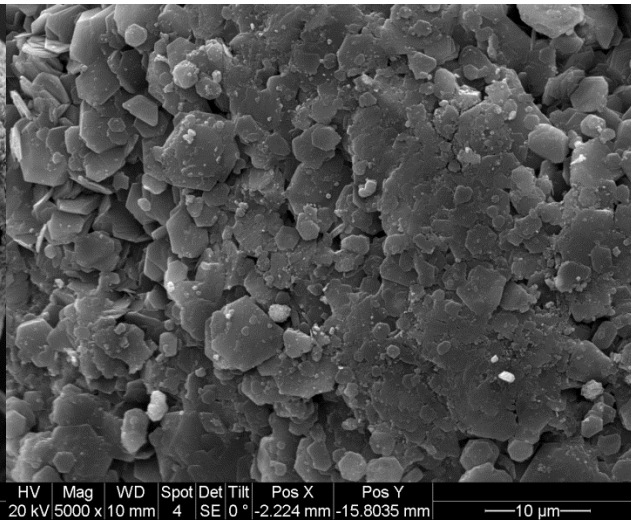

Figure B.5. External part of a non-calcined homogeneous pellet (5000X).

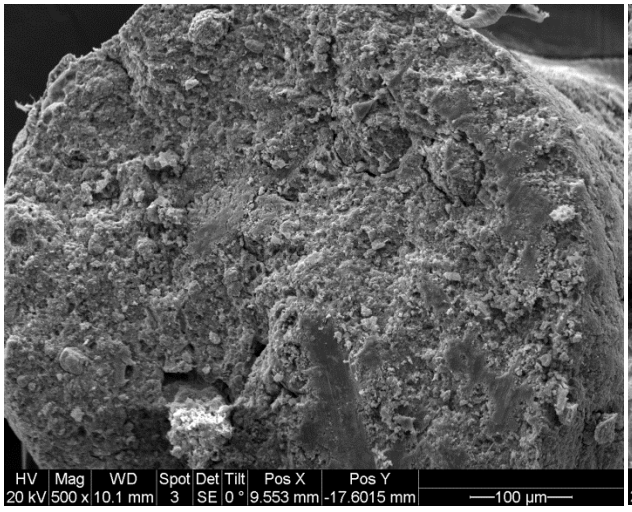

Figure B.6. Internal part of a calcined homogeneous pellet (500X).

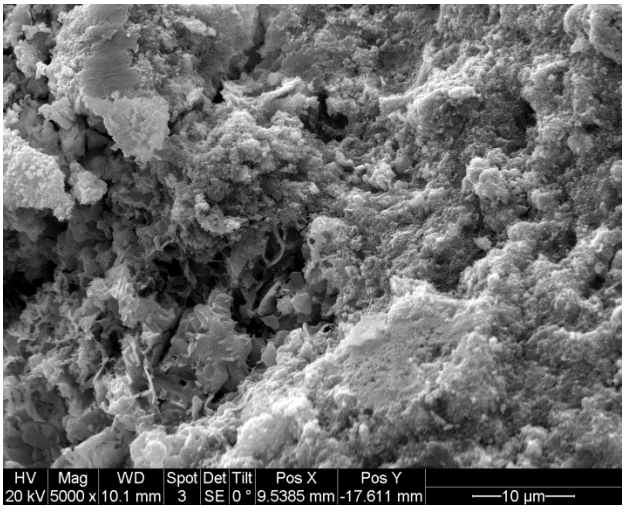

Figure B.7. Internal part of a calcined homogeneous pellet (5000X).

APPENDIX C – ADDITIONAL INFORMATION FOR HEAT TRANSFER MODEL. SOLUTION TO DIFFERENTIAL EQUATION AND PARAMETRIC STUDY

The procedure use to solve the differential equations posed in Chapter Four, and the solution of the parameters A, B, C, D, E and F of the final equations are provided. In addition, results obtained from the parametric study wherein the effects of time particle size, heat of reaction, thermal conductivity and time of reaction were examined. The carbonation stage was chosen as the basis to carry out this study. Thus, any parameter involved, such as density or diffusivities of gases, was kept unchanged.

C.1 – Procedure to solve the differential equations

To solve the differential equation, the following change of variable was made:

$$\Theta = rT$$

Hence,

$$\Theta_{non}(r,t) = r\left[A + B\left(1 - \left|erf\left(\frac{r}{2\sqrt{\alpha_{non}t}}\right)\right|\right)\right]$$

$$\Theta_{con}(r,t) = r\left[C + D\left(1 - \left|erf\left(\frac{r}{2\sqrt{\alpha_{con}t}}\right)\right|\right)\right]$$

$$\Theta_{shell}(r,t) = rE + r^2F$$

$$\Theta_o = rT_o$$

$$\Theta_\infty = rT_\infty$$

Also,

$$\frac{\partial T}{\partial r} = \frac{1}{r}\frac{\partial \Theta}{\partial r} - \frac{1}{r^2}\Theta$$

and,

$$\frac{\partial \Theta_{\text{non}}}{\partial r} = A + B\left(1 - \left|erf\left(\frac{r}{2\sqrt{\alpha_{non}t}}\right)\right|\right) - rB\frac{2}{\sqrt{\pi}}\frac{e^{-\frac{r^2}{4\alpha_{non}t}}}{2\sqrt{\alpha_{non}t}}\frac{erf\left(\frac{r}{2\sqrt{\alpha_{non}t}}\right)}{\left|erf\left(\frac{r}{2\sqrt{\alpha_{non}t}}\right)\right|}$$

$$\frac{\partial \Theta_{\text{non}}}{\partial r} = C + D\left(1 - \left|erf\left(\frac{r}{2\sqrt{\alpha_{con}t}}\right)\right|\right) - rD\frac{2}{\sqrt{\pi}}\frac{e^{-\frac{r^2}{4\alpha_{con}t}}}{2\sqrt{\alpha_{con}t}}\frac{erf\left(\frac{r}{2\sqrt{\alpha_{con}t}}\right)}{\left|erf\left(\frac{r}{2\sqrt{\alpha_{con}t}}\right)\right|}$$

$$\frac{\partial \Theta_{\text{shell}}}{\partial r} = = \text{E} + 2rF$$

Eventually, by applying this equations to the boundary conditions, the parameters A, B, C, D, E and F result as follows:

A = 873 or 1073

$$B = D\frac{1 - \left|erf\left(\frac{s}{2\sqrt{\alpha_{con}t}}\right)\right|}{1 - \left|erf\left(\frac{s}{2\sqrt{\alpha_{non}t}}\right)\right|}$$

C = 873 or 1073

$$\text{D} = \frac{\frac{\sqrt{\pi}}{2}\rho q\left(\frac{\partial s}{\partial t}\right)}{k_{con}\left[\frac{e^{-\frac{s^2}{4\alpha_{con}t}}}{2\sqrt{\alpha_{con}t}}\frac{\text{erf}\left(\frac{s}{2\sqrt{\alpha_{con}t}}\right)}{\left|\text{erf}\left(\frac{s}{2\sqrt{\alpha_{con}t}}\right)\right|}\right] + k_{non}\left[\left(\frac{1 - \left|\text{erf}\left(\frac{s}{2\sqrt{\alpha_{con}t}}\right)\right|}{1 - \left|\text{erf}\left(\frac{s}{2\sqrt{\alpha_{non}t}}\right)\right|}\right)\frac{e^{-\frac{s^2}{4\alpha_{non}t}}}{2\sqrt{\alpha_{non}t}}\frac{\text{erf}\left(\frac{s}{2\sqrt{\alpha_{non}t}}\right)}{\left|\text{erf}\left(\frac{s}{2\sqrt{\alpha_{non}t}}\right)\right|}\right]}$$

$$E = C + D\left(1 - \left|erf\left(\frac{R_{core}}{2\sqrt{\alpha_{con}t}}\right)\right|\right) - R_{core}F$$

$$F = \frac{C + D\left(1 - \left|erf\left(\frac{R_{core}}{2\sqrt{\alpha_{con}t}}\right)\right|\right) - T_{\infty}}{R_{core} - R_{pellet} - \frac{k_s}{h}}$$

The units for each parameter are degrees Kelvin (K).

C.2 – Particle size

The results obtained for four different radii are illustrated in Figures C.1 and C.2. The time of reaction was assumed to be the same as that of the original radius (~2400 min). For sizes of particle larger than the base case, the temperature differences should be larger as well since the resistance to heat transfer is increased. Figure C.1 shows that when the size of the particle is increased, the difference of temperature between the center of the pellet and the outer part of the shell becomes larger, although it still remains insignificant. For a radius 5 times larger, the difference does not exceed 0.10 K.

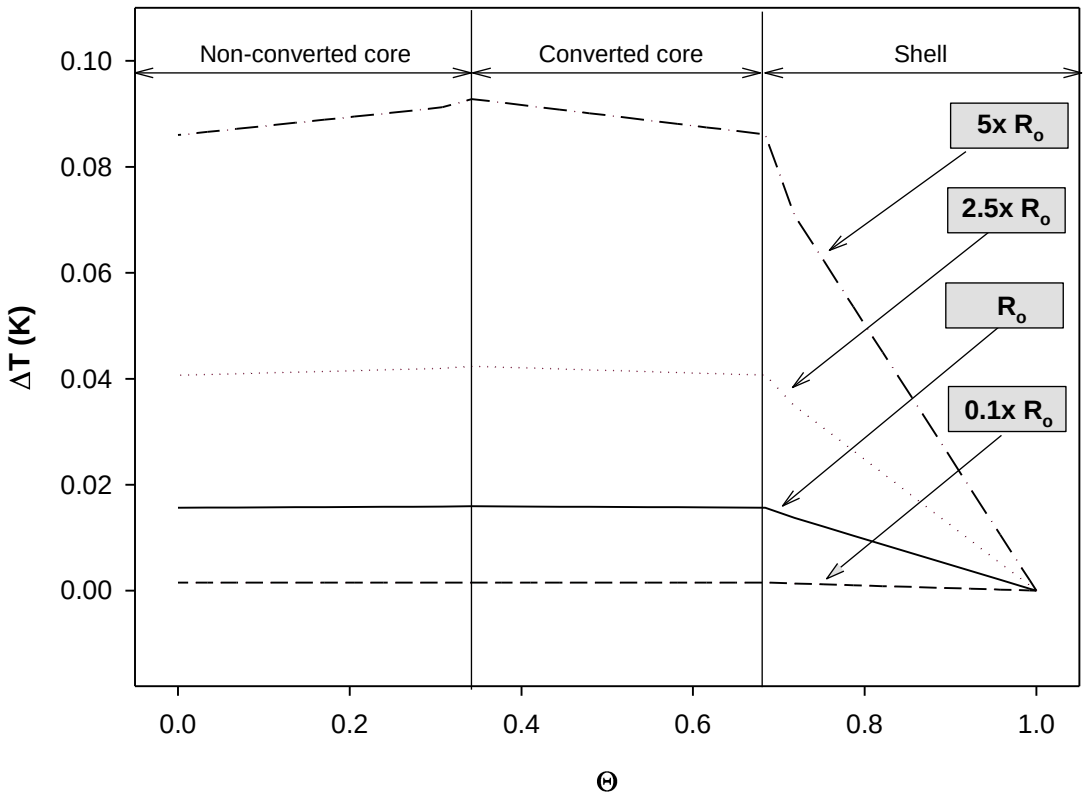

Figure C.1. Temperature increments for different sizes of pellets after 750 min vs normalized radius. Normalized radii have been used to represent and compare all the cases at once (Θ = R/Ro where Ro ≡ radius of pellet).

On the other hand, as shown in Figure C.2, the temperature evolution with time is more noticeable, but still not very significant. For a pellet 5 times larger, the final temperature predicted is 882 K, which is 9 K higher than the initial temperature. Therefore, even for larger particles, no significant temperature increases would be expected.

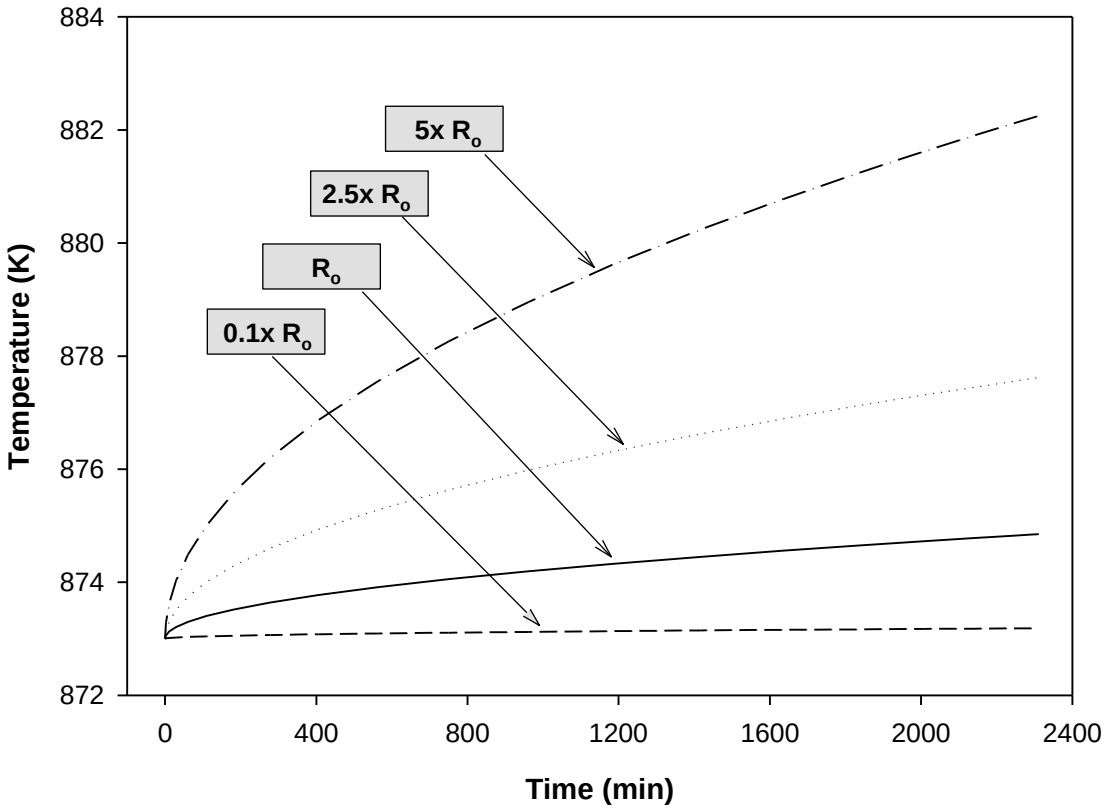

Figure C.2. Temperature evolution with time for different radii.

C.3 – Heat of reaction

Heat of reaction is another important model input parameter whose effect was examined. Figure C.3 illustrates the temperature profile within the pellet for four different cases. One corresponds to the base case heat of reaction of the carbonation reaction (-174.7 kJ/mol), and the other three correspond to heats of reaction 0.5, 1.5 and 2 times the original heat of reaction. As shown in Figure C.3, the largest temperature difference within the pellet for a heat of reaction 2 times the heat of the base case barely surpasses 0.03 K.

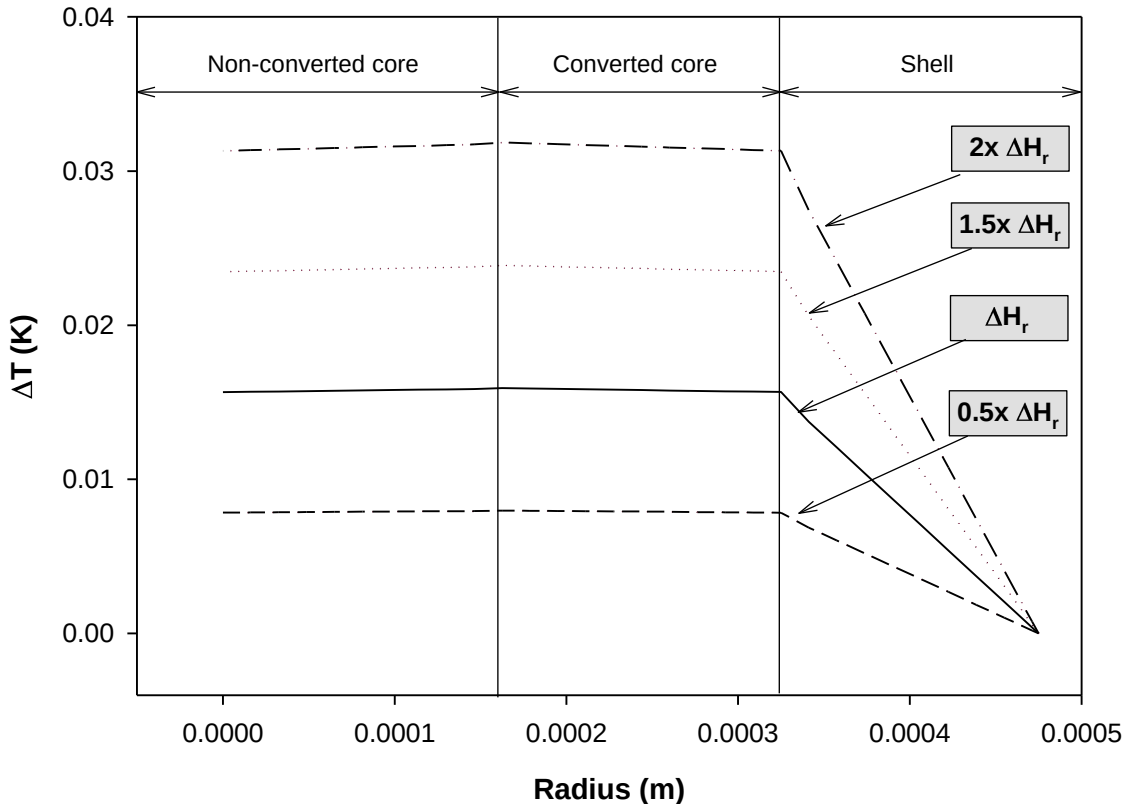

Figure C.3. Temperature increments for several heats of reaction after 750 min.

On the other hand, Figure C.4 depicts the evolution of the temperature with time. For a heat of reaction 2 times larger, the model predicts almost 877 K as the final temperature, which is 2 degrees higher than the base case. Therefore, it seems that the heat of reaction has little impact on the temperature difference, although it is possible that for shorter reactions its effect would be more significant.

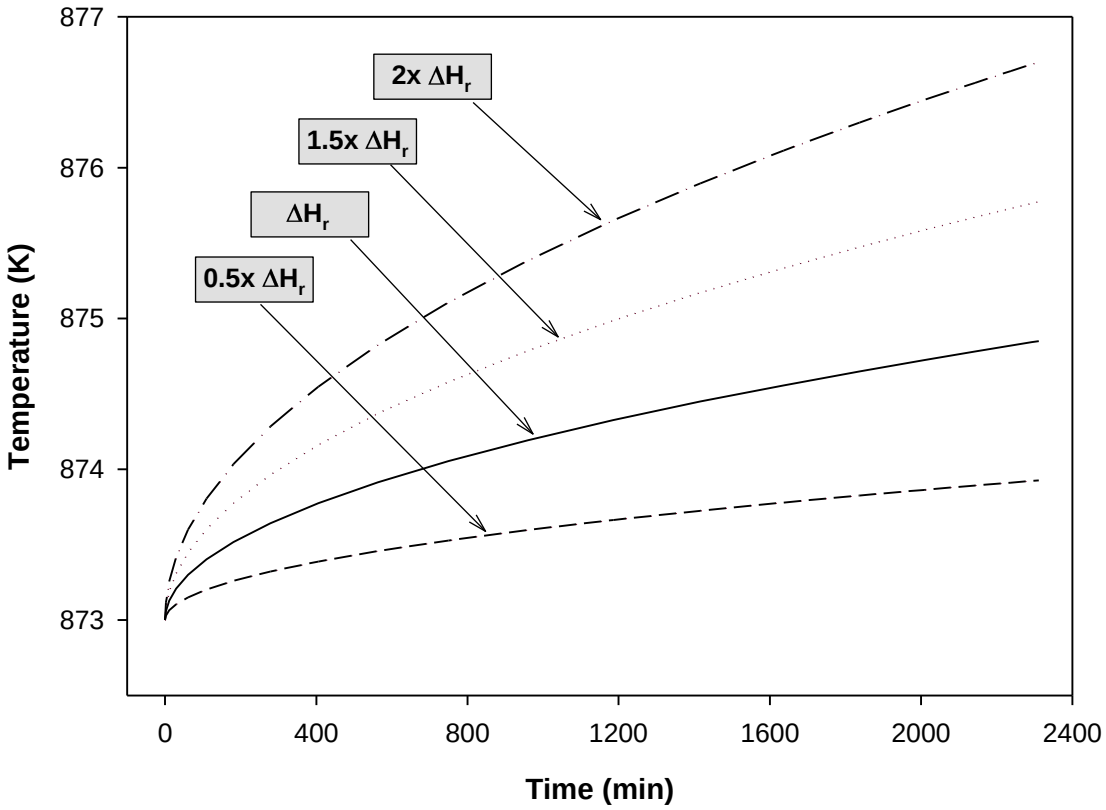

Figure C.4. Evolution of the temperature with time for several heats of reaction.

C.4 – Thermal conductivity

Another parameter studied was the thermal conductivity. Figure C.5 shows that higher values of thermal conductivity lead to smaller temperatures increases. On the other hand, when lower values of thermal conductivity are tried, the maximum temperature becomes larger. In agreement with these results are the temperature profiles illustrated in Figure C.6. Higher values of thermal conductivity lead to flatter temperature profiles, while lower values lead to larger temperature differences within the pellet.

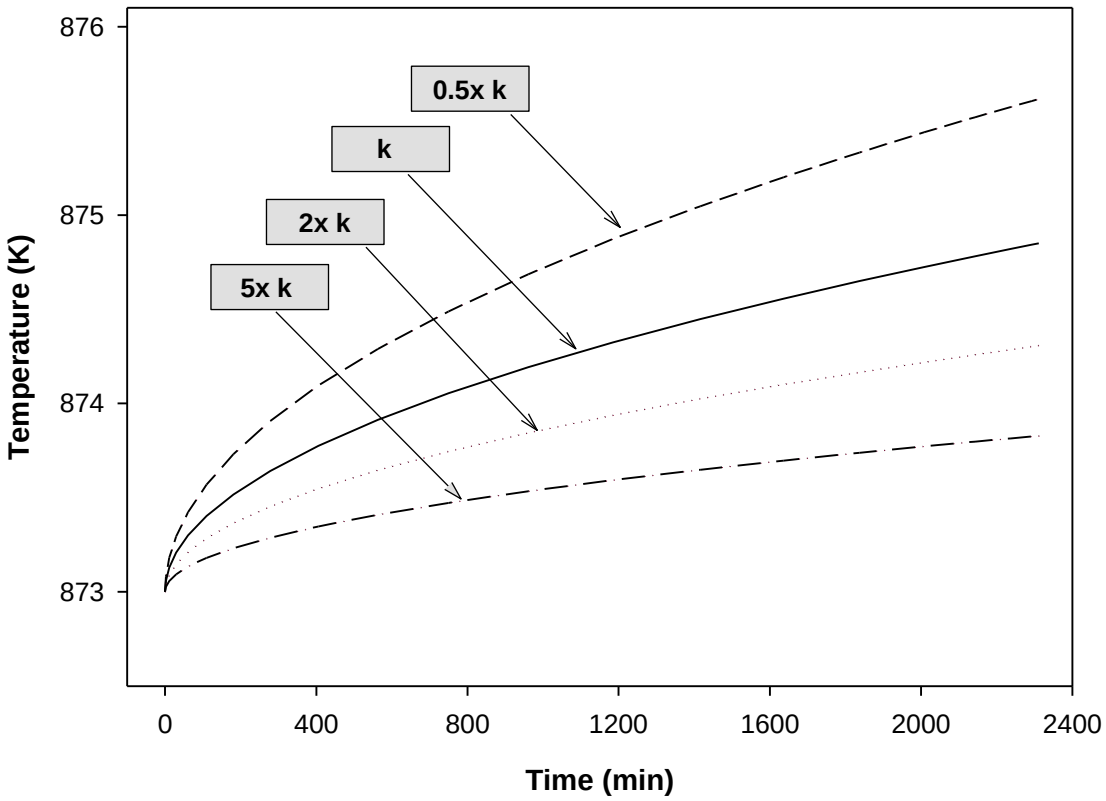

Figure C.5. Evolution of moving boundary temperature with time for several values of thermal conductivity.

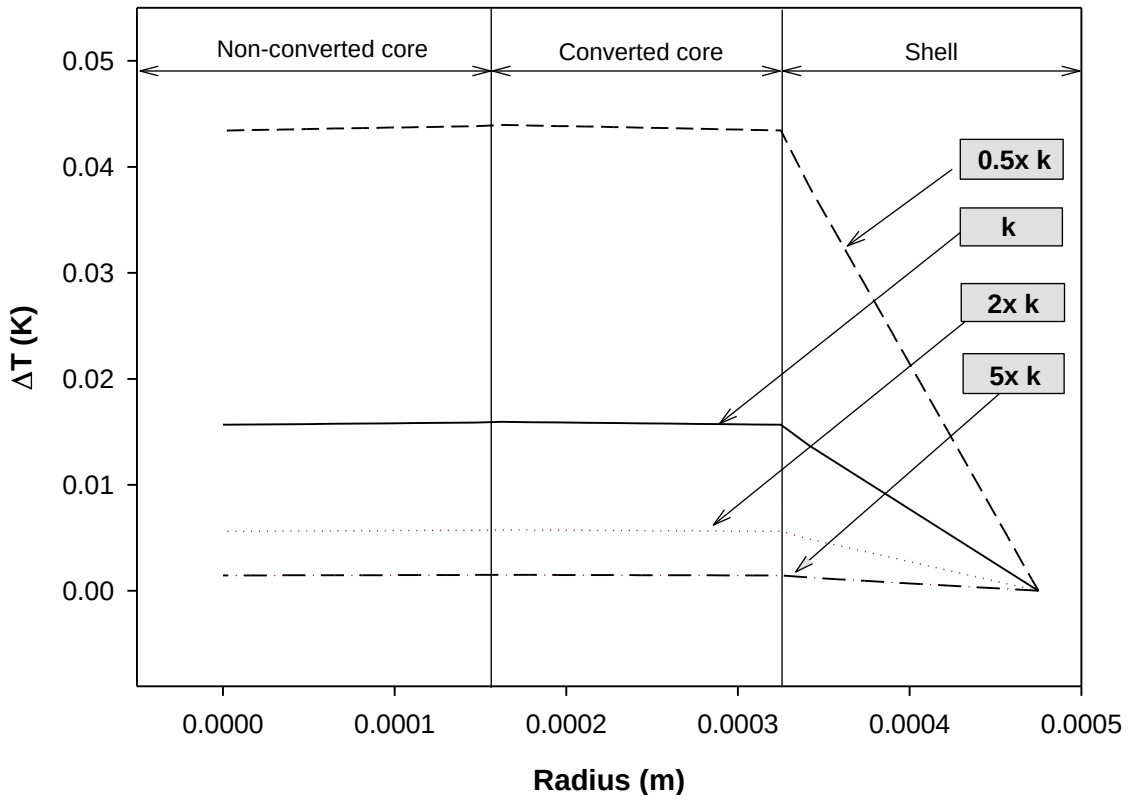

Figure C.6. Temperature changes from the center of the pellet to the outer part of the shell for several thermal conductivities after 750 min.

C.5 – Time of reaction

As mentioned before, the time of reaction seemed to have an important role in the temperature evolution and temperature difference within the pellet. In this section, four different times of reaction for the carbonation are tested. Since the time for complete carbonation was long (~2400 min), the times of reaction tested are shorter, namely, 10, 50 and 100 times shorter. In Figure C.7 is depicted the temperature evolution over time and it is observed that if the carbonation would be 100 times faster, the temperature increase would be ~18 K, which is

approximately 10 times the temperature increase for the base case. On the other hand, in Figure C.8 are illustrated the temperature differences within the pellet. In this case, the largest difference is still smaller than 0.25 K. This result is significant if the estimated temperature increase for the reduction is taken into account (see Chapter Four, Section 4.3.1).

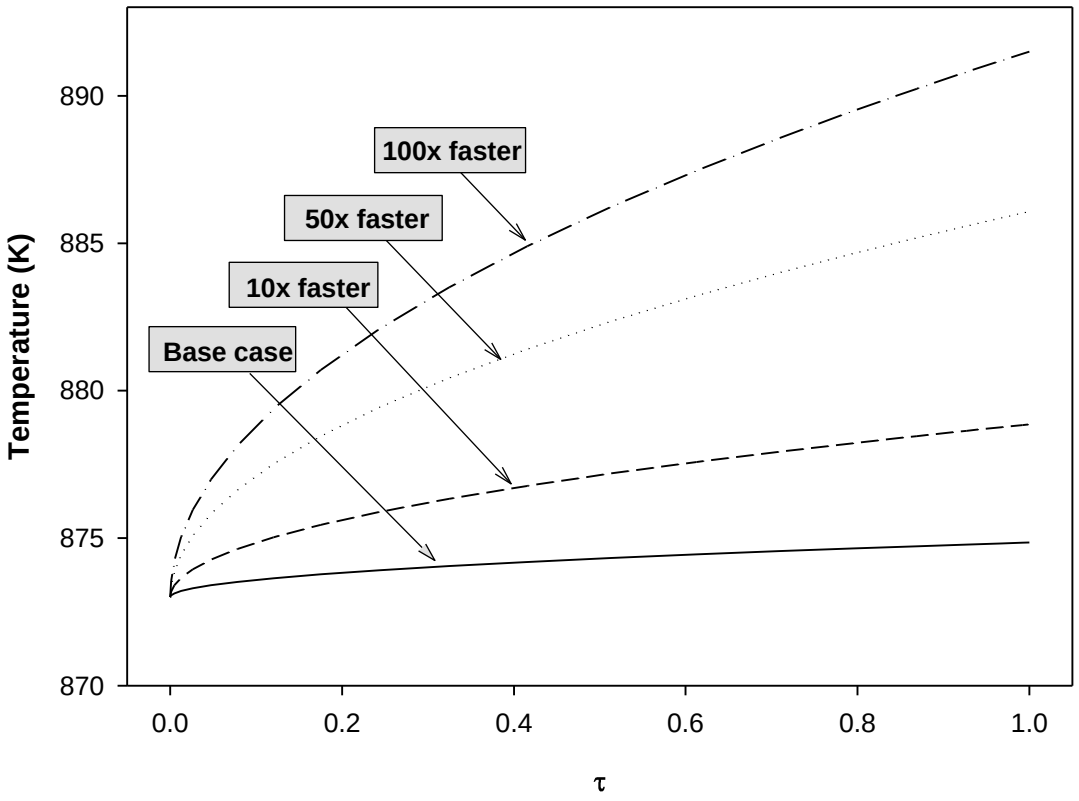

Figure C.7. Temperature evolution over time for four different times of reaction ($\tau = t/t_r$ where $t_r \equiv$ time of reaction).

For the reduction, the estimated temperature difference within the pellet was 3.8 K, which is substantially larger than 0.25 K (note that the time of reaction for the 100-times-faster carbonation reaction is shorter than that of the reduction, 24 min versus 82 min). To explain this

result the thermal conductivity must be taken into consideration. For the carbonation reaction, the thermal conductivities of the CaO, $CaCO_3$, and Al_2O_3 are similar, while in the reduction, the thermal conductivity of Cu is much larger than those of CuO and Al_2O_3 (see Table 4.2). On the other hand, the increase of temperature over time is larger for the fastest carbonation case than for the reduction, 18 K versus 6 K, which is in agreement with the idea that shorter reaction times lead to larger temperature increases over time.

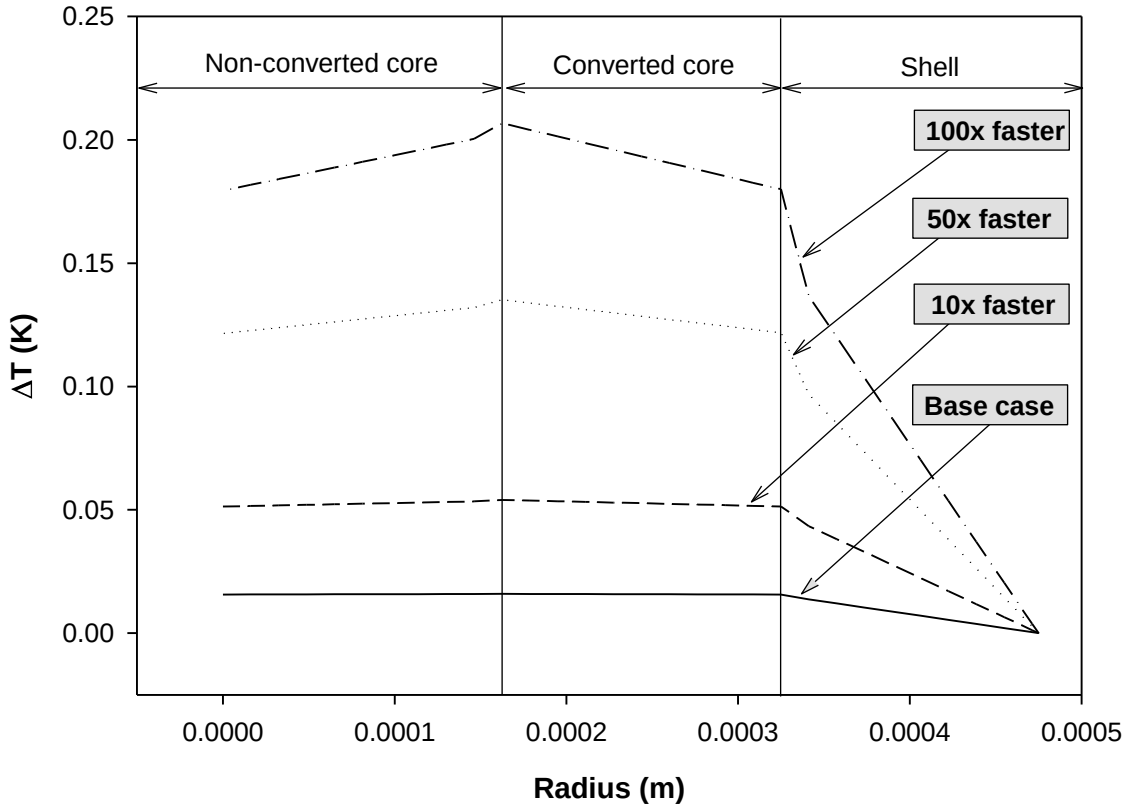

Figure C.8. Temperature difference within the pellet for four different times of reaction.

APPENDIX D – ADDITIONAL INFORMATION FOR CHAPTER FIVE

D.1 – Results from XRD analyses

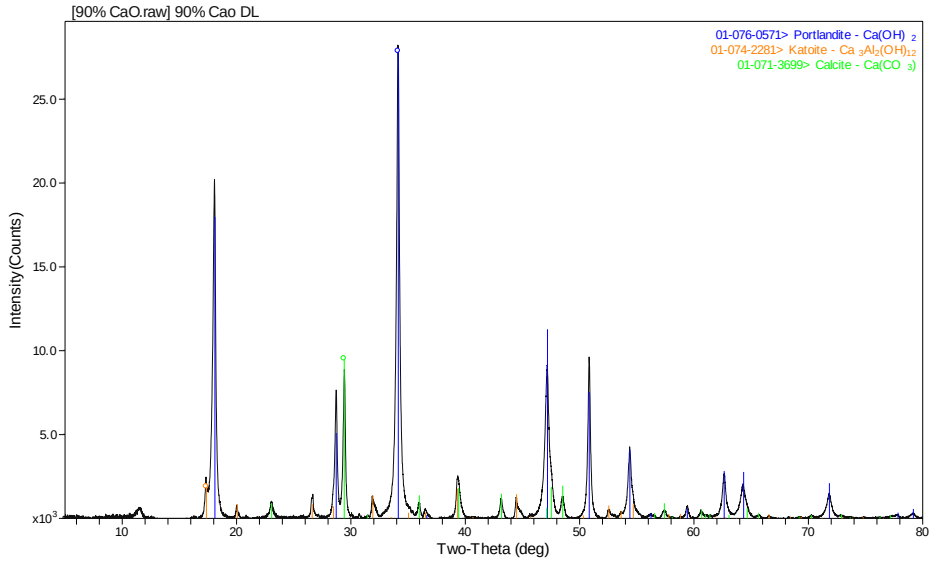

Figure D.1. XRD analysis of raw 90/10 pellets.

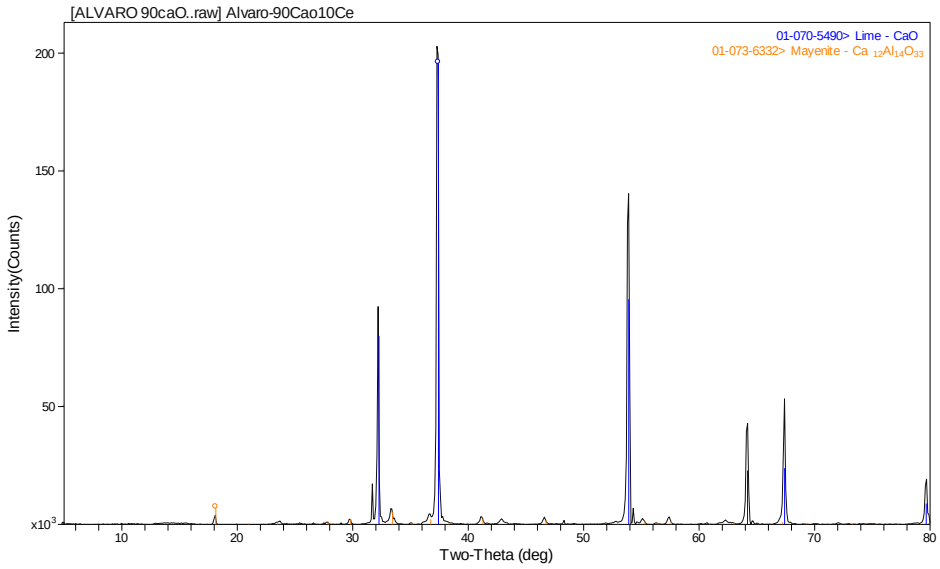

Figure D.2. XRD analysis of 90/10 pellets subjected to 50 cycles of carbonation/calcination.

D.2 – Calculation of mayenite content based on data from XRD analyses

Assuming 1 g of 90/10 pellets, according to Table 5.3, the content of the sample would be:

0.063 g of $Ca_3Al_2(OH)_{12}$ - katoite

0.745 g of $Ca(OH)_2$

0.179 g of $CaCO_3$

0.014 g of SiO_2

Molecular weights:

Katoite: $Ca_3Al_2(OH)_{12}$ = 378 g/mol

Portlandite: $Ca(OH)_2$ = 74 g/mol

Calcite: $CaCO_3$ = 100 g/mol

Quartz: SiO_2 = 60 g/mol

Mayenite: $Ca_{12}Al_{14}O_{33}$ = 1386 g/mol

Lime: CaO = 56 g/mol

Recalling that:

$$7\ Ca_3Al_2(OH)_{12} \rightarrow Ca_{12}Al_{14}O_{33} + 9\ CaO + 42\ H_2O$$

And assuming that 1 mol of $Ca(OH)_2$ and 1 mol of $CaCO_3$ will produce 1 mol of CaO, and that SiO_2 will remain stable, then the following calculations apply:

- Mayenite formed from katoite

  $7 \cdot n_{mayenite} = n_{katoite}$

  $7 \cdot (m_{mayenite}/MW_{mayenite}) = m_{katoite}/MW_{katoite}$

  $m_{mayenite} = m_{katoite} \cdot MW_{mayenite} / (7 \cdot MW_{katoite}) = (0.063)(1386)/((7)(378)) = 0.033$ g

- Lime formed from katoite

  $7 \cdot n_{CaO} = 9 \cdot n_{katoite}$

  $7 \cdot (m_{CaO}/MW_{CaO}) = 9 \cdot (m_{katoite}/MW_{katoite})$

  $m_{CaO} = 9 \cdot m_{katoite} \cdot MW_{CaO} / (7 \cdot MW_{katoite}) = (9)(0.063)(56)/((7)(378)) = 0.012$ g

- Lime formed from portlandite

  $n_{CaO} = n_{Ca(OH)2}$

  $m_{CaO}/MW_{CaO} = m_{Ca(OH)2}/MW_{Ca(OH)2}$

  $m_{CaO} = m_{Ca(OH)2} \cdot MW_{CaO} / MW_{Ca(OH)2} = (0.745)(56)/(74) = 0.564$ g

- Lime formed from calcite

  $n_{CaO} = n_{CaCO3}$

  $m_{CaO}/MW_{CaO} = m_{CaCO3}/MW_{CaCO3}$

  $m_{CaO} = m_{CaCO3} \cdot MW_{CaO} / MW_{CaCO3} = (0.179)(56)/(100) = 0.100$ g

- Final mass

  $m_{CaO(katoite)} + m_{CaO(calcite)} + m_{CaO(portlandite)} + m_{mayenite} + m_{SiO2} = 0.012 + 0.564 + 0.100 +$

  $0.033 + 0.014 = 0.723$ g

- Fractions of each component

  CaO = (0.012 + 0.564 +0.100)/(0.723) = 0.935 → 93.5%

  Mayenite = 0.033/0.723 = 0.046 → 4.6%

  Quartz = 0.014/0.723 = 0.019 → 1.9%

D.3 – Tables of results for 50/40/10, 50/50 and 90/10 pellets

Table D.1. Results of 16 cycles of calcium looping and chemical looping combustion for 50/40/10 pellets.

Cycle	$\chi_{oxidation}$ (%)	$\chi_{carbonation}$ (%)	O_2 Capacity (gO_2/gPellets)	CO_2 Capacity (gCO_2/gPellets)	OCL (%)[a]	CCL (%)[b]
1	85.3 ± 2.6	16.0 ± 1.8	0.107 ± 0.003	0.050 ± 0.005	N/A	N/A
2	87.3 ± 1.8	12.5 ± 0.8	0.110 ± 0.002	0.039 ± 0.003	-2.4 ± 1.5	22.0 ± 3.7
3	87.6 ± 1.7	10.9 ± 0.5	0.110 ± 0.002	0.034 ± 0.001	-2.8 ± 1.3	31.6 ± 8.4
4	87.9 ± 1.8	9.4 ± 0.3	0.111 ± 0.002	0.030 ± 0.001	-3.1 ± 1.1	40.7 ± 7.3
5	87.9 ± 2.2	8.4 ± 0.3	0.111 ± 0.003	0.026 ± 0.001	-3.1 ± 0.7	47.4 ± 7.2
6	87.8 ± 2.4	7.7 ± 0.3	0.111 ± 0.003	0.024 ± 0.001	-3.0 ± 0.4	51.6 ± 5.8
7	87.9 ± 2.2	7.0 ± 0.5	0.111 ± 0.003	0.022 ± 0.002	-3.1 ± 0.5	55.8 ± 4.6
8	87.7 ± 1.8	6.6 ± 0.2	0.110 ± 0.002	0.021 ± 0.001	-2.9 ± 1.0	58.3 ± 4.3
9	88.0 ± 1.8	6.2 ± 0.3	0,111 ± 0.002	0.020 ± 0.001	-3.3 ± 1.1	60.9 ± 4.2
10	87.7 ± 1.7	5.9 ± 0.2	0.110 ± 0.002	0.018 ± 0.001	-2.9 ± 1.2	63.2 ± 3.8
11	88.5 ± 1.7	5.8 ± 0.1	0.111 ± 0.002	0.018 ± 0.001	-3.8 ± 1.4	63.9 ± 3.4
12	88.1 ± 1.5	5.4 ± 0.4	0.111 ± 0.002	0.017 ± 0.001	-3.3 ± 1.4	66.3 ± 4.8
13	88.4 ± 1.3	5.2 ± 0.4	0.111 ± 0.002	0.016 ± 0.001	-3.7 ± 1.6	67.5 ± 5.7
14	87.9 ± 1.5	4.9 ± 0.5	0.111 ± 0.002	0.015 ± 0.001	-3.2 ± 1.4	69.1 ± 6.0
15	88.1 ± 2.0	4.8 ± 0.5	0.111 ± 0.002	0.015 ± 0.001	-3.4 ± 0.8	70.0 ± 6.6
16	88.2 ± 1.7	4.2 ± 1.0	0.111 ± 0.002	0.013 ± 0.003	-3.5 ± 1.2	73.2 ± 8.1

[a]CCL (%) = CO_2 Capacity Loss
[b]OCL (%) = O_2 Capacity Loss

Table D.2. Results of 20 cycles of chemical looping combustion for 50/50 pellets.

Cycle	$\chi_{oxidation}$ (%)	O_2 Capacity (gO_2/gPellets)	OCL (%)*
1	87.8 ± 1.7	0.111 ± 0.002	N/A
2	88.0 ± 2.1	0.111 ± 0.003	-0.2 ± 0.6
3	88.9 ± 2.1	0.112 ± 0.003	-1.2 ± 0.5
4	88.5 ± 1.9	0.111 ± 0.002	-0.8 ± 0.2
5	88.9 ± 1.8	0.112 ± 0.002	-1.3 ± 0.2
6	89.3 ± 2.0	0.112 ± 0.002	-1.7 ± 0.6
7	89.3 ± 2.3	0.112 ± 0.003	-1.7 ± 0.7
8	89.7 ± 2.2	0.113 ± 0.003	-2.2 ± 1.0
9	89.9 ± 2.3	0.113 ± 0.003	-2.3 ± 0.9
10	89.6 ± 2.4	0.113 ± 0.003	-2.1 ± 1.0
11	90.0 ± 2.6	0.113 ± 0.003	-2.4 ± 1.4
12	90.0 ± 2.7	0.113 ± 0.003	-2.5 ± 1.5
13	89.8 ± 2.7	0.113 ± 0.003	-2.3 ± 1.5
14	89.9 ± 2.5	0.113 ± 0.003	-2.3 ± 1.4
15	89.8 ± 2.9	0.113 ± 0.004	-2.3 ± 1.7
16	89.6 ± 3.1	0.113 ± 0.004	-2.1 ± 1.9
17	89.6 ± 3.3	0.113 ± 0.004	-2.1 ± 2.2
18	89.3 ± 3.1	0.112 ± 0.004	-1.7 ± 2.0
19	89.2 ± 3.3	0.112 ± 0.004	-1.6 ± 2.3
20	89.2 ± 3.4	0.112 ± 0.004	-1.6 ± 2.4

*OCL (%) = O_2 Capacity Loss

Table D.3- Results of 20 cycles of calcium looping for 90/10 pellets.

Cycle	$\chi_{carbonation}$ (%)	CO_2 Capacity (gCO_2/gPellets)	CCL (%)*
1	65.8 ± 0.5	0.465 ± 0.004	N/A
2	47.3 ± 1.4	0.334 ± 0.010	28.2 ± 1.5
3	40.0 ± 1.3	0.283 ± 0.009	39.2 ± 1.5
4	36.0 ± 1.2	0.255 ± 0.008	45.2 ± 1.4
5	33.4 ± 1.1	0.236 ± 0.008	49.2 ± 1.3
6	31.4 ± 1.0	0.222 ± 0.007	52.2 ± 1.2
7	29.9 ± 1.0	0.211 ± 0.007	54.5 ± 1.2
8	28.7 ± 1.0	0.202 ± 0.007	56.5 ± 1.2
9	27.6 ± 1.0	0.195 ± 0.007	58.1 ± 1.2
10	26.6 ± 1.1	0.188 ± 0.008	59.6 ± 1.5
11	25.9 ± 0.9	0.183 ± 0.007	60.6 ± 1.2
12	25.2 ± 0.9	0.178 ± 0.007	61.7 ± 1.2
13	24.6 ± 1.0	0.174 ± 0.007	62.6 ± 1.2
14	24.1 ± 0.9	0.170 ± 0.006	63.3 ± 1.2
15	23.7 ± 0.9	0.167 ± 0.007	64.0 ± 1.2
16	23.3 ± 1.0	0.165 ± 0.007	64.6 ± 1.2
17	22.9 ± 1.0	0.162 ± 0.007	65.1 ± 1.3
18	22.6 ± 1.0	0.160 ± 0.007	65.6 ± 1.4
19	22.4 ± 1.0	0.158 ± 0.007	66.0 ± 1.4
20	22.2 ± 1.0	0.157 ± 0.007	66.3 ± 1.4

*CCL (%) = CO_2 Capacity Loss

D.4 – Copyright of permission for Table 5.6

ROYAL SOCIETY OF CHEMISTRY LICENSE TERMS AND CONDITIONS

Mar 13, 2015

This is a License Agreement between Alvaro Recio ("You") and Royal Society of Chemistry ("Royal Society of Chemistry") provided by Copyright Clearance Center ("CCC"). The license consists of your order details, the terms and conditions provided by Royal Society of Chemistry, and the payment terms and conditions.

All payments must be made in full to CCC. For payment instructions, please see information listed at the bottom of this form.

License Number	3587380389150
License date	Mar 13, 2015
Licensed content publisher	Royal Society of Chemistry
Licensed content publication	Energy & Environmental Science
Licensed content title	Recent advances in solid sorbents for CO2 capture and new development trends
Licensed content author	Junya Wang,Liang Huang,Ruoyan Yang,Zhang Zhang,Jingwen Wu,Yanshan Gao,Qiang Wang,Dermot O'Hare,Ziyi Zhong
Licensed content date	Aug 6, 2014
Volume number	7
Issue number	11
Type of Use	Thesis/Dissertation
Requestor type	academic/educational
Portion	figures/tables/images
Number of figures/tables /images	5
Format	print and electronic
Distribution quantity	20
Will you be translating?	no
Order reference number	None
Title of the thesis/dissertation	Study of Composite Sorbent Pellets for Integration of Calcium Looping and Chemical Looping Combustion
Expected completion date	Apr 2015
Estimated size	140
Total	0.00 CAD

Terms and Conditions

This License Agreement is between {Requestor Name} ("You") and The Royal Society of Chemistry ("RSC") provided by the Copyright Clearance Center ("CCC"). The license consists of your order details, the terms and conditions provided by the Royal Society of Chemistry, and the payment terms and conditions.

RSC / TERMS AND CONDITIONS

INTRODUCTION

The publisher for this copyrighted material is The Royal Society of Chemistry. By clicking "accept" in connection with completing this licensing transaction, you agree that the following terms and conditions apply to this transaction (along with the Billing and Payment terms and conditions established by CCC, at the time that you opened your RightsLink account and that are available at any time at .

LICENSE GRANTED

The RSC hereby grants you a non-exclusive license to use the aforementioned material anywhere in the world subject to the terms and conditions indicated herein. Reproduction of the material is confined to the purpose and/or media for which permission is hereby given.

RESERVATION OF RIGHTS

The RSC reserves all rights not specifically granted in the combination of (i) the license details provided by your and accepted in the course of this licensing transaction; (ii) these terms and conditions; and (iii) CCC's Billing and Payment terms and conditions.

REVOCATION

The RSC reserves the right to revoke this license for any reason, including, but not limited to, advertising and promotional uses of RSC content, third party usage, and incorrect source figure attribution.

THIRD-PARTY MATERIAL DISCLAIMER

If part of the material to be used (for example, a figure) has appeared in the RSC publication with credit to another source, permission must also be sought from that source. If the other source is another RSC publication these details should be included in your RightsLink request. If the other source is a third party, permission must be obtained from the third party. The RSC disclaims any responsibility for the reproduction you make of items owned by a third party.

PAYMENT OF FEE

If the permission fee for the requested material is waived in this instance, please be advised that any future requests for the reproduction of RSC materials may attract a fee.

ACKNOWLEDGEMENT

The reproduction of the licensed material must be accompanied by the following acknowledgement:

Reproduced ("Adapted" or "in part") from {Reference Citation} (or Ref XX) with permission of The Royal Society of Chemistry.

If the licensed material is being reproduced from New Journal of Chemistry (NJC), Photochemical & Photobiological Sciences (PPS) or Physical Chemistry Chemical Physics (PCCP) you must include one of the following acknowledgements:

For figures originally published in NJC:

Reproduced ("Adapted" or "in part") from {Reference Citation} (or Ref XX) with permission of The Royal Society of Chemistry (RSC) on behalf of the European Society for Photobiology, the European Photochemistry Association and the RSC.

For figures originally published in PPS:

Reproduced ("Adapted" or "in part") from {Reference Citation} (or Ref XX) with permission of The Royal Society of Chemistry (RSC) on behalf of the Centre National de la Recherche Scientifique (CNRS) and the RSC.

For figures originally published in PCCP:

Reproduced ("Adapted" or "in part") from {Reference Citation} (or Ref XX) with permission of the PCCP Owner Societies.

HYPERTEXT LINKS

With any material which is being reproduced in electronic form, you must include a hypertext link to the original RSC article on the RSC's website. The recommended form for the hyperlink is http://dx.doi.org/10.1039/DOI suffix, for example in the link http://dx.doi.org/10.1039/b110420a the DOI suffix is 'b110420a'. To find the relevant DOI suffix for the RSC article in question, go to the Journals section of the website and locate the article in the list of papers for the volume and issue of your specific journal. You will find the DOI suffix quoted there.

LICENSE CONTINGENT ON PAYMENT

While you may exercise the rights licensed immediately upon issuance of the license at the end of the licensing process for the transaction, provided that you have disclosed complete and accurate details of your proposed use, no license is finally effective unless and until full payment is received from you (by CCC) as provided in CCC's Billing and Payment terms and conditions. If full payment is not received on a timely basis, then any license preliminarily granted shall be deemed automatically revoked and shall be void as if never granted. Further, in the event that you breach any of these terms and conditions or any of CCC's Billing and Payment terms and conditions, the license is automatically revoked and shall be void as if never granted. Use of materials as described in a revoked license, as well as any use of the materials beyond the scope of an unrevoked license, may constitute copyright infringement and the RSC reserves the right to take any and all action to protect its copyright in the materials.

WARRANTIES
The RSC makes no representations or warranties with respect to the licensed material.

INDEMNITY
You hereby indemnify and agree to hold harmless the RSC and the CCC, and their respective officers, directors, trustees, employees and agents, from and against any and all claims arising out of your use of the licensed material other than as specifically authorized pursuant to this licence.

NO TRANSFER OF LICENSE
This license is personal to you or your publisher and may not be sublicensed, assigned, or transferred by you to any other person without the RSC's written permission.

NO AMENDMENT EXCEPT IN WRITING
This license may not be amended except in a writing signed by both parties (or, in the case of "Other Conditions, v1.2", by CCC on the RSC's behalf).

OBJECTION TO CONTRARY TERMS
You hereby acknowledge and agree that these terms and conditions, together with CCC's Billing and Payment terms and conditions (which are incorporated herein), comprise the entire agreement between you and the RSC (and CCC) concerning this licensing transaction, to the exclusion of all other terms and conditions, written or verbal, express or implied (including any terms contained in any purchase order, acknowledgment, check endorsement or other writing prepared by you). In the event of any conflict between your obligations established by these terms and conditions and those established by CCC's Billing and Payment terms and conditions, these terms and conditions shall control.

JURISDICTION
This license transaction shall be governed by and construed in accordance with the laws of the District of Columbia. You hereby agree to submit to the jurisdiction of the courts located in the District of Columbia for purposes of resolving any disputes that may arise in connection with this licensing transaction.

LIMITED LICENSE
The following terms and conditions apply to specific license types:

Translation
This permission is granted for non-exclusive world English rights only unless your license was granted for translation rights. If you licensed translation rights you may only translate this content into the languages you requested. A professional translator must perform all translations and reproduce the content word for word preserving the integrity of the article.

Intranet
If the licensed material is being posted on an Intranet, the Intranet is to be password-protected and made available only to bona fide students or employees only. All content

posted to the Intranet must maintain the copyright information line on the bottom of each image. You must also fully reference the material and include a hypertext link as specified above.

Copies of Whole Articles
All copies of whole articles must maintain, if available, the copyright information line on the bottom of each page.

Other Conditions
v1.2

Gratis licenses (referencing $0 in the Total field) are free. Please retain this printable license for your reference. No payment is required.

If you would like to pay for this license now, please remit this license along with yourpayment made payable to "COPYRIGHT CLEARANCE CENTER" otherwise you will be invoiced within 48 hours of the license date. Payment should be in the form of a check or money order referencing your account number and this invoice number {Invoice Number}.

Once you receive your invoice for this order, you may pay your invoice by credit card.

Please follow instructions provided at that time.

Make Payment To:
Copyright Clearance Center
Dept 001
P.O. Box 843006
Boston, MA 02284-3006

For suggestions or comments regarding this order, contact Rightslink Customer Support: customercare@copyright.com or +1-855-239-3415 (toll free in the US) or +1-978-646-2777.

Questions? customercare@copyright.com or +1-855-239-3415 (toll free in the US) or +1-978-646-2777.

Gratis licenses (referencing $0 in the Total field) are free. Please retain this printable license for your reference. No payment is required.

APPENDIX E – ADDITIONAL INFORMATION FOR CHAPTER SIX

E.1 – Pellets thermally pre-treated - results

Table E.1. Results of TT1.5N-90/10 pellets.

Cycle	$\chi_{carbonation}$ (%)	CO_2 Capacity (CO_2/gPellets)	CCL (%)*
1	57.2 ± 0.7	0.404 ± 0.005	N/A
2	45.8 ± 0.7	0.323 ± 0.005	20.1 ± 2.1
3	40.5 ± 0.9	0.286 ± 0.006	29.2 ± 2.3
4	37.5 ± 1.0	0.265 ± 0.007	34.4 ± 2.4
5	35.5 ± 1.0	0.251 ± 0.007	37.9 ± 2.3
6	34.0 ± 1.1	0.240 ± 0.007	40.6 ± 2.4
7	32.9 ± 1.0	0.232 ± 0.007	42.5 ± 2.3
8	31.9 ± 0.9	0.225 ± 0.006	44.2 ± 2.2
9	31.3 ± 0.9	0.221 ± 0.007	45.3 ± 2.2
10	30.7 ± 1.0	0.217 ± 0.007	46.3 ± 2.4
11	30.1 ± 1.1	0.213 ± 0.008	47.4 ± 2.5
12	29.6 ± 1.1	0.209 ± 0.008	48.2 ± 2.5
13	29.3 ± 1.1	0.207 ± 0.008	48.8 ± 2.5
14	29.0 ± 1.1	0.205 ± 0.008	49.4 ± 2.5
15	28.7 ± 1.1	0.203 ± 0.008	49.9 ± 2.5
16	28.5 ± 1.1	0.201 ± 0.008	50.2 ± 2.6
17	28.3 ± 1.1	0.200 ± 0.008	50.5 ± 2.6
18	28.2 ± 1.3	0.199 ± 0.009	50.7 ± 2.9
19	28.2 ± 1.6	0.199 ± 0.011	50.7 ± 3.2
20	28.3 ± 1.9	0.200 ± 0.014	50.5 ± 3.8

*CCL (%) = CO_2 Capacity Loss

Table E.2. Results of TT1.5A-90/10 pellets.

Cycle	$\chi_{carbonation}$ (%)	CO_2 Capacity ($gCO_2/gPellets$)	CCL (%)*
1	58.6 ± 0.5	0.414 ± 0.004	N/A
2	46.4 ± 0.7	0.327 ± 0.005	20.9 ± 1.6
3	40.5 ± 1.3	0.286 ± 0.010	30.9 ± 2.9
4	37.3 ± 1.5	0.264 ± 0.011	36.3 ± 3.2
5	35.3 ± 1.7	0.249 ± 0.012	39.7 ± 3.4
6	33.8 ± 1.7	0.238 ± 0.012	42.4 ± 3.4
7	32.7 ± 1.8	0.231 ± 0.013	44.2 ± 3.6
8	31.8 ± 1.9	0.224 ± 0.013	45.7 ± 3.7
9	31.1 ± 1.9	0.219 ± 0.013	47.0 ± 3.6
10	30.6 ± 1.6	0.216 ± 0.011	47.7 ± 3.2
11	29.8 ± 2.0	0.211 ± 0.014	49.0 ± 3.9
12	29.5 ± 2.0	0.208 ± 0.014	49.7 ± 3.9
13	29.1 ± 1.8	0.205 ± 0.013	50.4 ± 3.5
14	29.0 ± 1.7	0.205 ± 0.012	50.5 ± 3.3
15	28.4 ± 2.0	0.201 ± 0.014	51.4 ± 3.8
16	28.3 ± 2.0	0.200 ± 0.014	51.7 ± 3.8
17	28.1 ± 2.0	0.198 ± 0.014	52.0 ± 3.8
18	28.0 ± 2.0	0.197 ± 0.014	52.2 ± 3.8
19	27.8 ± 2.0	0.197 ± 0.014	52.5 ± 3.9
20	27.7 ± 2.0	0.196 ± 0.014	52.7 ± 3.8

*CCL (%) = CO_2 Capacity Loss

Table E.3. Results of TT7.5N-90/10 pellets.

Cycle	$\chi_{carbonation}$ (%)	CO_2 Capacity (gCO_2/gPellets)	CCL (%)*
1	55.4 ± 0.8	0.391 ± 0.006	N/A
2	46.2 ± 0.5	0.326 ± 0.003	16.6 ± 0.6
3	41.7 ± 0.3	0.294 ± 0.002	24.8 ± 0.9
4	38.9 ± 0.2	0.274 ± 0.001	29.8 ± 0.8
5	37.0 ± 0.3	0.261 ± 0.002	33.2 ± 0.5
6	35.6 ± 0.3	0.251 ± 0.002	35.8 ± 0.5
7	34.6 ± 0.3	0.244 ± 0.002	37.6 ± 0.4
8	33.7 ± 0.3	0.238 ± 0.002	39.2 ± 0.3
9	32.9 ± 0.4	0.233 ± 0.002	40.5 ± 0.3
10	32.4 ± 0.3	0.229 ± 0.002	41.6 ± 0.3
11	31.8 ± 0.4	0.225 ± 0.003	42.6 ± 0.1
12	31.4 ± 0.3	0.221 ± 0.002	43.4 ± 0.3
13	31.0 ± 0.4	0.219 ± 0.003	44.0 ± 0.2
14	30.7 ± 0.4	0.217 ± 0.003	44.5 ± 0.1
15	30.5 ± 0.4	0.215 ± 0.003	44.9 ± 0.1
16	30.2 ± 0.3	0.213 ± 0.002	45.5 ± 0.2
17	30.1 ± 0.4	0.212 ± 0.003	45.7 ± 0.1
18	29.8 ± 0.7	0.210 ± 0.005	46.2 ± 0.7
19	29.6 ± 0.6	0.209 ± 0.004	46.5 ± 0.7
20	29.6 ± 0.6	0.209 ± 0.004	46.6 ± 0.6

*CCL (%) = CO_2 Capacity Loss

E.2 – Calculation of reaction rate

The reaction rate was calculated following the equation below:

$$(-R_A) = \frac{dX_A}{dt} \qquad \text{E-1}$$

The conversion was calculated following the same procedure that was explained in Appendix B.6:

$$\chi_A = \chi_{carbonation} = \frac{m_{carb} - m_{calc}}{m_{calcined} y_{CaO} \left(\frac{MW_{CaCO_3}}{MW_{CaO}} - 1\right)} \qquad \text{E-2}$$

Then, the differential increments are approximated to finite increments:

$$(-R_A) = \frac{\Delta X_A}{\Delta t} \qquad \text{E-3}$$

Finally, the reaction rate is calculated using the smoothed data. Δt used was 5 seconds.

$$(-R_A) = \frac{\Delta X_A}{\Delta t} = \frac{X_{A,i} - X_{A,i-1}}{t_i - t_{i-1}} \qquad \text{E-3}$$

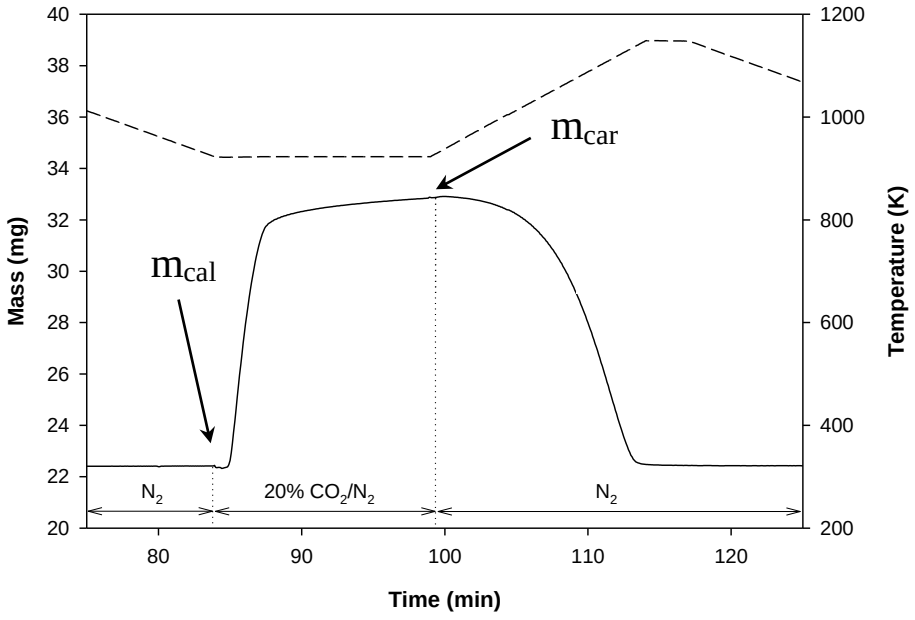

Figure E.1 – Carbonation/calcination cycle for 90/10 pellets with labels of m_{carb} and m_{calc}.

E.3 – Smoothing of raw data

To calculate the reaction rates showed in Chapter Six, the raw data was smoothed by means of the Lowess local regression smoothing method. The smoothing process consists of reducing the number of data points by calculating the smoothed value using the neighbouring data points within a defined a span. For the data points within the span, a regression weight function is defined. Then, for each span, there is a weight function, which is calculated from the regression of the weights of each data point within the span. The equation used to calculate the weights is as follows:

$$w_i = \left(1 - \left|\frac{x - x_i}{d(x)}\right|^3\right)^3$$

where x is the predictor value associated with the response value to be smoothed, x_i are the nearest neighbours of x as defined by the span, and $d(x)$ is the distance along the abscissa from x to the most distant predictor value within the span.

Once the weights for the data points within the span are calculated, a weighted linear least squares regression is performed. For the Lowess method the regression uses a second degree polynomial. Finally, the smoothed value is calculated using the weighted regression at the predictor value of interest. These steps are repeated for each span.

Figure E.2 illustrates the result obtained for the 5% K-impregnated pellets. The noise and fluctuations are greatly reduced, and the trend of the reaction rate is conserved.

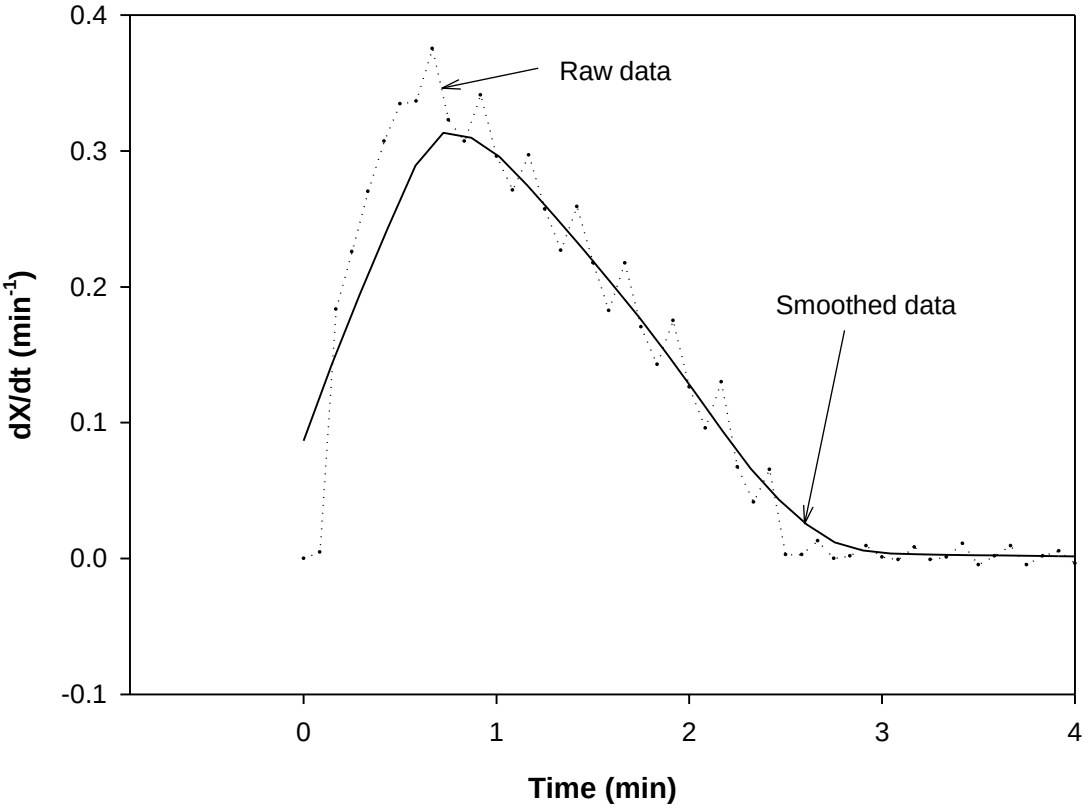

Figure E.2 – Comparison of raw and smoothed data for 5% K-impregnated pellets.

.

E.4 – Pellets subjected to carbonation with steam - results

Table E.4. Results of 90/10 pellets without using steam during the carbonation stage.

Cycle	$\chi_{carbonation}$ (%)	CO_2 Capacity ($gCO_2/gPellets$)	CCL (%)*
1	65.1 ± 14.9	0.46 ± 0.11	N/A
2	55.2 ± 15.5	0.39 ± 0.11	15.8 ± 7.6
3	38.8 ± 4.4	0.28 ± 0.03	39.4 ± 8.9
4	33.5 ± 2.2	0.24 ± 0.02	47.3 ± 10.1
5	29.8 ± 1.7	0.21 ± 0.02	53.0 ± 9.7
6	27.3 ± 1.7	0.19 ± 0.01	57.0 ± 8.9
7	25.3 ± 1.5	0.18 ± 0.01	60.2 ± 8.2
8	24.1 ± 1.5	0.17 ± 0.01	62.1 ± 7.6
9	22.9 ± 1.3	0.16 ± 0.01	64.0 ± 7.4
10	22.1 ± 0.9	0.16 ± 0.01	65.0 ± 8.7
11	20.7 ± 0.5	0.15 ± 0.01	67.2 ± 8.6
12	19.9 ± 0.4	0.14 ± 0.01	68.6 ± 7.6
13	19.1 ± 0.7	0.14 ± 0.01	69.9 ± 6.5
14	18.5 ± 0.2	0.13 ± 0.01	70.6 ± 7.6
15	18.2 ± 0.4	0.13 ± 0.01	71.3 ± 6.7

*CCL (%) = CO_2 Capacity Loss

Table E.5. Results of 90/10 pellets using 10% steam during the carbonation stage.

Cycle	$\chi_{carbonation}$ (%)	CO_2 Capacity ($gCO_2/gPellets$)	CCL (%)*
1	69.2 ± 6.2	0.49 ± 0.04	N/A
2	53.0 ± 3.8	0.37 ± 0.03	23.1 ± 9.6
3	45.0 ± 3.0	0.32 ± 0.02	34.6 ± 7.8
4	39.2 ± 3.6	0.28 ± 0.03	43.0 ± 8.5
5	32.1 ± 3.2	0.23 ± 0.02	53.3 ± 7.7
6	32.6 ± 4.2	0.23 ± 0.03	52.5 ± 8.4
7	31.1 ± 5.8	0.22 ± 0.04	54.7 ± 10.0
8	29.5 ± 6.5	0.21 ± 0.05	57.0 ± 10.8
9	27.8 ± 5.7	0.20 ± 0.04	59.6 ± 9.6
10	26.8 ± 6.2	0.19 ± 0.04	60.9 ± 10.3
11	25.6 ± 6.2	0.18 ± 0.04	62.7 ± 10.2
12	25.0 ± 6.2	0.18 ± 0.04	63.6 ± 10.1
13	24.6 ± 7.3	0.17 ± 0.05	64.2 ± 11.3
14	24.6 ± 9.0	0.17 ± 0.06	64.2 ± 13.5
15	24.3 ± 9.6	0.17 ± 0.07	64.6 ± 14.3

*CCL (%) = CO_2 Capacity Loss

Table E.6. Results of 90/10 pellets using 30% steam during the carbonation stage.

Cycle	$\chi_{carbonation}$ (%)	CO_2 Capacity ($gCO_2/gPellets$)	CCL (%)*
1	65.9 ± 8.8	0.47± 0.06	N/A
2	64.2 ± 10.2	0.46± 0.07	-0.4± 18.7
3	55.9 ± 4.7	0.40± 0.04	12.2± 14.7
4	56.3± 8.3	0.40± 0.05	13.1± 7.5
5	50.5± 7.2	0.36± 0.05	20.3± 16.3
6	47.8± 8.9	0.34± 0.06	26.7± 6.5
7	45.6± 4.7	0.33± 0.05	27.5± 17.1
8	47.7± 9.1	0.34± 0.06	26.6± 10.3
9	43.0± 4.8	0.31± 0.04	31.4± 16.8
10	39.9± 10.3	0.29± 0.07	39.0± 11.2
11	38.8± 4.0	0.28± 0.04	38.4± 14.5
12	42.3± 7.5	0.30± 0.05	35.1± 5.6
13	38.0± 6.1	0.27± 0.05	39.3± 16.0
14	39.1± 6.4	0.28± 0.04	39.9± 4.6
15	38.0± 4.4	0.27± 0.04	39.8± 13.3

*CCL (%) = CO_2 Capacity Loss

**Note: these results show the average of 5 experiments, and the performance in each cycle was not always the same because of condensation issues.

E.5 – t-Test results

The t-Test analysis was performed using Excel 2010.

1st cycle

t-Test: Paired Two Sample for Means

	No steam	*10% steam*
Mean	0.463383	0.488631
Variance	0.009068	0.001492
Observations	3	3
Pearson Correlation	0.140146	
Hypothesized Mean Difference	0	
df	2	
t Stat	**-0.448**	
P(T<=t) one-tail	0.349003	
t Critical one-tail	**2.919986**	
P(T<=t) two-tail	0.698005	
t Critical two-tail	4.302653	

2nd cycle

t-Test: Paired Two Sample for Means

	No steam	*10% steam*
Mean	0.392872	0.374065
Variance	0.009948	0.000555
Observations	3	3
Pearson Correlation	-0.90584	
Hypothesized Mean Difference	0	
df	2	
t Stat	**0.268139**	
P(T<=t) one-tail	0.406858	
t Critical one-tail	**2.919986**	
P(T<=t) two-tail	0.813716	
t Critical two-tail	4.302653	

3rd cycle

t-Test: Paired Two Sample for Means

	No steam	*10% steam*
Mean	0.276077	0.317975
Variance	0.000893	0.000345
Observations	3	3
Pearson Correlation	-0.82587	
Hypothesized Mean Difference	0	
df	2	
t Stat	**-1.56381**	
P(T<=t) one-tail	0.129154	
t Critical one-tail	**2.919986**	
P(T<=t) two-tail	0.258308	
t Critical two-tail	4.302653	

4th cycle

t-Test: Paired Two Sample for Means

	No steam	*10% steam*
Mean	0.238653	0.27672
Variance	0.00027	0.000512
Observations	3	3
Pearson Correlation	-0.58672	
Hypothesized Mean Difference	0	
df	2	
t Stat	**-1.88896**	
P(T<=t) one-tail	0.099745	
t Critical one-tail	**2.919986**	
P(T<=t) two-tail	0.19949	
t Critical two-tail	4.302653	

5th cycle

t-Test: Paired Two Sample for Means

	No steam	*10% steam*
Mean	0.212313	0.226769
Variance	0.000176	0.000405
Observations	3	3
Pearson Correlation	0.971308	
Hypothesized Mean Difference	0	
df	2	
t Stat	**-3.17172**	
P(T<=t) one-tail	0.043338	
t Critical one-tail	**2.919986**	
P(T<=t) two-tail	0.086677	
t Critical two-tail	4.302653	

6th cycle

t-Test: Paired Two Sample for Means

	No steam	*10% steam*
Mean	0.194322	0.230417
Variance	0.000172	0.000677
Observations	3	3
Pearson Correlation	-0.43161	
Hypothesized Mean Difference	0	
df	2	
t Stat	**-1.84854**	
P(T<=t) one-tail	0.102886	
t Critical one-tail	**2.919986**	
P(T<=t) two-tail	0.205771	
t Critical two-tail	4.302653	

7th cycle

t-Test: Paired Two Sample for Means

	No steam	*10% steam*
Mean	0.180096	0.219973
Variance	0.000127	0.001313
Observations	3	3
Pearson Correlation	-0.60247	
Hypothesized Mean Difference	0	
df	2	
t Stat	**-1.57173**	
P(T<=t) one-tail	0.128312	
t Critical one-tail	**2.919986**	
P(T<=t) two-tail	0.256625	
t Critical two-tail	4.302653	

8th cycle

t-Test: Paired Two Sample for Means

	No steam	*10% steam*
Mean	0.171608	0.208446
Variance	0.000126	0.001663
Observations	3	3
Pearson Correlation	-0.6266	
Hypothesized Mean Difference	0	
df	2	
t Stat	**-1.3126**	
P(T<=t) one-tail	0.159858	
t Critical one-tail	**2.919986**	
P(T<=t) two-tail	0.319717	
t Critical two-tail	4.302653	

9th cycle

t-Test: Paired Two Sample for Means

	No steam	*10% steam*
Mean	0.162663	0.196044
Variance	9.59E-05	0.001247
Observations	3	3
Pearson Correlation	-0.59248	
Hypothesized Mean Difference	0	
df	2	
t Stat	**-1.38091**	
P(T<=t) one-tail	0.150684	
t Critical one-tail	**2.919986**	
P(T<=t) two-tail	0.301368	
t Critical two-tail	4.302653	

10th cycle

t-Test: Paired Two Sample for Means

	No steam	*10% steam*
Mean	0.157162	0.189586
Variance	5.67E-05	0.0015
Observations	3	3
Pearson Correlation	-0.00501	
Hypothesized Mean Difference	0	
df	2	
t Stat	**-1.42202**	
P(T<=t) one-tail	0.145475	
t Critical one-tail	**2.919986**	
P(T<=t) two-tail	0.290951	
t Critical two-tail	4.302653	

11th cycle

t-Test: Paired Two Sample for Means

	No steam	*10% steam*
Mean	0.147197	0.180657
Variance	1.5E-06	0.001511
Observations	3	3
Pearson Correlation	-0.26369	
Hypothesized Mean Difference	0	
df	2	
t Stat	**-1.47798**	
P(T<=t) one-tail	0.13874	
t Critical one-tail	**2.919986**	
P(T<=t) two-tail	0.277479	
t Critical two-tail	4.302653	

12th cycle

t-Test: Paired Two Sample for Means

	No steam	*10% steam*
Mean	0.141241	0.176564
Variance	6.22E-06	0.00151
Observations	3	3
Pearson Correlation	-0.99874	
Hypothesized Mean Difference	0	
df	2	
t Stat	**-1.47953**	
P(T<=t) one-tail	0.138559	
t Critical one-tail	**2.919986**	
P(T<=t) two-tail	0.277118	
t Critical two-tail	4.302653	

13th cycle

t-Test: Paired Two Sample for Means

	No steam	*10% steam*
Mean	0.135626	0.173839
Variance	2.55E-05	0.002072
Observations	3	3
Pearson Correlation	-0.97542	
Hypothesized Mean Difference	0	
df	2	
t Stat	**-1.31187**	
P(T<=t) one-tail	0.159959	
t Critical one-tail	**2.919986**	
P(T<=t) two-tail	0.319918	
t Critical two-tail	4.302653	

14th cycle

t-Test: Paired Two Sample for Means

	No steam	*10% steam*
Mean	0.131821	0.173889
Variance	3.2E-07	0.003153
Observations	3	3
Pearson Correlation	-0.37559	
Hypothesized Mean Difference	0	
df	2	
t Stat	**-1.29262**	
P(T<=t) one-tail	0.162669	
t Critical one-tail	**2.919986**	
P(T<=t) two-tail	0.325338	
t Critical two-tail	4.302653	

15th cycle

t-Test: Paired Two Sample for Means

	No steam	*10% steam*
Mean	0.129409	0.171973
Variance	1.33E-05	0.003557
Observations	3	3
Pearson Correlation	-0.7969	
Hypothesized Mean Difference	0	
df	2	
t Stat	**-1.17795**	
P(T<=t) one-tail	0.179998	
t Critical one-tail	**2.919986**	
P(T<=t) two-tail	0.359996	
t Critical two-tail	4.302653	